

Svensk Kärnbränslehantering AB
Kapsellaboratoriet
Box 925
572 29 OSKARSHAMN

Residual stress measuring by incremental hole drilling technique

(5 appendices)

This is a revised report. A new Appendix 5 has been included in the report. This appendix contains the measured stresses converted to the global coordinate system of the insert tube. The reason for doing this conversion was that the results from this measurement should be presented in the same manner as the results from a measurement done with the Deep-hole Drilling technique. The latter results are presented in Ref. [10]

A second revision of the report is done. In this revision calculated stresses in Appendix 4 and 5 are considered to be unreliable if the corresponding von Mises effective stress is larger than 70% of the yield stress. All such calculated stress values are now shaded in both appendices. Some minor typing errors are also corrected. A wrong reference in this revision is corrected in Rev2a.

1 Test objects

- A 75mm thick sample from a PWR insert tube Ø950 mm. The sample was marked IP8
- A 75mm thick sample from a BWR insert tube Ø950 mm. The sample was marked I54
- A 50mm thick copper sample. Test block (TB) annealed at 225°

The test samples were cut out from the insert tubes and their surfaces ground by the customer before they were transported to SP. The test objects arrived to SP October 2008.

2 Assignment

The objective was to carry out residual stress measurement at different locations of the test samples. The locations are shown in sketches in *Appendix 1*. The layout of the strain gages are shown on *Figure A4:1* in *Appendix 4*.

3 Summary

From the measured strains residual stresses were calculated by the method outlined in the ASTM Standard procedure E837, Ref. [4]. It was then found that the requirements for a uniform residual stress field given in the standard were not fulfilled and therefore the stresses were calculated with the Integral Method described in Ref. [6]. This method is suggested in Ref. [8] for highly non-uniform stress distributions. The calculations were done by a computer program written by G.S. Schajer, Ref. [7].

Residual stress measurements were done on the samples in the state they had when they were delivered to SP, but also after the samples had been stress-relieve annealed. The annealing was done by Bodycote Värmebehandling AB in Angered.

SP Technical Research Institute of Sweden

4 Date of the measurement

The measurement was done during the period October – December, 2008 (on the original samples) and in March, 2009 (on the annealed sample).

5 Equipment used at the measurement

A Milling Guide Model RS-200 from Measurements Group was used for drilling the holes. According to recommendation from the supplier of the equipment a high-speed air turbine and carbide-tipped 1.6mm cutters were used.

The strains were measured by CEA-06-062UL-120 gages. This type of gages is manufactured by the supplier of the hole drilling equipment and recommended for this type of tests.

The strains were sampled to a computer by an MGCPlus data acquisition system from HBM equipped with an AP814 and an ML801 card for conditioning and sampling single strain gages.

Photographs from the measurement and sketches of the hole drilling equipment are given in *Appendix 2*.

6 Implementation of the measurement

- The strain gages were bonded to the test samples according to instructions from the strain gage manufacturer. To minimize effects of temperature changes in the lead wires, three-wire quarter-bridge circuits were used.
- Before the drilling was started it was checked that all three gages gave stable readings on the data acquisition system
- The stand for the drilling equipment was cemented to the sample and aligned with respect to the centring marks of the strain gage rosette.
- The drilling was done in 15 steps from zero hole depth down to 1.91 mm (slightly deeper than the hole diameter). For each increment the strains were sampled to the computer and stored in an EXCEL-sheet. When the strain was measured the drill was retracted from the hole.
- After the drilling was completed it was checked that the readings of the strain gages were stable.
- After the completion of the drilling the hole diameter was measured in three directions and a mean value of the measurements calculated and used in the analysis.

7 Material data

In the analysis material data according to *Table 1* were used. The data was given to SP by SKB and can be found in Ref:s [1], [2] and [3].

Table 1: Material data used in the calculations.

Material	Young's modulus	Poisson's ratio	Yield stress
BWR (Nodular Cast Iron EN 1563; SKBdok 1064461)	166 GPa	0.30	272 MPa
PWR (Nodular Cast Iron EN 1563; SKBdok 1064461)	166 GPa	0.30	299 MPa
Copper (Cu-OFE EN 1976; SKBdok 1064458)	117 GPa	0.35	Ca 50 MPa

8 Uncertainty in reported values

There are a lot of uncertainties in these types of investigations. Errors due to deviation in instrument reading and uncertainties in the used material data are in most cases small and their influence on the final result is also rather easy to estimate. When doing measurements with the hole drilling method it is essential that the drilling is very soft so no additional residual stresses are introduced and that no heating of the material occur. These types of errors are much more difficult to estimate as they are to a relative large amount depending on the skilfulness of the person doing the drilling. In this application the stress distribution was non-uniform and a calculation of the stress gradient had to be done by a commercial computer program. According to the manual for this program the calculations require engineering judgment. Below we have listed possible errors and discussed them briefly. The order of the different errors is the order of the different moments in the measurement.

Bonding and alignment of the strain gages

If the gages are not properly bonded to the target their deformation will not correspond to the deformation of the target and inaccurate readings are obtained. Poor bonding to the target can be present from the beginning of the measurement or the gages can loosen during the measurement. The person responsible for the bonding of the gages at this project is very experienced in this type of work. In other projects SP has bonded redundant gages to the test object and we have compared their readings and only found deviations of some microstrains, i.e. close to the resolution of the measurement system.

In this project it was rather easy to bond the gages as the samples were large and lying on a working desk. After terminating the measurement we checked the bonding of some of the gages by scraping them by a knife and got no indication of poor bonding.

Each gage element consists of three gages and the element should be aligned on the sample in order to be able to evaluate the strains in well defined directions. If the element is not properly aligned the calculated values of the direction of the principal stresses will be wrong, but their values will still be correct. The misalignment of a gage and then the fault in the direction of the calculated principal stresses should be within a few degrees.

Positioning and fixing the stand of the drilling equipment to specimens

The hole must be drilled in the centre of the gage element. On the foil with the gages the centre is marked by a circle with a diameter very close to the diameter of the cutter. By inserting a special-purpose microscope in the stand it was possible to, by X-Y-adjusting screws position the guide over the centre of the gage element. It was also easy to after the drilling check that the hole was drilled centrally. According to the manufacture of the drilling equipment, Ref. [5], the errors in calculated stresses due to inaccurate alignment should be less than 3 %.

The stand of the drilling equipment must be very rigidly fixed to the sample when the hole is drilled. The stand has three feet which are mounted in pads cemented to the sample. After doing a drilling and measurement these pads had to be removed and used at the next measurement location. This was done by striking them in a transverse direction. If the pads had been poorly cemented to the surface of the sample, it should be observed when they were removed. No such fault was observed.

Detection of the zero depth

The zero depth is the point at which drilling into the sample is started and the entire gage backing has been removed. This source of error is discussed in Ref. [8] but no estimate of the size of the error is given.

At this project the gage backing material was carefully removed by a hand operated drill and when this was done the special-purpose microscope was positioned in the stand and it was checked that the zero depth was achieved.

Even if the gage backing is correctly removed errors due to inaccurate alignment, concave profile of the drill cutting edge, axial clearance in the drill motor bearings and the surface roughness can cause errors in the determination of the zero depth.

These types of errors can lead to serious degradation in the quality of the first stress data.

By calculating the residual stresses with slightly different hole depths (simulating errors in detection of the zero depth) SP has found that the errors in the first stress data can be 5 %, but the error decreases rapidly with increasing hole depth.

Drilling the hole

This is another critical moment of the measurement. It's well known that heating of the material during the drilling and / or bending in the cutter can give inaccurate results. Before we started this project we discussed the implementation of the measurement with supplier of the milling equipment. Their recommendation was to use a high speed air turbine (400000 rpm), carbide tipped cutters (diameter 1.6mm), a slow feed rate of the cutter and to use a new cutter for each hole. We have followed these recommendations.

The drilling depth should be measured at each increment. This was done by a micrometer built into the drilling equipment. According to Ref. [9] this type of error is negligible in commercial systems. By simulating errors in the reading of the hole depth SP has also found that these errors are less than 2 % for all calculated stresses with exception for the stress just below the surface.

It is well known that hole drilling in cast iron is difficult. A hole will pass through different phases of the material and this can cause sudden changes in the measured strains. Some of the measurement series showed large jumps and these results are not presented in this report.

Measuring strains

Errors in measured strains can be due to errors in instrument reading or temperature drift in the strain gages or the lead wires to the gages. The bridge amplifier, used at the measurement, is annually calibrated and its inaccuracy is less than 1 %.

To reduce temperature drift we used three wire connection of the gages to the amplifier and used temperature compensated gages. Before and after the drilling each hole we observed the

reading from the gages during several minutes and made sure that they were stable. This indicates that the measured strains didn't change due to temperature fluctuations.

The errors in the reported stress values due to errors in the measured strains are therefore small, Ref. [9] estimates the error to be less than 5 %.

Measuring the hole dimensions

The hole dimension was measured by an optical head placed in the drilling rig and the hole diameter was measured in three direction and a mean-value of these measurements calculated. The reading was done against an optical scale. By measuring the hole diameter in three directions it was also checked that a circular hole was obtained. The deviation in diameters measured in three directions was less than 2 %. Ref. [9] states that this type of error is negligible.

Material data used by the computer program

According to Ref [9] the error due to uncertainties in the Young's modulus, E , is estimated to be less than 1 % and the error due to uncertainties in the Poisson's ratio, ν , to be less than 3 %.

Evaluating stresses from measured strains

As mentioned in the summary the stresses were calculated by the Integral Method as this method has the greatest capacity of resolving fine details. However, this method is sensitive to strain measurement errors.

A commercial computer program, written by a world leading expert in field Ref [7], has been used. The software has a built in regularization for smoothing the calculated stresses and thereby reducing the effect of experimental errors when using the Integral Method.

A middle choice between using the Integral method and calculating uniform stresses is to use the Power method. This method involves averaging and is then less sensitive to experimental errors. But when this method was checked by looking at the misfit between the measured strains and the strains corresponding to the obtained stress solution was rather great. Therefore the method was not used.

According to the manual to the computer program Ref. [7], “*the nature of the residual stresses being measured is generally not known in advance, the choice of calculation method to be used is difficult to predict. A good strategy is to try all three methods in reverse order (Integral, Power Series, and Uniform Stress). Again, good engineering judgment, combined with a knowledge of the stresses expected, should be used to choose the most appropriate stress calculation method. Similar judgment is also essential when interpreting the meaning and reliability of the results obtained*

It should also be mentioned that the accuracy of the calculated stresses decrease with the distance from the surface. The used computer program does not calculate stresses at greater deep than 1 mm.

Errors when the calculated residual stresses are not considerable lower than the yield stress

The calculation of stresses from measured strains requires that the material is linear elastic, i.e. yielding may not occur. If yielding occurs the calculated residual stresses will be too large. ASTM Standard procedure E837, Ref. [4], recommend that the calculated stresses should be

less than 50 % of the yield stress whilst the manufacture of the drilling equipment, Ref. [5], suggest a limit of 70 %.

The yield stress has been determined to be 272 MPa for the BWR sample, 299 MPa for the PWR sample and 50 MPa for the copper sample. SP has used the von Mises effective stress as yielding criterion and assumed that calculated stresses are reliable if the corresponding von Mises stress is less than 70 % of the yield stress. If the von Mises stress is larger, the calculated stresses should be regarded to be uncertain. Such values are shaded in the tables with results in *Appendix 4* and *Appendix 5*

Table 2 A summary of the discussion about the uncertainties in the reported stress values

Type of error	Uncertainty	Remarks
Bonding and alignment of the strain gages	Strain values: Negligible Direction of principal stresses: < a few degree	Estimated by SP
Positioning and fixing the stand of the drilling equipment to specimens	<3 %	Ref. [5]
Detection of zero depth	<5 % (only important for stresses just below the surface)	Estimated by SP
Drilling the hole (measuring hole depth)	Negligible (or <2%)	Ref. [9] (Estimated by SP)
Measuring strains	<5 %	Ref. [9]
Measuring the hole dimensions	Negligible	Ref. [9]
Error in the Young's modulus, E	1 %	Ref. [9]
Error in the Poisson's ratio, ν ,	3 %	Ref. [9]
Evaluating stresses from measured strains	$\pm 15\%^{1)}$	Ref. [9]
Errors when the calculated residual stresses are not considerable lower than the yield stress	<50 % Rp: Negligible 50-70 % Rp: $\pm 10\%$ >70 % Rp.: Unknown	Ref. [9]

¹⁾ This figure is an estimate of the error when a 3-axial stress field (the stresses are varying with the hole depth) is evaluated as a uniform stress field. In this report the stresses are evaluated under the assumption of a non-uniform stress field. SP has found that evaluating the residual stresses with different methods (evaluated as uniform stress, using the power method or using the integral method) can give a larger scatter in the results. The actual uncertainty is therefore not fully known, but this figure indicates that the error can be large.

From *Table 2* it can be seen that the dominating error is the error when the non-uniform stresses are calculated. The contribution from the other errors are therefore small and the total uncertainty in the calculated stress values will be less than 20 %.

9 Measurement program

The locations at which measurements were done are shown on the sketches supplied in *Appendix 1*.

After finishing the original measurement program it was decided that both the BWR and PWR test samples should be heat treated and some new measurements performed. For these supplement measurements the letter 'T' is included in identification label. Some of the new measurements were done on the back side of the test samples, the identification labels for these measurements contains the letter 'B'.

10 Results

Raw data as measured strains are given in *Appendix 3*.

The calculated residual stresses are presented as max / min principal stresses in *Appendix 4*.

The stresses are also expressed in local coordinate systems referring to the gages and in a global coordinate system referring to the insert tube in *Appendix 5*.

SP Technical Research Institute of Sweden SP Structural and Solid Mechanics - Life and Reliability

Performed by



Gunnar Kjell

Examined by



Billy Alvarsson

Appendices

- | | |
|------------|---|
| Appendix 1 | Sketches showing the measuring positions (8 pages) |
| Appendix 2 | Photographs of the test set-up (7 pages) |
| Appendix 3 | Raw data (measured strains) (28 pages) |
| Appendix 4 | Max / min principal stresses calculated by the Integral method (31 pages) |
| Appendix 5 | Normal and shear stresses in a global coordinate system (32 pages) |

References

- [1] P. Dillström, L. Alverlind, M. Andersson, 2010. "Framtagning av acceptanskriterier samt skadetåighetsanalyser av segjärnsinsatsen". SKB R-10-11, Svensk Kärnbränslehantering AB
- [2] M. Wihed "Materialprovning av segjärnsinsats I54". *SKBdoc1078585*, Swerea SweCast AB, 2007.
- [3] M. Wihed "Materialprovning av segjärnsinsats IP8". *SKBdoc1171612*. Swerea SweCast AB, 2007.

- [4] ASTM E 387-08 Standard Test method for Determining Residual Stresses by the Hole-Drilling Strain-Gage Method, 2008
- [5] Technical Note TN-503-6, Measurement of Residual Stresses by the Hole-Drilling Strain Gage Method, Vishay Measurement Group, 2007.
- [6] G.S. Schajer. "Measurement of Non-Uniform Residual Stresses Using the Hole-Drilling Method. *Journal of Engineering Materials and Technology*, Vol.110, No.4, 1988. "Part I Stress Calculation Procedures," pp.338-343, "Part II Practical Application of the Integral Method," pp 344-349.
- [7] G.S. Schajer "H-Drill – Hole-Drilling Residual Stress Calculation Program" Ver 3.10 User guide, 2007
- [8] PV Grant, PD Lord, PS Whitehead. "The measurement of residual stresses by the incremental hole drilling technique, measurement good practice guide 53". National Physical Laboratory UK, 2002.
- [9] R. Oettel "The Determination of Uncertainties in residual Stress Measurement (Using the hole drilling technique)". *Manual of Codes of Practice for determination of uncertainties in mechanical tests on metallic material*. Project UNCERT, EU Contract SMT4-CT97-2165, Standards Measurement & Testing Programme, ISBN 0 946754 41 1, Issue 1, September.
- [10] "DHD residual stress measurements within the cast iron insert of a radioactive waste canister - report No R11-001", SKBDoc 1321056, version 2.0

Appendix 1

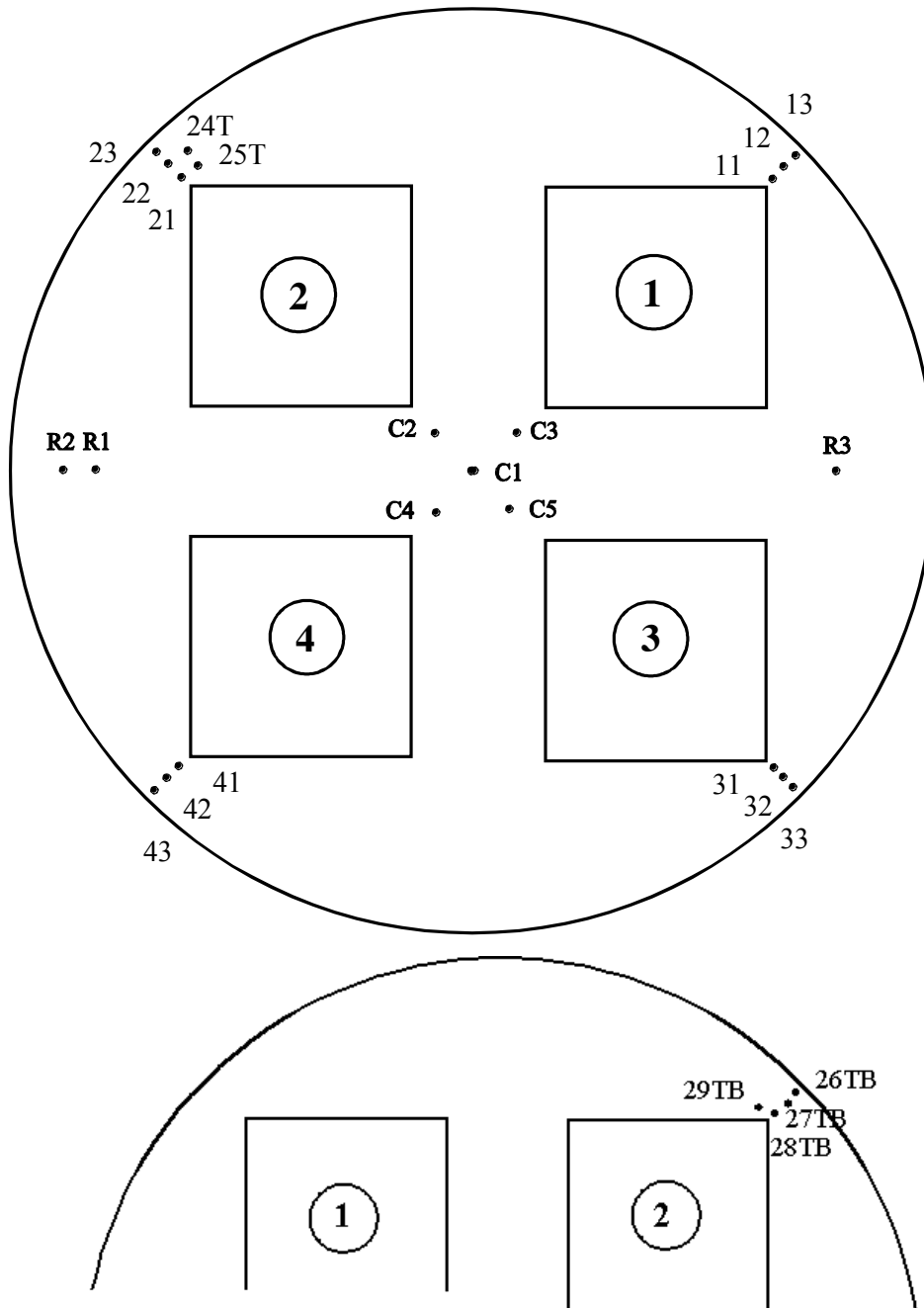
Sketches showing the measuring positions

Figure A1:1 The sample from the PWR insert tube. The sketch shows the locations of the different measuring points (indicated as filled circles). R1, R2 and R3 are Reference 1,2 & 3. C1, C2, C3, C4 & C5 are Centrum 1, 2, 3 ,4 & 5. The other measuring points have a two figure labelling where the first figure refers to the number of the space (i.e. 1, 2, 3 or 4) and the second figure refers to the position of the hole. For space 2 five measurements were done after thermal treatment, two on the front side (24T and 25T) and four on the back side (26TB, 27TB, 28TB and 29TB)

Appendix 1

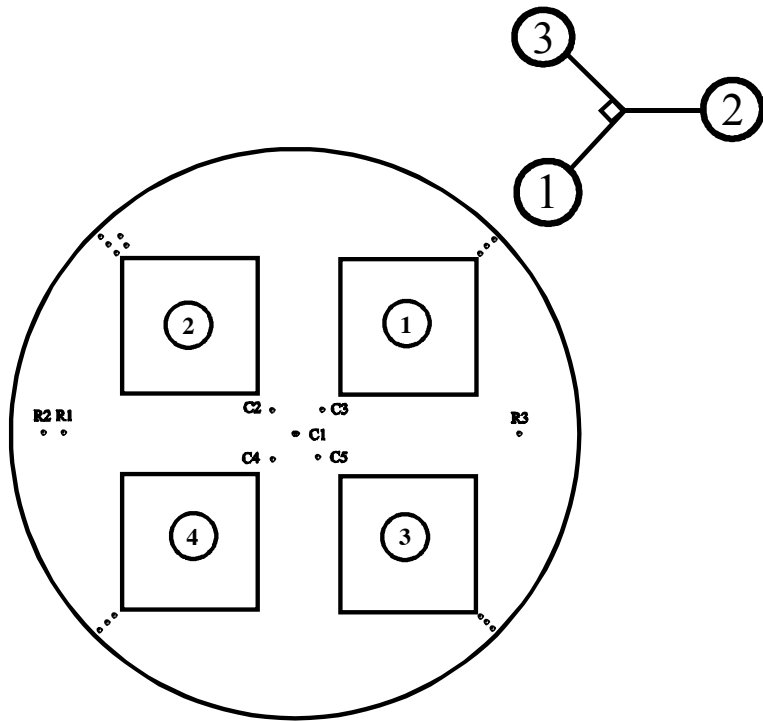


Figure A1:2 The orientation of the strain gages in the rosette for points 11, 12, 13 and C4

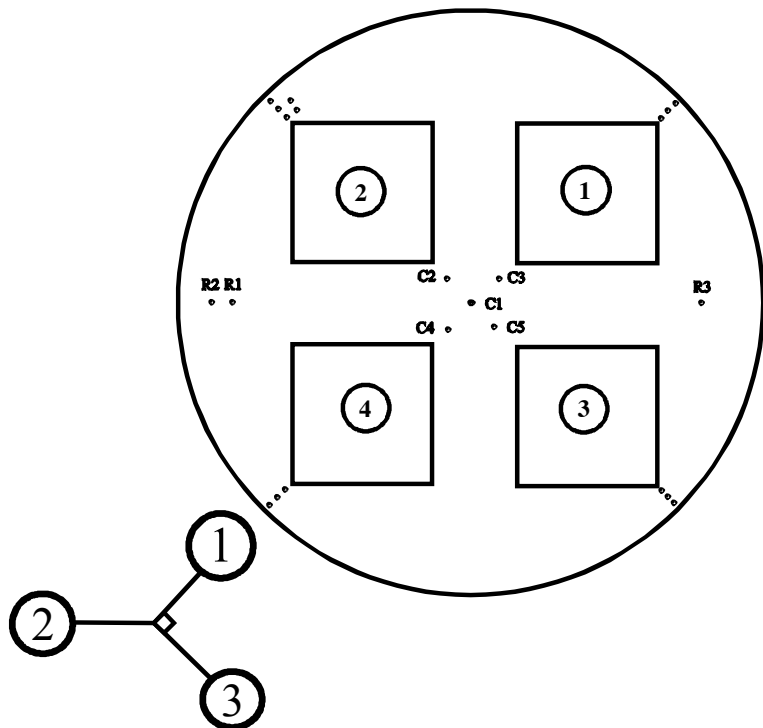


Figure A1:3 The orientation of the strain gages in the rosette for points 41, 42, 43 and C3

Appendix 1

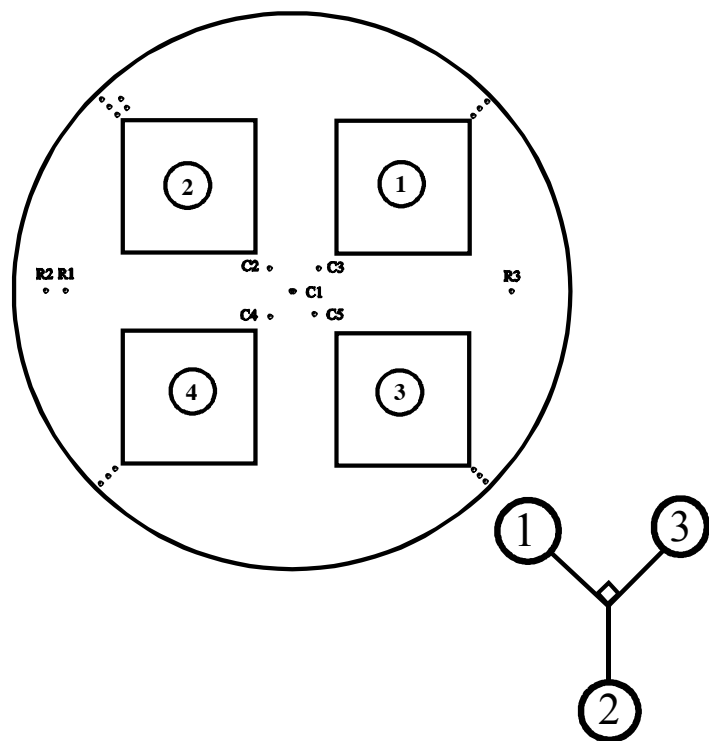


Figure A1:4 The orientation of the strain gages in the rosette for points 31, 32, 33 and C2

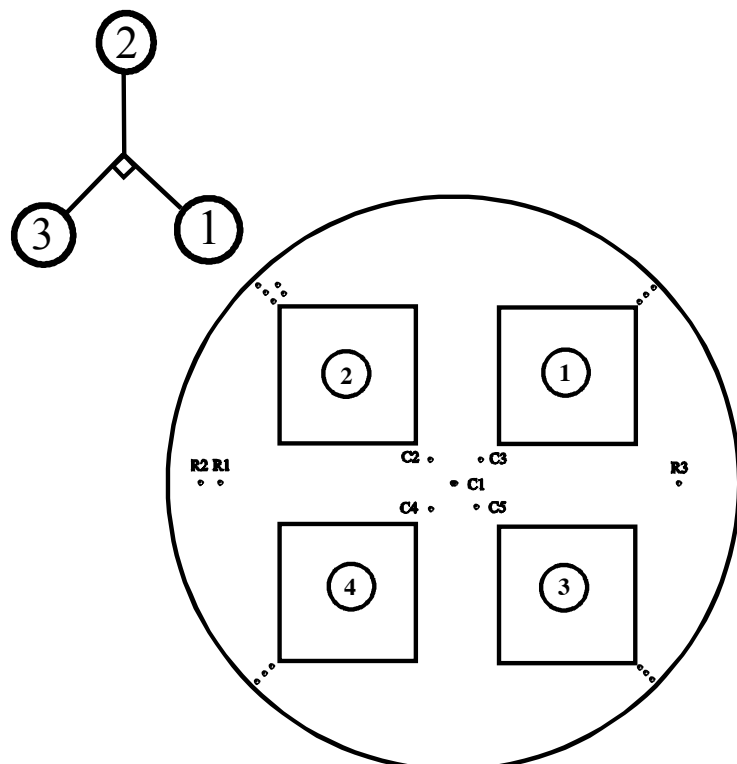


Figure A1:5 The orientation of the strain gages in the rosette for points 21, 22, 23, 24T, 25T and C5

Appendix 1

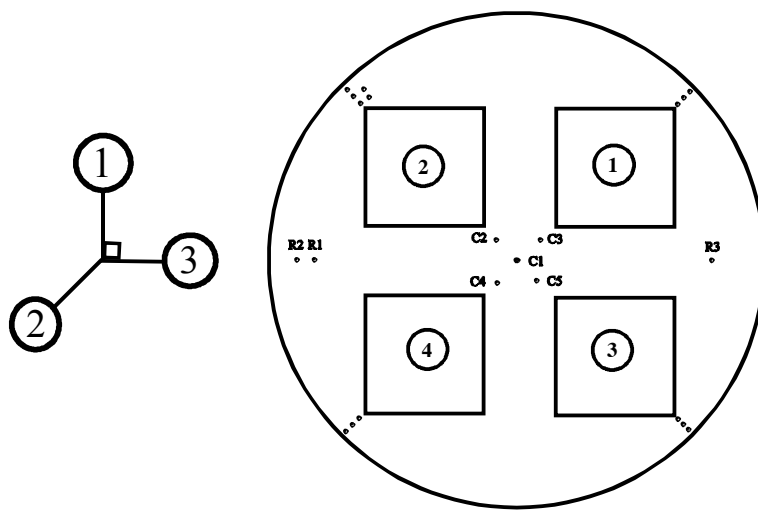


Figure A1:6 The orientation of the strain gages in the rosette for points R1, R2, R3 and C1

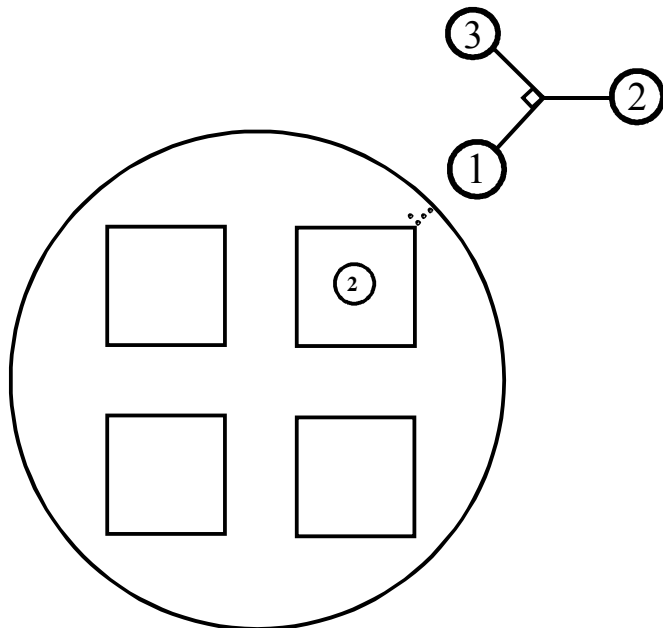


Figure A1:7 The orientation of the strain gages in the rosette for points 26TB, 27TB, 28TB and 29TB

Appendix 1

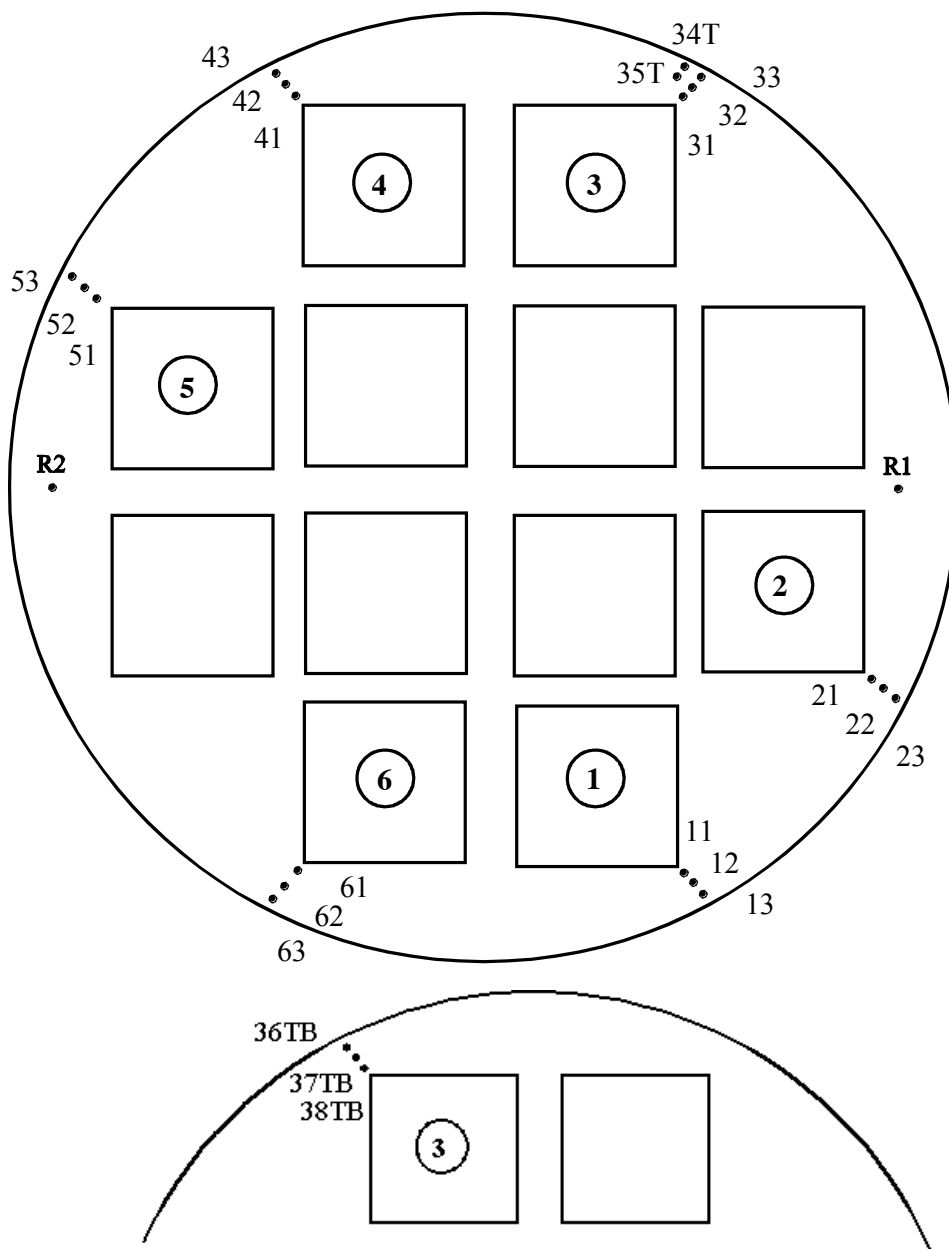


Figure A1:8 The sample from the BWR insert tube. The upper sketch shows the front side and the lower the back side. The sketches show the locations of the different measuring points (indicated as filled circles). R1, and R2 are Reference 1 & 2. The other measuring points have a two figure labelling where the first figure refers to the number of the space (i.e. 1, 2, 3, 4, 5 or 6) and the second figure refers to the position of the hole. For space 3 five measurements were done after thermal treatment, two on the front side (34T and 35T) and three on the back side (36T, 37T and 38T)

Appendix 1

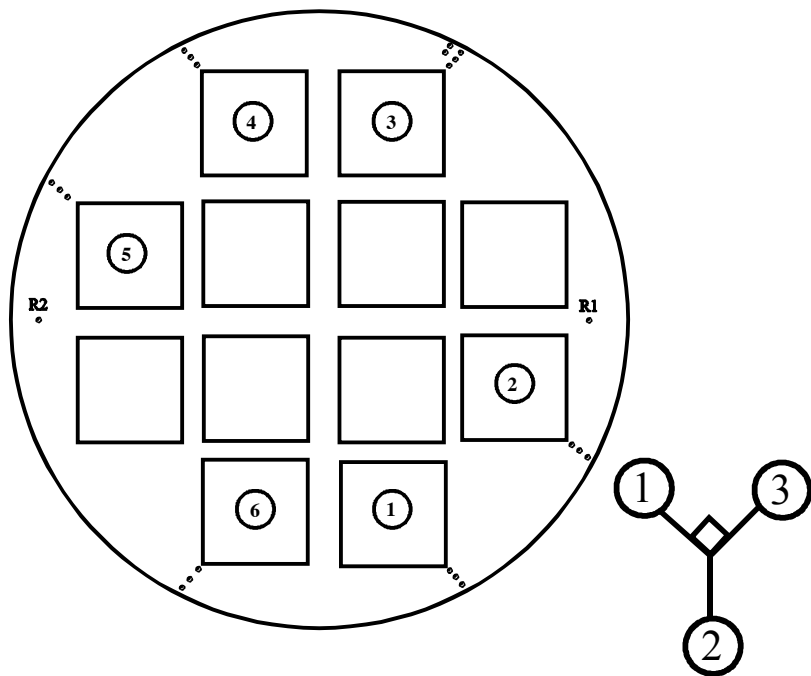


Figure A1:9 The orientation of the strain gages in the rosette for points 11, 12, 13, 21, 22 and 23.

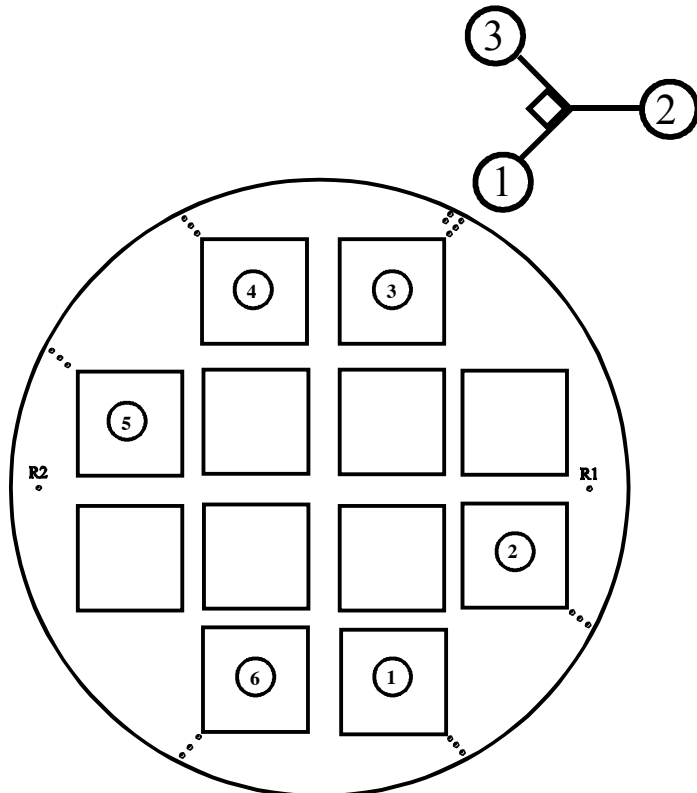


Figure A1:10 The orientation of the strain gages in the rosette for points 31, 32 33, 34T and 35T.

Appendix 1

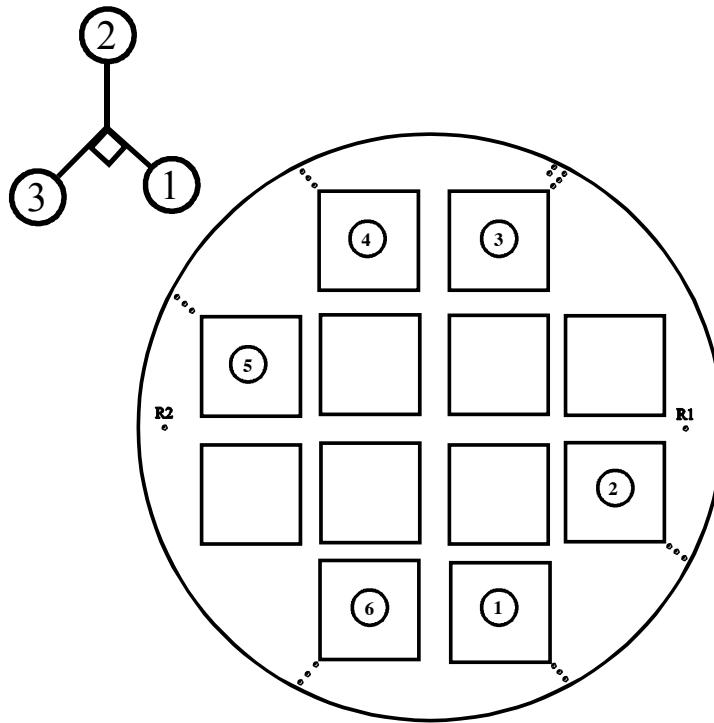


Figure A1:11 The orientation of the strain gages in the rosette for points 41, 42, 43, 51, 52 and 53.

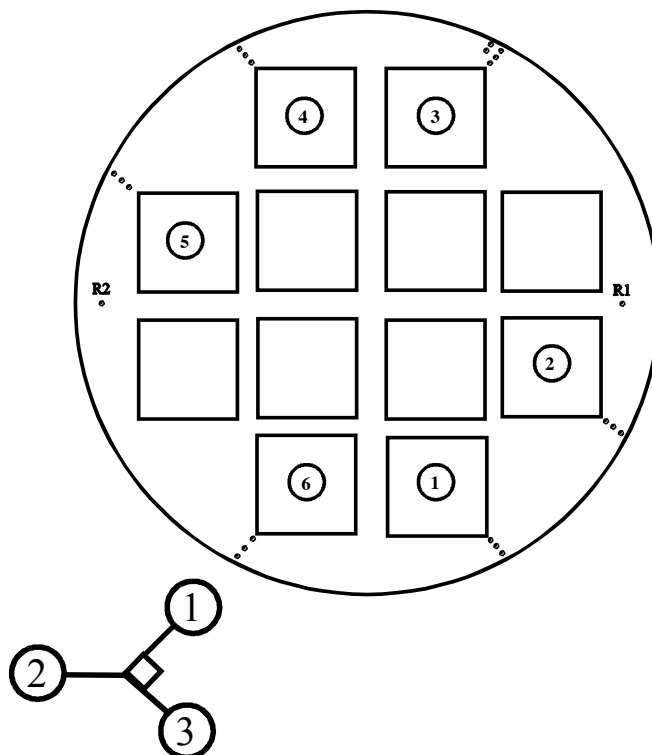


Figure A1:12 The orientation of the strain gages in the rosette for points 61, 62 and 63.

Appendix 1

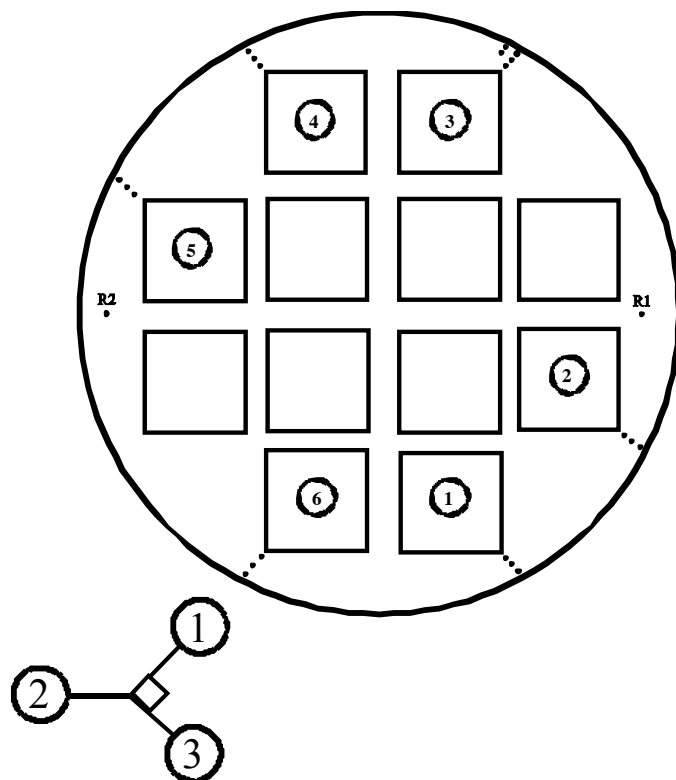


Figure A1:13 The orientation of the strain gages in the rosette for points R1 and R2.

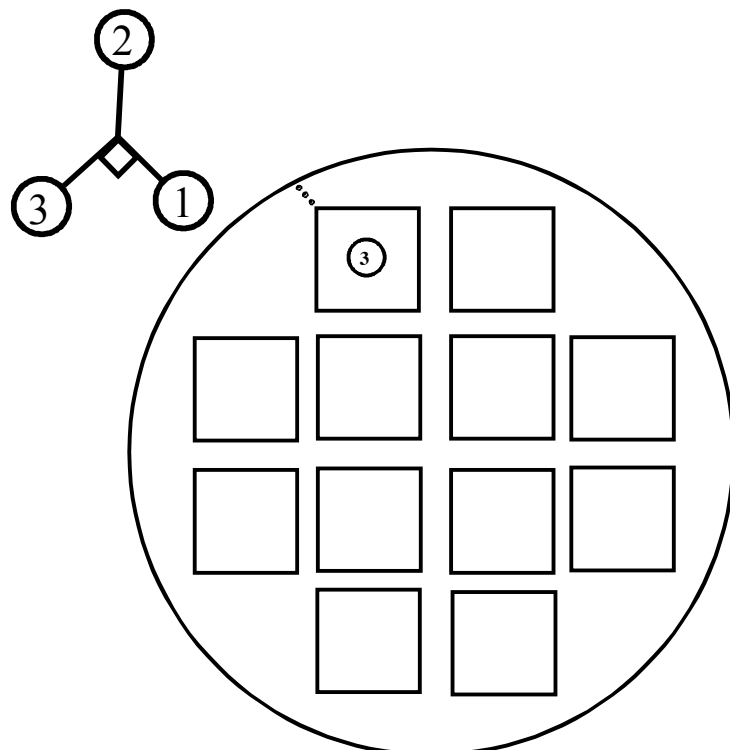


Figure A1:14 The orientation of the strain gages in the rosette for points 36T, 37T and 38T.

Appendix 2

Photographs of the test set-up

Figure A2:1 The BWR sample lying on the packing pallet before the start of the measurement.



Figure A2:2 The marking on the BWR sample.

Appendix 2

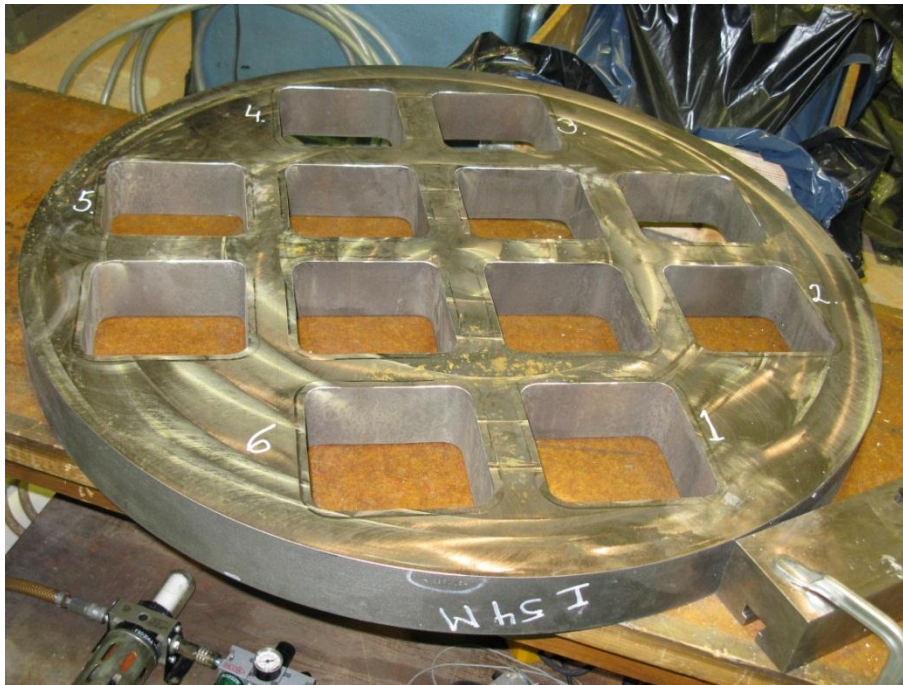


Figure A2:3 The numbering of the spaces (No: 1, 2, 3, 4, 5 & 6) where the measurements were done on the BWR sample.

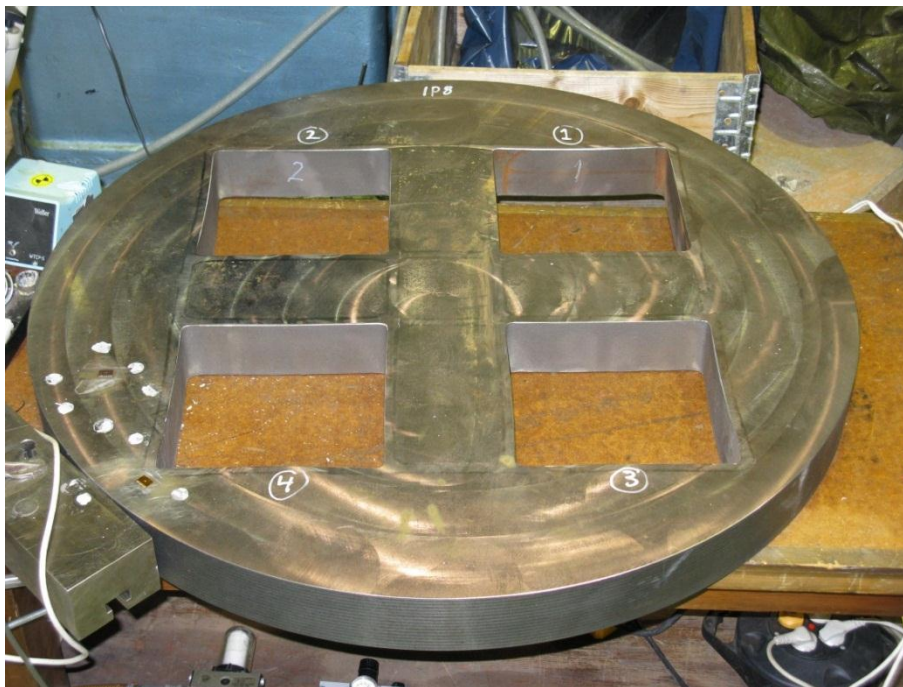


Figure A2:4 The numbering of the spaces (No: 1, 2, 3 & 4) where the measurements were done on the PWR sample.

Appendix 2



Figure A2:5 The marking on the PWR sample.



Figure A2:6 The PWR sample. The corner of space, molten material has loosened from the tube. Similar release was found close to space 3

Appendix 2

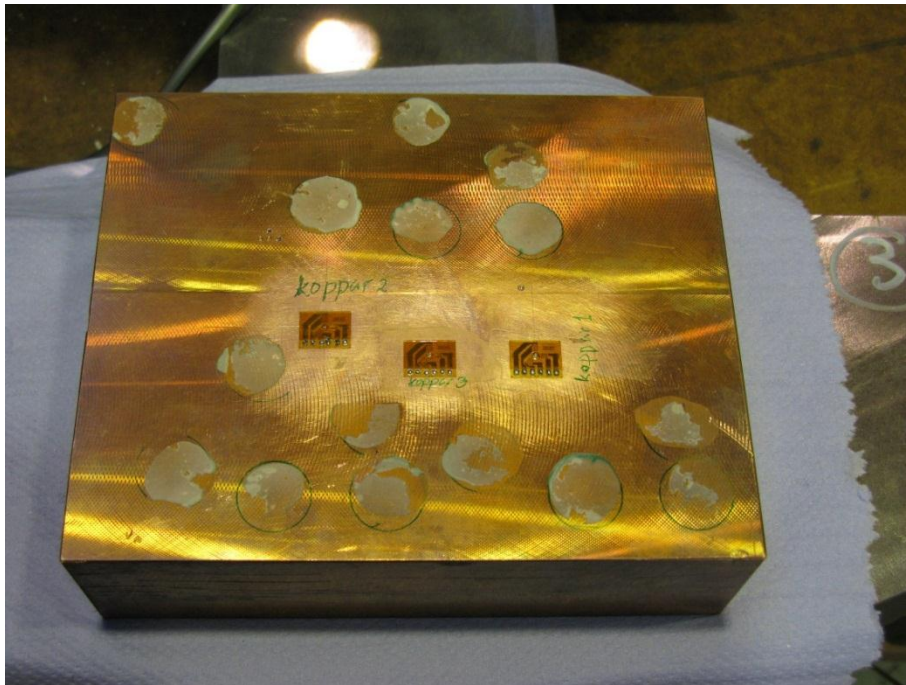


Figure A2:7 The copper sample.



Figure A2:8 The hole drilling rig cemented to the PWR sample at space 4. As the hole should be drilled close to the outer edge of the sample the third foot of the rig had to be placed on a metal block lying close to the sample. As the block must be immovable, it was clamped to the work bench.

Appendix 2

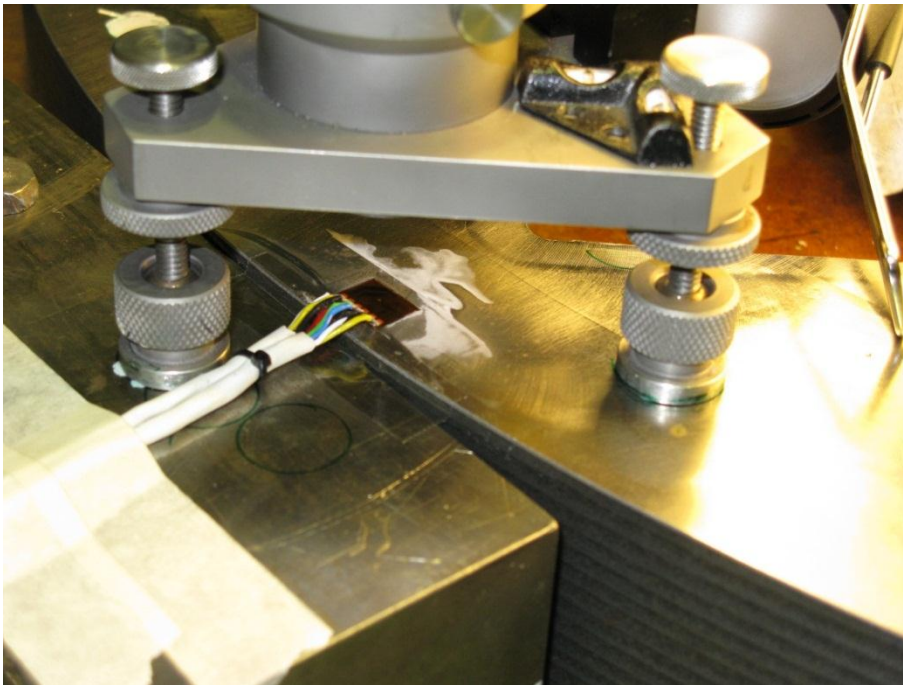


Figure A2:9 A second photograph showing the hole drilling rig cemented to the PWR sample.

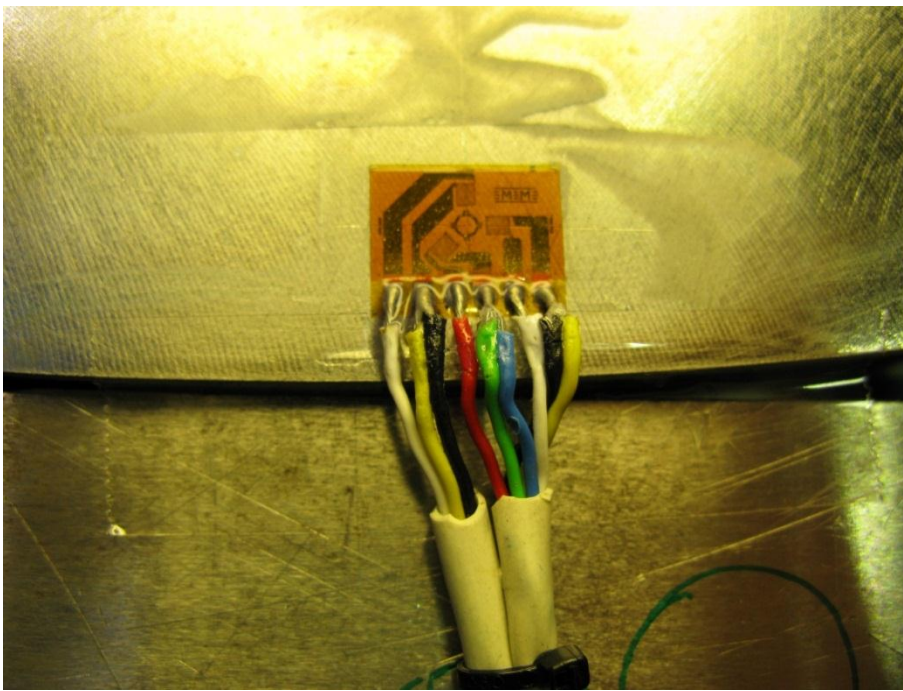


Figure A2:10 The 062UL strain gage bonded to the sample just before the drilling.

Appendix 2

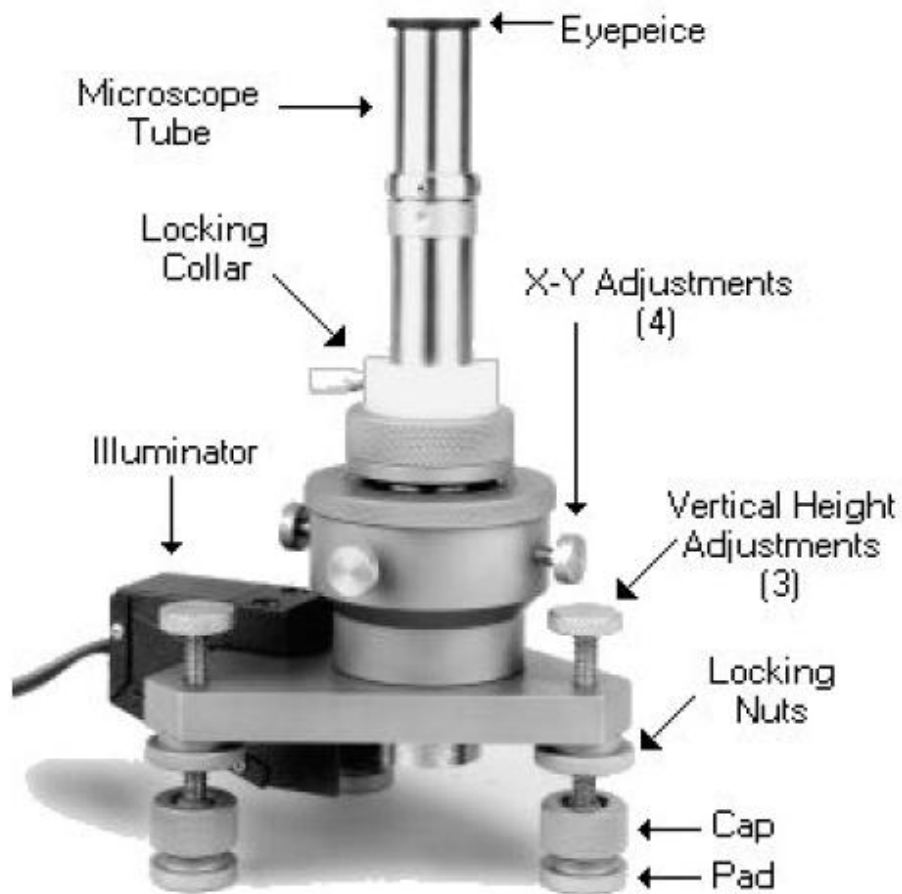


Figure A2:11 A picture of the milling guide supplied by the manufacture. A microscope is inserted in the milling guide so the guide can be the X-Y adjusting screws positioned over the centre of the gage.

Appendix 2

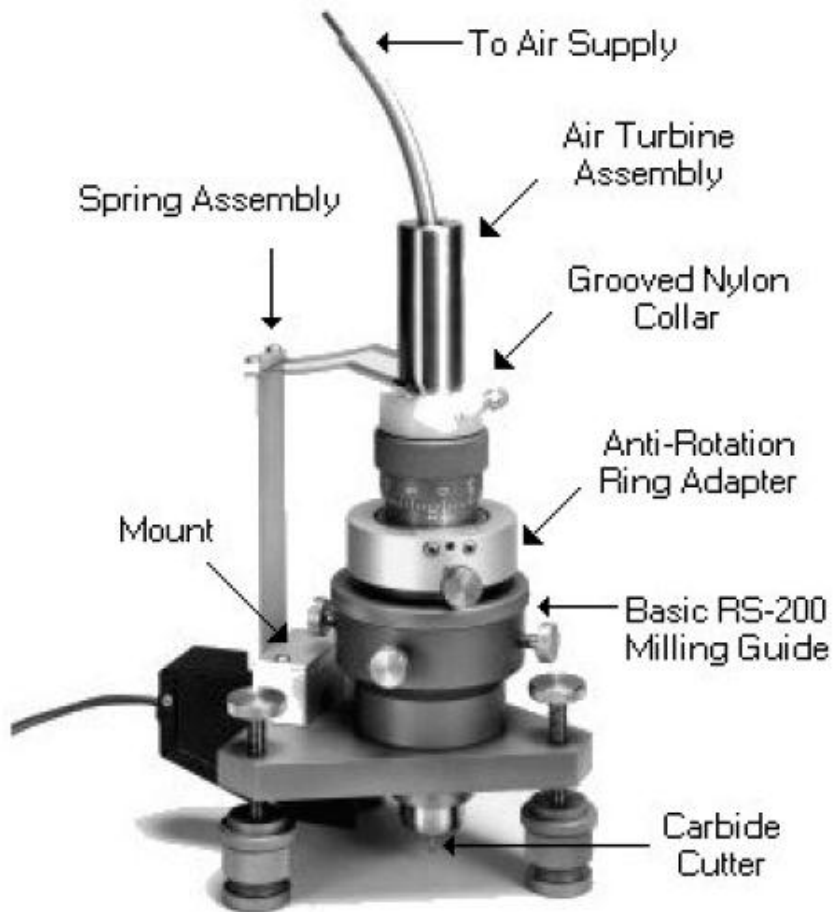


Figure A2:12 A picture of the milling guide supplied by the manufacture. A high speed air turbine is mounted in the guide.

Appendix 3

Raw data (measured strains)

This appendix contains raw data from the measurements. For each measuring point the data are listed in a table and plotted as a graph.

Table 1: Figures with raw data from the measurements on the BWR sample

Measuring point	Figure	Measuring point	Figure	Measuring point	Figure
R1	Fig: A3:1	R2	Fig: A3:2	---	---
11	Fig: A3:3	12	Fig: A3:4	13	Fig: A3:5
21	Fig: A3:6	22	Fig: A3:7	23	Fig: A3:8
31	Fig: A3:9	32	Fig: A3:10	33	Fig: A3:11
34T	Fig: A3:12	35T	Fig: A3:13	---	---
36TB	Fig: A3:14	37TB	Fig: A3:15	38TB	Fig: A3:16
41	Fig: A3:17	42	Fig: A3:18	43	Fig: A3:19
51	Fig: A3:20	52	Fig: A3:21	53	Fig: A3:22
61	Fig: A3:23	62	Fig: A3:24	63	Fig: A3:25

Table 2: Figures with raw data from the measurements on the PWR sample

Measuring point	Figure	Measuring point	Figure	Measuring point	Figure
R1	Fig: A3:26	R2	Fig: A3:27	R3	Fig: A3:28
C1	Fig: A3:29	C2	Fig: A3:30	C3	Fig: A3:31
C4	Fig: A3:32	C5	Fig: A3:33	---	---
11	Fig: A3:34	12	Fig: A3:35	13	Fig: A3:36
21	Fig: A3:37	22	Fig: A3:38	23	Fig: A3:39
24T	Fig: A3:40	25T	Fig: A3:41	---	---
26TB	Fig: A3:42	27TB	Fig: A3:43	28TB	Fig: A3:44
29TB	Fig: A3:45	---	---	---	---
31	Fig: A3:46	32	Fig: A3:47	33	Fig: A3:48
41	---	42	Fig: A3:49	43	Fig: A3:50

Table 3: Figures with raw data from the measurements on the Copper sample

Measuring point	Figure	Measuring point	Figure	Measuring point	Figure
2	Fig: A3:51	3	Fig: A3:52	5	Fig: A3:53

Appendix 3

Depth mm	Gage 1 $\mu\text{m/m}$	Gage 2 $\mu\text{m/m}$	Gage 3 $\mu\text{m/m}$
0.00	1	-1	0
0.13	11	21	23
0.25	5	31	33
0.38	-5	35	35
0.51	-13	37	34
0.64	-19	39	34
0.76	-23	42	33
0.89	-26	43	30
1.02	-26	44	27
1.14	-28	44	24
1.27	-28	45	23
1.40	-28	45	23
1.52	-27	45	23
1.65	-27	45	22
1.78	-27	45	21
1.91	-27	44	21

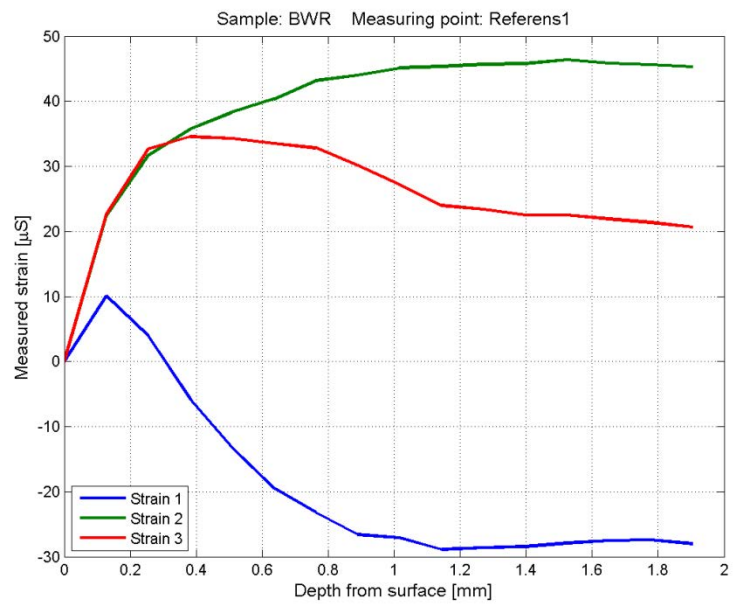


Figure A3:1 Raw data from measurement point R1 on the BWR sample

Depth mm	Gage 1 $\mu\text{m/m}$	Gage 2 $\mu\text{m/m}$	Gage 3 $\mu\text{m/m}$
0.00	0	-1	0
0.13	30	33	34
0.25	51	59	58
0.38	62	73	70
0.51	68	81	77
0.64	72	88	82
0.76	76	94	85
0.89	79	97	89
1.02	81	99	89
1.14	81	102	89
1.27	82	103	90
1.40	83	103	90
1.52	84	104	91
1.65	83	104	91
1.78	84	105	91
1.91	84	105	90

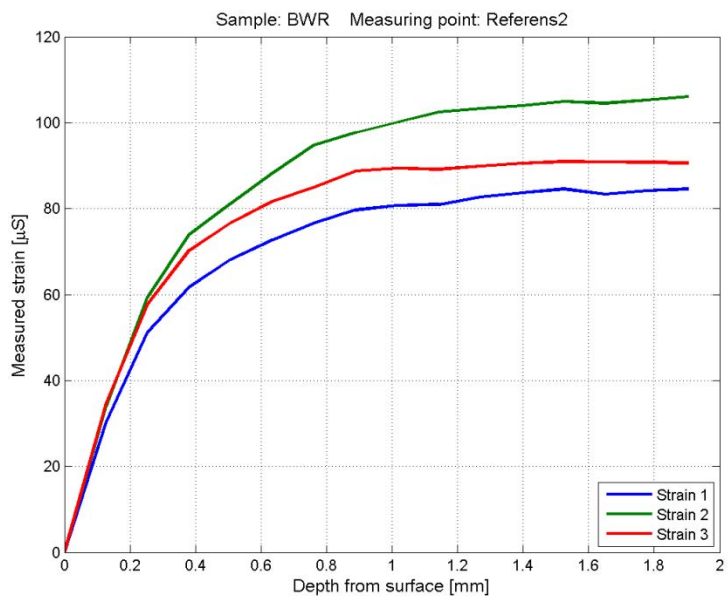


Figure A3:2 Raw data from measurement point R2 on the BWR sample

Appendix 3

Depth mm	Gage 1 $\mu\text{m}/\text{m}$	Gage 2 $\mu\text{m}/\text{m}$	Gage 3 $\mu\text{m}/\text{m}$
0.00	0	-1	0
0.13	22	28	28
0.25	37	39	35
0.38	46	42	37
0.51	51	44	38
0.64	56	47	40
0.76	57	48	42
0.89	59	51	45
1.02	58	51	47
1.14	57	51	49
1.27	56	53	51
1.40	55	52	53
1.52	55	53	54
1.65	55	54	55
1.78	54	54	56
1.91	53	54	56

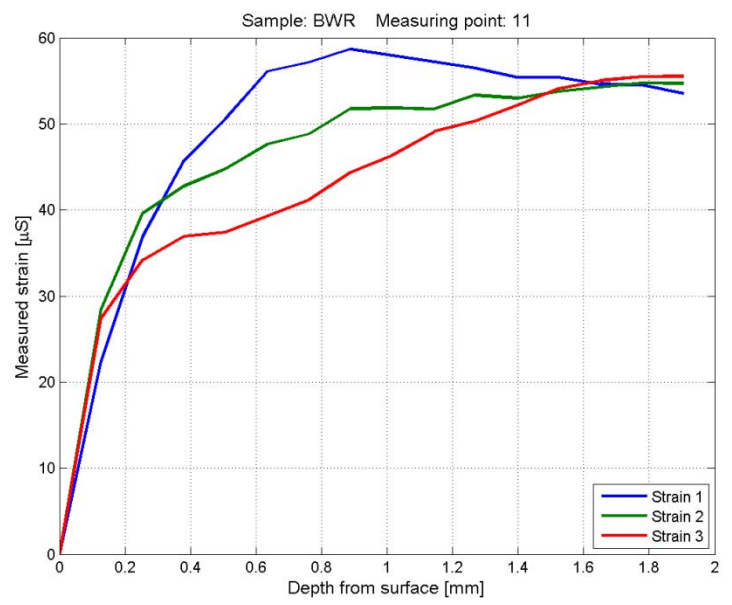


Figure A3:3 Raw data from measurement point 11 on the BWR sample

Depth mm	Gage 1 $\mu\text{m}/\text{m}$	Gage 2 $\mu\text{m}/\text{m}$	Gage 3 $\mu\text{m}/\text{m}$
0.00	0	-1	0
0.13	19	19	23
0.25	31	28	35
0.38	33	27	39
0.51	34	23	41
0.64	33	16	43
0.76	33	12	44
0.89	32	11	46
1.02	32	11	49
1.14	33	11	51
1.27	32	11	52
1.40	31	11	53
1.52	29	10	54
1.65	30	10	54
1.78	29	10	54
1.91	29	10	54

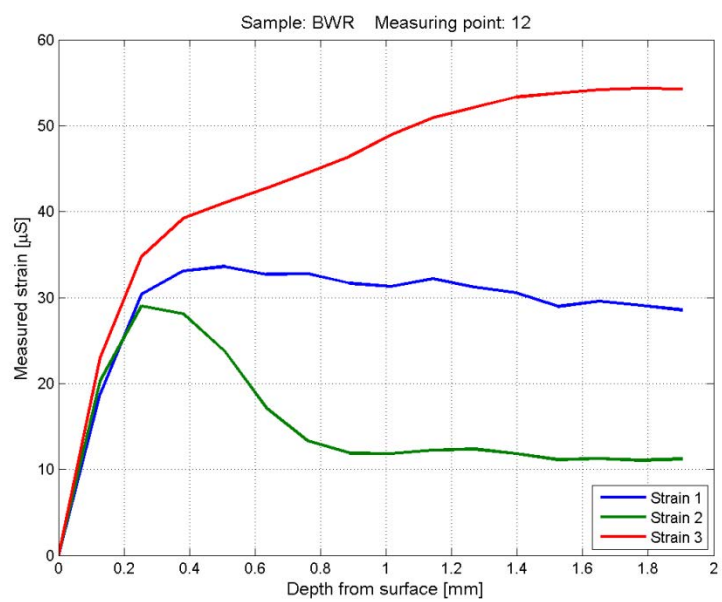


Figure A3:4 Raw data from measurement point 12 on the BWR sample

Appendix 3

Depth mm	Gage 1 $\mu\text{m}/\text{m}$	Gage 2 $\mu\text{m}/\text{m}$	Gage 3 $\mu\text{m}/\text{m}$
0.00	-1	-1	0
0.13	30	29	30
0.25	42	38	41
0.38	44	39	46
0.51	45	38	49
0.64	46	39	53
0.76	47	40	58
0.89	46	41	62
1.02	46	43	65
1.14	46	43	68
1.27	45	44	68
1.40	44	43	70
1.52	44	44	71
1.65	44	44	70
1.78	43	43	70
1.91	43	44	71

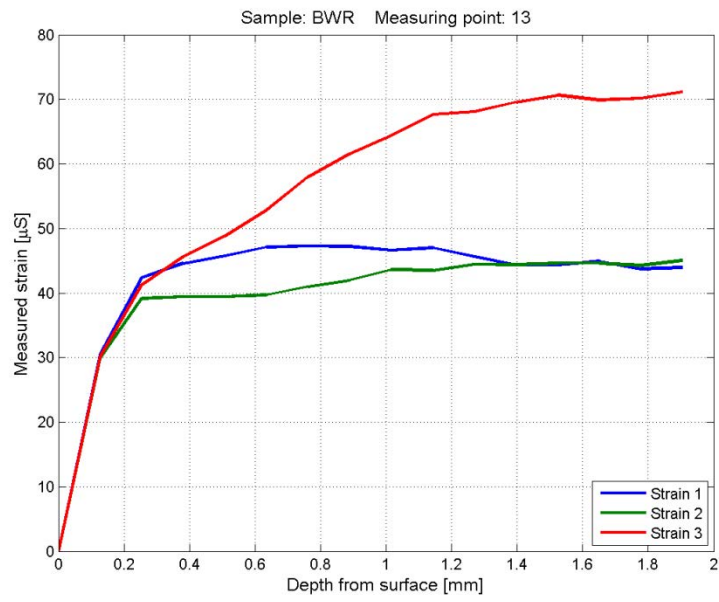


Figure A3:5 Raw data from measurement point 13 on the BWR sample

Depth mm	Gage 1 $\mu\text{m}/\text{m}$	Gage 2 $\mu\text{m}/\text{m}$	Gage 3 $\mu\text{m}/\text{m}$
0.00	1	-1	1
0.13	18	13	20
0.25	25	3	22
0.38	28	-7	20
0.51	26	-16	18
0.64	26	-27	16
0.76	26	-33	18
0.89	25	-37	19
1.02	25	-39	20
1.14	23	-41	22
1.27	23	-41	23
1.40	23	-42	23
1.52	22	-41	24
1.65	22	-42	25
1.78	21	-41	25
1.91	21	-41	26

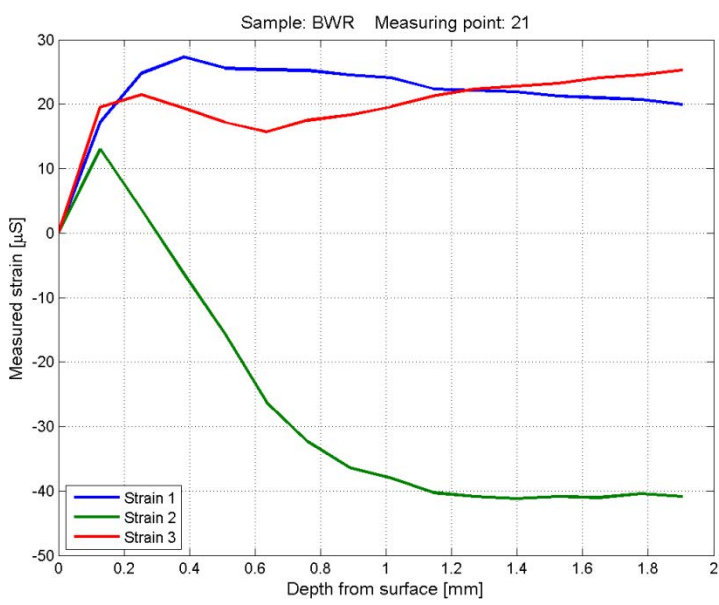


Figure A3:6 Raw data from measurement point 21 on the BWR sample

Appendix 3

Depth mm	Gage 1 $\mu\text{m}/\text{m}$	Gage 2 $\mu\text{m}/\text{m}$	Gage 3 $\mu\text{m}/\text{m}$
0.00	-1	-1	-1
0.13	5	6	25
0.25	-4	-2	36
0.38	-14	-12	41
0.51	-22	-19	44
0.64	-33	-26	46
0.76	-42	-31	48
0.89	-47	-34	51
1.02	-52	-35	52
1.14	-54	-36	52
1.27	-55	-37	51
1.40	-56	-37	52
1.52	-56	-37	52
1.65	-56	-36	52
1.78	-56	-36	52
1.91	-58	-37	52

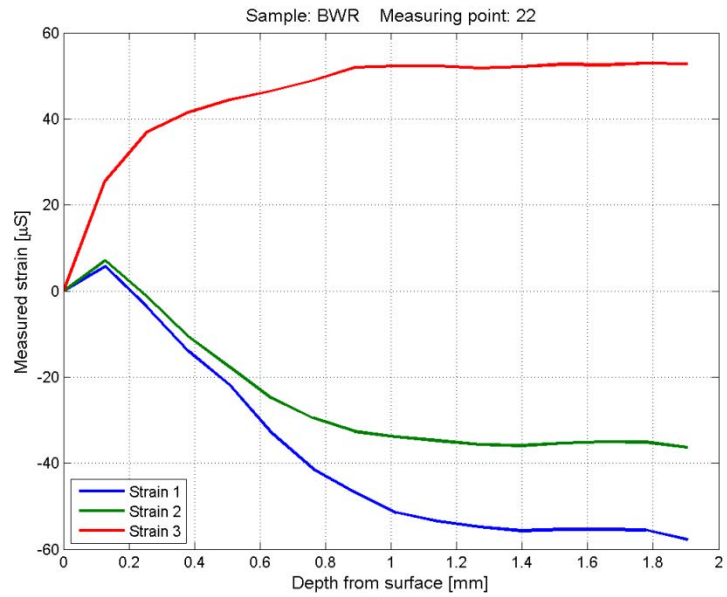


Figure A3:7 Raw data from measurement point 22 on the BWR sample

Depth mm	Gage 1 $\mu\text{m}/\text{m}$	Gage 2 $\mu\text{m}/\text{m}$	Gage 3 $\mu\text{m}/\text{m}$
0.00	0	-1	0
0.13	11	13	26
0.25	5	6	38
0.38	-2	-4	43
0.51	-10	-11	45
0.64	-16	-19	48
0.76	-22	-24	50
0.89	-24	-23	52
1.02	-23	-21	56
1.14	-24	-21	57
1.27	-26	-22	58
1.40	-26	-22	59
1.52	-27	-22	59
1.65	-27	-22	60
1.78	-28	-22	59
1.91	-28	-22	60

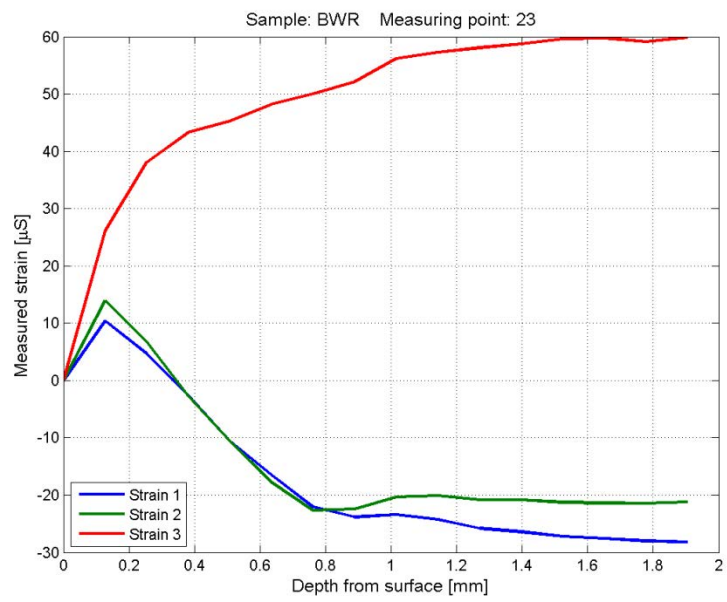


Figure A3:8 Raw data from measurement point 23 on the BWR sample

Appendix 3

Depth mm	Gage 1 $\mu\text{m}/\text{m}$	Gage 2 $\mu\text{m}/\text{m}$	Gage 3 $\mu\text{m}/\text{m}$
0.00	1	0	0
0.13	23	8	13
0.25	36	-3	3
0.38	38	-22	-12
0.51	39	-40	-25
0.64	39	-58	-37
0.76	41	-74	-47
0.89	41	-85	-55
1.02	41	-93	-60
1.14	41	-99	-65
1.27	39	-103	-67
1.40	39	-105	-67
1.52	39	-107	-67
1.65	39	-109	-68
1.78	38	-109	-68
1.91	36	-110	-67

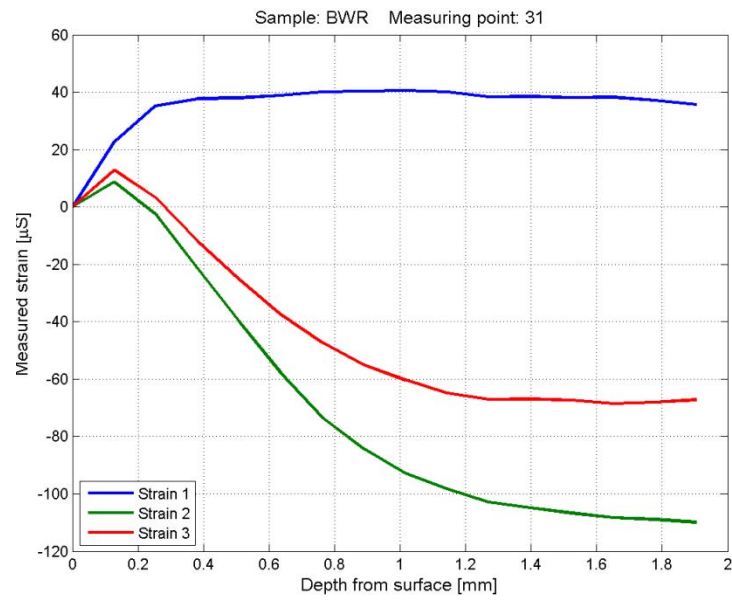


Figure A3:9 Raw data from measurement point 31 on the BWR sample

Depth mm	Gage 1 $\mu\text{m}/\text{m}$	Gage 2 $\mu\text{m}/\text{m}$	Gage 3 $\mu\text{m}/\text{m}$
0.00	0	-1	0
0.13	11	7	25
0.25	3	-12	26
0.38	-11	-38	16
0.51	-20	-56	10
0.64	-30	-76	5
0.76	-39	-92	-1
0.89	-49	-112	-7
1.02	-53	-121	-9
1.14	-56	-130	-12
1.27	-58	-133	-12
1.40	-59	-137	-12
1.52	-60	-139	-13
1.65	-60	-141	-14
1.78	-60	-141	-14
1.91	-60	-142	-14

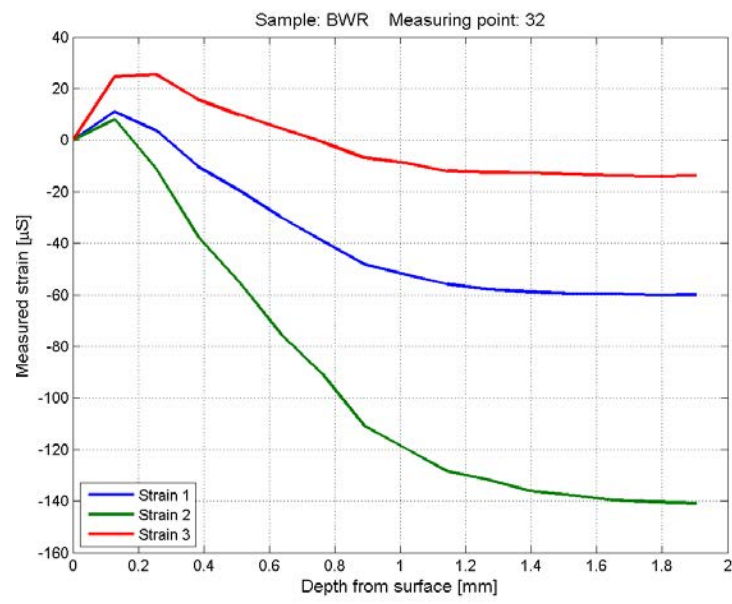


Figure A3:10 Raw data from measurement point 32 on the BWR sample

Appendix 3

Depth mm	Gage 1 $\mu\text{m/m}$	Gage 2 $\mu\text{m/m}$	Gage 3 $\mu\text{m/m}$
0.00	0	-1	0
0.13	7	11	24
0.25	-4	-5	29
0.38	-16	-27	28
0.51	-26	-44	26
0.64	-40	-63	22
0.76	-46	-76	23
0.89	-54	-85	23
1.02	-59	-90	22
1.14	-63	-93	21
1.27	-64	-95	21
1.40	-66	-97	21
1.52	-66	-97	21
1.65	-67	-97	21
1.78	-68	-98	21
1.91	-69	-98	21

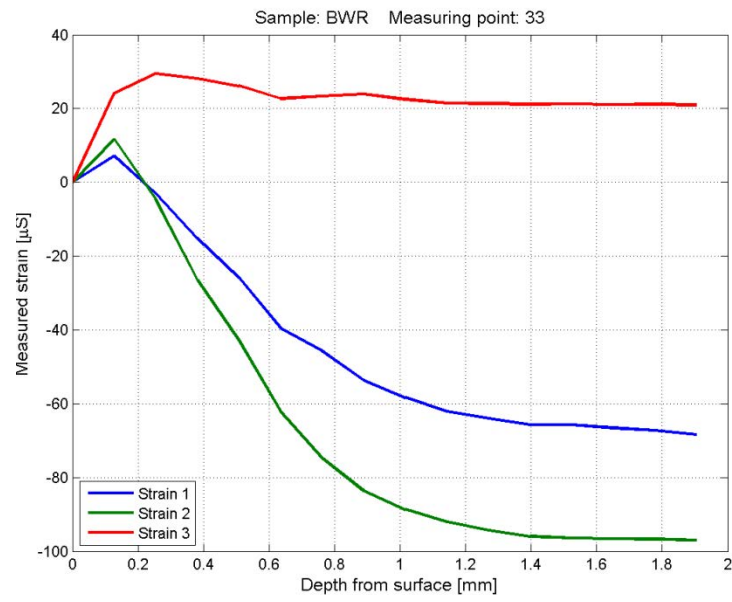


Figure A3:11 Raw data from measurement point 33 on the BWR sample

Depth mm	Gage 1 $\mu\text{m/m}$	Gage 2 $\mu\text{m/m}$	Gage 3 $\mu\text{m/m}$
0.00	0	0	-1
0.13	2	3	14
0.25	-12	-11	19
0.38	-27	-25	20
0.51	-36	-35	23
0.64	-46	-47	23
0.76	-55	-57	24
0.89	-60	-64	24
1.02	-62	-68	25
1.14	-64	-70	24
1.27	-66	-71	23
1.40	-67	-71	22
1.52	-68	-72	21
1.65	-68	-71	22
1.78	-68	-71	23
1.91	-70	-72	21

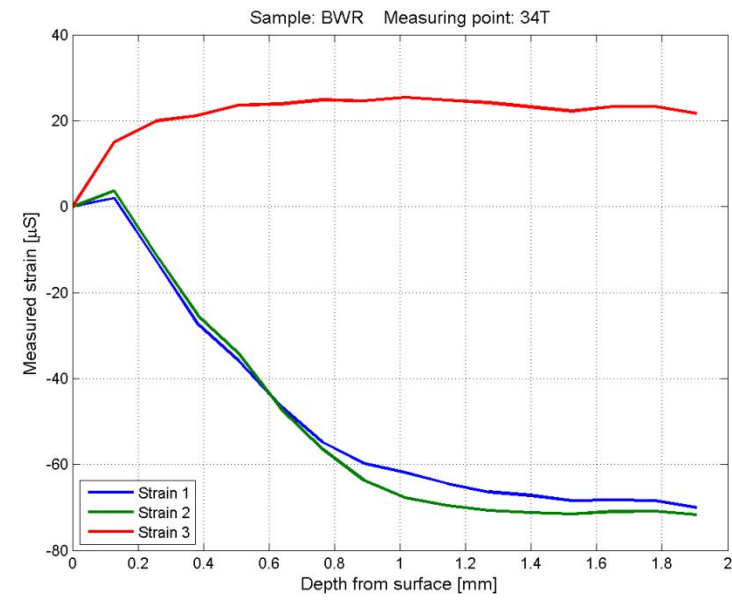


Figure A3:12 Raw data from measurement point 34T on the BWR sample

Appendix 3

Depth mm	Gage 1 $\mu\text{m}/\text{m}$	Gage 2 $\mu\text{m}/\text{m}$	Gage 3 $\mu\text{m}/\text{m}$
0.00	0	0	-1
0.13	8	14	15
0.25	-4	0	18
0.38	-17	-20	18
0.51	-31	-38	15
0.64	-44	-53	11
0.76	-56	-68	9
0.89	-65	-80	7
1.02	-68	-88	7
1.14	-73	-93	5
1.27	-75	-96	6
1.40	-77	-97	5
1.52	-78	-99	5
1.65	-79	-100	4
1.78	-78	-99	5
1.91	-79	-100	5

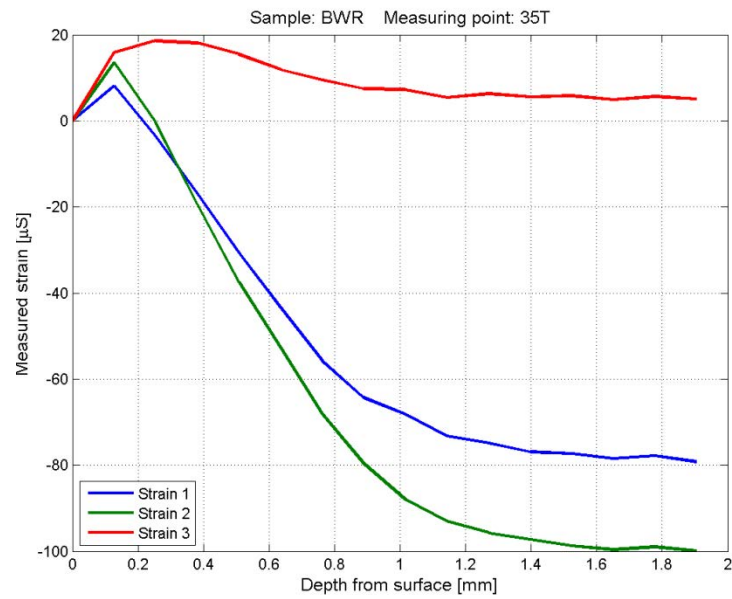


Figure A3:13 Raw data from measurement point 35T on the BWR sample

Depth mm	Gage 1 $\mu\text{m}/\text{m}$	Gage 2 $\mu\text{m}/\text{m}$	Gage 3 $\mu\text{m}/\text{m}$
0.00	0	1	0
0.13	13	13	15
0.25	20	19	22
0.38	24	22	26
0.51	26	24	29
0.64	28	26	32
0.76	30	27	34
0.89	30	26	34
1.02	32	26	36
1.14	33	25	38
1.27	32	25	38
1.40	32	25	39
1.52	32	25	39
1.65	33	25	38
1.78	33	25	39
1.91	31	24	38

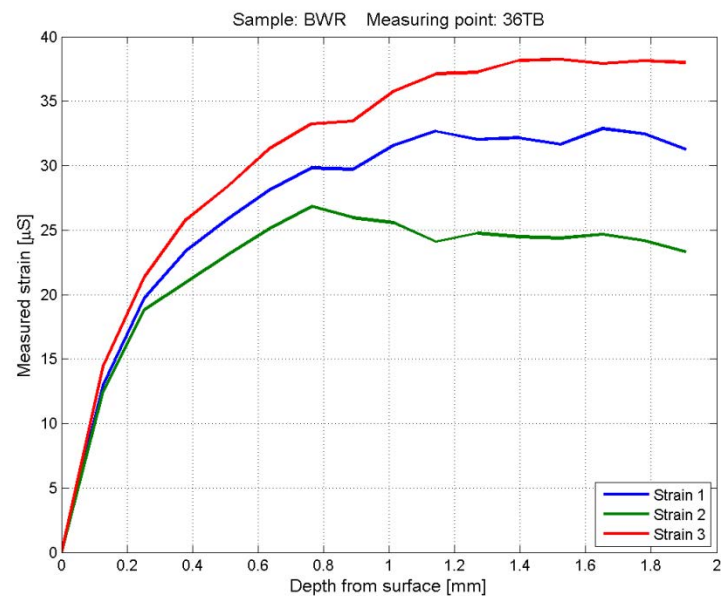


Figure A3:14 Raw data from measurement point 36TB on the BWR sample

Appendix 3

Depth mm	Gage 1 µm/m	Gage 2 µm/m	Gage 3 µm/m
0.00	0	0	0
0.13	13	15	13
0.25	20	21	18
0.38	24	23	23
0.51	24	23	25
0.64	26	24	26
0.76	27	23	27
0.89	29	25	30
1.02	29	24	30
1.14	30	23	32
1.27	30	23	32
1.40	30	22	32
1.52	31	22	33
1.65	30	22	33
1.78	30	21	33
1.91	29	21	33

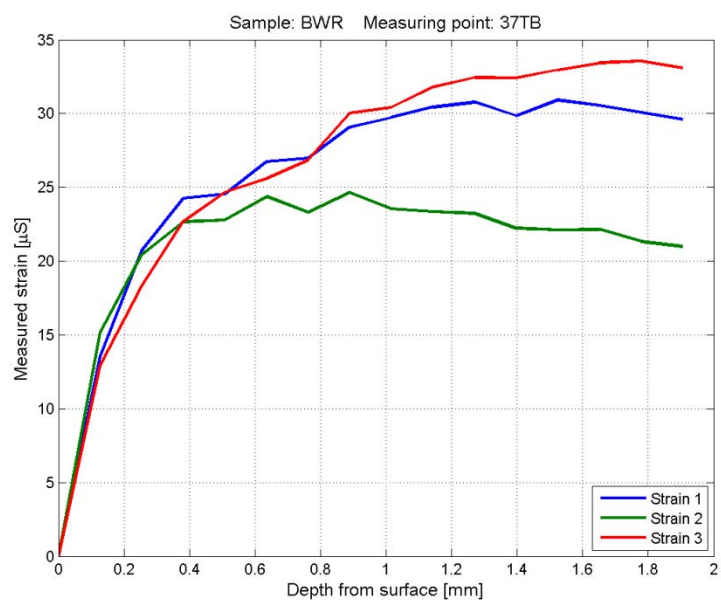


Figure A3:15 Raw data from measurement point 37TB on the BWR sample

Depth mm	Gage 1 µm/m	Gage 2 µm/m	Gage 3 µm/m
0.00	0	-1	-1
0.13	16	17	14
0.25	23	22	20
0.38	25	24	23
0.51	24	24	27
0.64	25	24	30
0.76	25	25	34
0.89	24	25	38
1.02	21	24	39
1.14	19	22	41
1.27	19	23	42
1.40	18	23	43
1.52	17	22	45
1.65	17	22	46
1.78	15	21	44
1.91	15	21	44

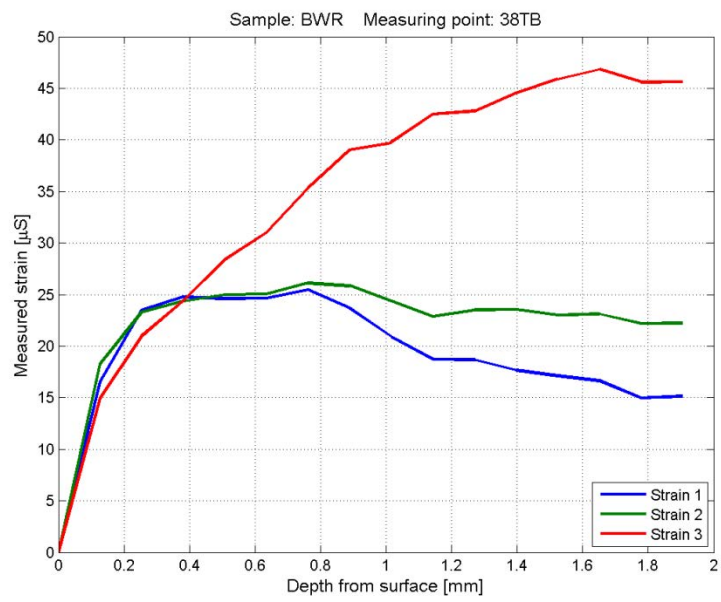


Figure A3:16 Raw data from measurement point 38TB on the BWR sample

Appendix 3

Depth mm	Gage 1 µm/m	Gage 2 µm/m	Gage 3 µm/m
0.00	0	1	1
0.13	26	28	25
0.25	49	40	27
0.38	61	38	13
0.51	70	36	1
0.64	74	32	-13
0.76	77	24	-28
0.89	81	17	-42
1.02	83	15	-50
1.14	85	13	-57
1.27	86	11	-61
1.40	87	11	-64
1.52	86	9	-64
1.65	86	10	-65
1.78	85	9	-65
1.91	84	9	-65

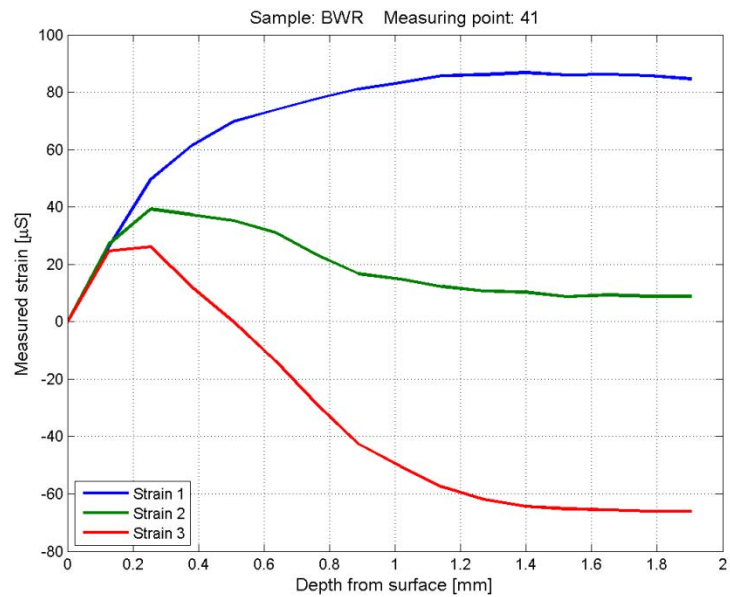


Figure A3:17 Raw data from measurement point 41 on the BWR sample

Depth mm	Gage 1 µm/m	Gage 2 µm/m	Gage 3 µm/m
0.00	0	-1	0
0.13	22	24	26
0.25	35	29	26
0.38	43	24	17
0.51	47	18	8
0.64	49	9	-2
0.76	52	2	-9
0.89	56	-3	-14
1.02	58	-7	-18
1.14	58	-11	-21
1.27	59	-14	-23
1.40	58	-16	-24
1.52	58	-18	-24
1.65	57	-19	-26
1.78	58	-20	-25
1.91	57	-21	-25

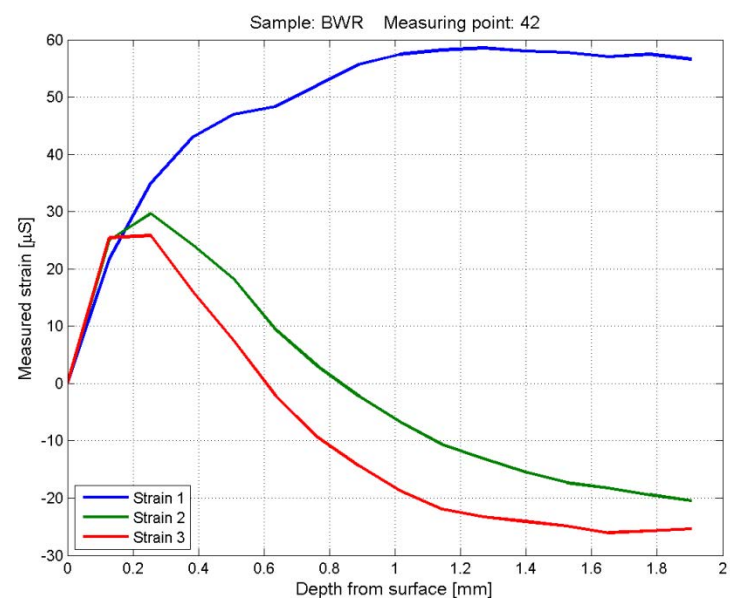


Figure A3:18 Raw data from measurement point 42 on the BWR sample

Appendix 3

0 mm	Gage 1 µm/m	Gage 2 µm/m	Gage 3 µm/m
0.00	-1	-1	0
0.13	21	22	26
0.25	35	30	36
0.38	41	27	35
0.51	46	24	32
0.64	47	21	28
0.76	49	17	23
0.89	50	14	19
1.02	50	13	17
1.14	50	13	17
1.27	49	12	14
1.40	49	11	13
1.52	49	11	13
1.65	48	11	12
1.78	48	11	12
1.91	47	11	12

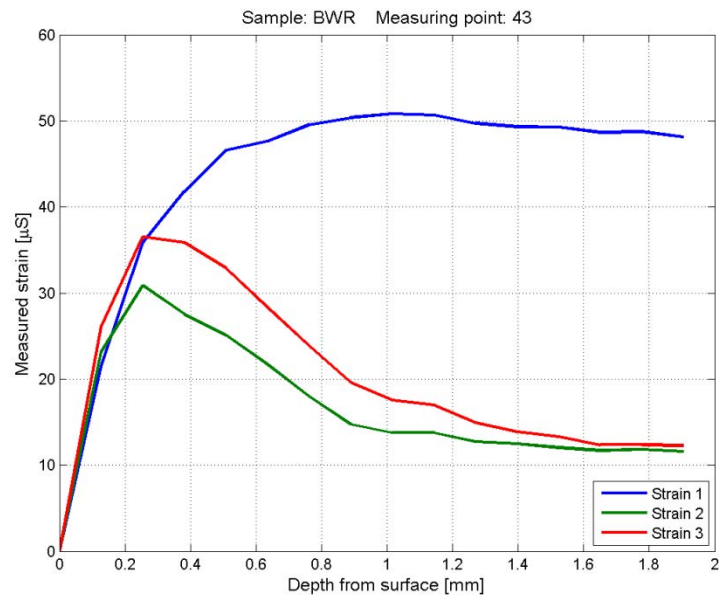


Figure A3:19 Raw data from measurement point 43 on the BWR sample

Depth mm	Gage 1 µm/m	Gage 2 µm/m	Gage 3 µm/m
0.00	0	-1	1
0.13	32	31	36
0.25	46	45	60
0.38	49	50	70
0.51	50	54	76
0.64	52	58	83
0.76	52	62	92
0.89	51	67	97
1.02	51	69	100
1.14	50	72	102
1.27	48	73	102
1.40	47	74	103
1.52	46	75	104
1.65	46	75	105
1.78	45	76	105
1.91	45	76	106

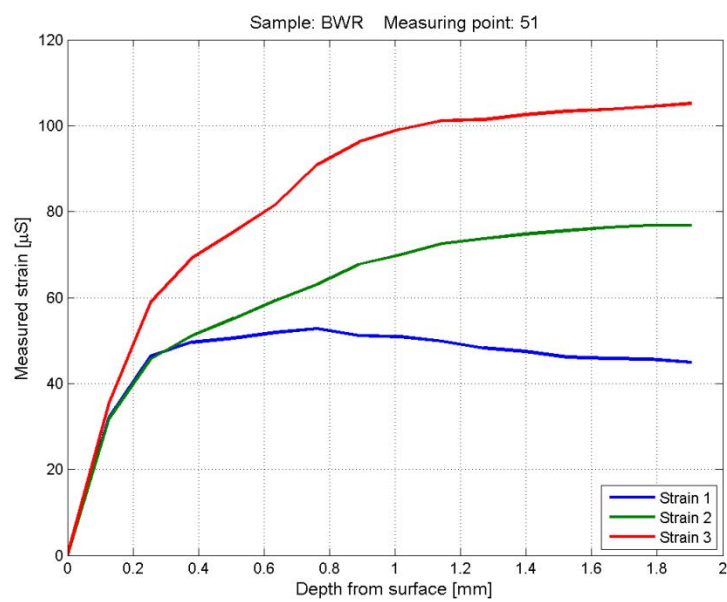


Figure A3:20 Raw data from measurement point 51 on the BWR sample

Appendix 3

Depth mm	Gage 1 $\mu\text{m}/\text{m}$	Gage 2 $\mu\text{m}/\text{m}$	Gage 3 $\mu\text{m}/\text{m}$
0.00	-1	-1	-1
0.13	22	26	34
0.25	26	32	57
0.38	25	36	69
0.51	24	40	78
0.64	23	43	84
0.76	23	47	88
0.89	23	51	94
1.02	24	55	97
1.14	24	58	100
1.27	24	60	102
1.40	24	62	103
1.52	24	63	104
1.65	24	64	104
1.78	24	64	105
1.91	23	64	105

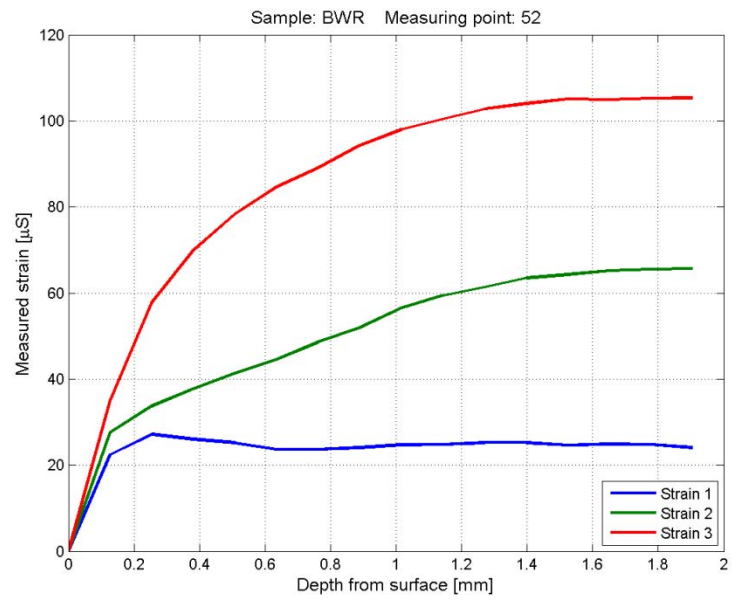


Figure A3:21 Raw data from measurement point 52 on the BWR sample

Depth mm	Gage 1 $\mu\text{m}/\text{m}$	Gage 2 $\mu\text{m}/\text{m}$	Gage 3 $\mu\text{m}/\text{m}$
0.00	-1	-1	0
0.13	19	25	22
0.25	26	36	40
0.38	26	42	49
0.51	27	47	55
0.64	28	52	60
0.76	28	58	64
0.89	30	65	69
1.02	31	70	72
1.14	31	73	75
1.27	31	74	75
1.40	30	75	77
1.52	31	76	77
1.65	31	77	77
1.78	30	76	77
1.91	29	76	77

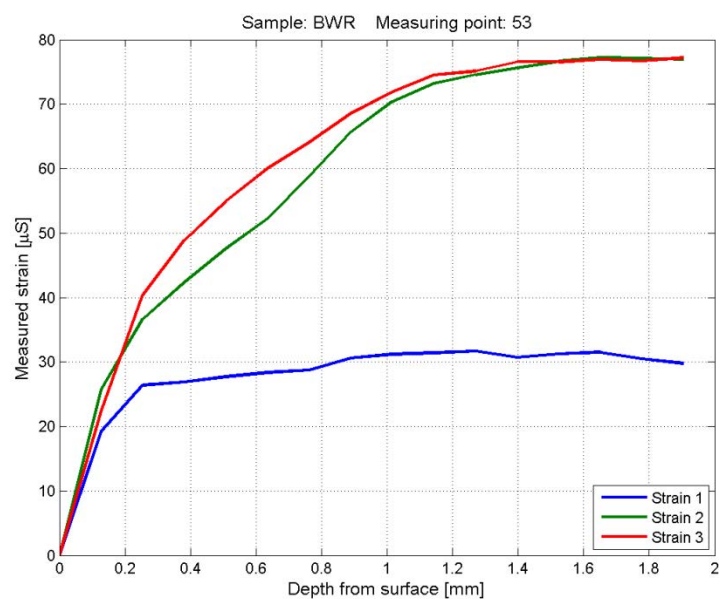


Figure A3:22 Raw data from measurement point 53 on the BWR sample

Appendix 3

Depth mm	Gage 1 $\mu\text{m}/\text{m}$	Gage 2 $\mu\text{m}/\text{m}$	Gage 3 $\mu\text{m}/\text{m}$
0.00	0	0	0
0.13	24	16	31
0.25	41	11	44
0.38	48	0	50
0.51	49	-8	55
0.64	50	-14	63
0.76	48	-23	72
0.89	44	-28	81
1.02	43	-33	88
1.14	40	-36	94
1.27	39	-39	98
1.40	37	-41	101
1.52	37	-42	104
1.65	36	-43	105
1.78	34	-44	107
1.91	33	-46	107

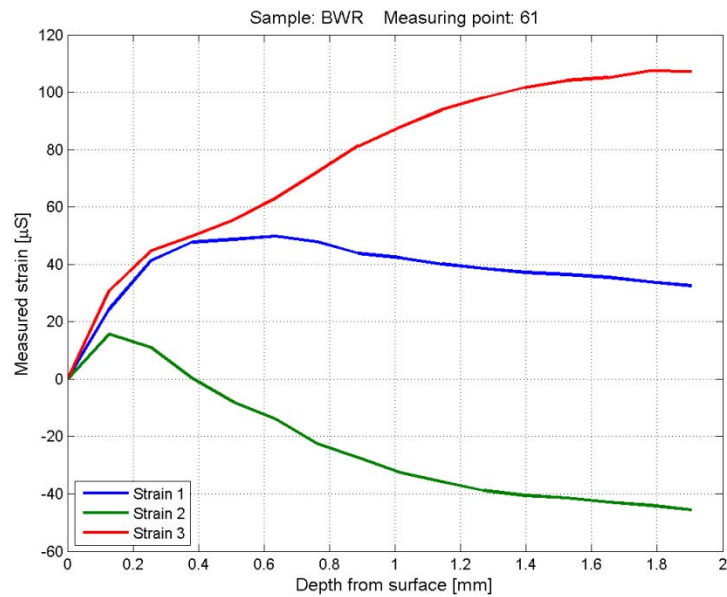


Figure A3:23 Raw data from measurement point 61 on the BWR sample

Depth mm	Gage 1 $\mu\text{m}/\text{m}$	Gage 2 $\mu\text{m}/\text{m}$	Gage 3 $\mu\text{m}/\text{m}$
0.00	0	-1	0
0.13	21	20	31
0.25	18	15	48
0.38	10	7	58
0.51	2	1	65
0.64	-6	-5	70
0.76	-11	-10	78
0.89	-17	-14	84
1.02	-24	-18	89
1.14	-27	-21	93
1.27	-30	-22	96
1.40	-33	-24	97
1.52	-34	-25	98
1.65	-35	-26	100
1.78	-36	-26	100
1.91	-37	-27	100

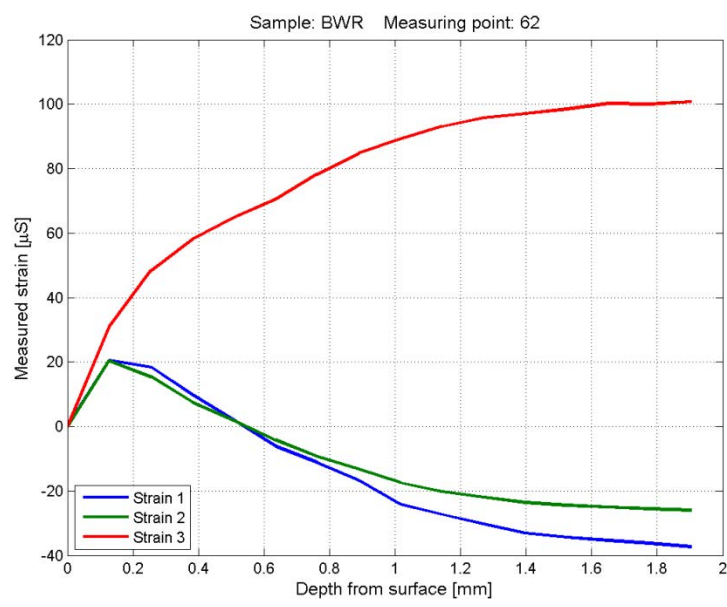


Figure A3:24 Raw data from measurement point 62 on the BWR sample

Appendix 3

Depth mm	Gage 1 $\mu\text{m}/\text{m}$	Gage 2 $\mu\text{m}/\text{m}$	Gage 3 $\mu\text{m}/\text{m}$
0.00	0	0	0
0.13	11	16	27
0.25	3	13	43
0.38	-7	6	50
0.51	-16	1	55
0.64	-25	-4	60
0.76	-30	-6	66
0.89	-35	-7	71
1.02	-40	-8	75
1.14	-43	-8	78
1.27	-46	-9	80
1.40	-47	-10	81
1.52	-48	-10	81
1.65	-50	-10	81
1.78	-50	-10	81
1.91	-51	-11	81

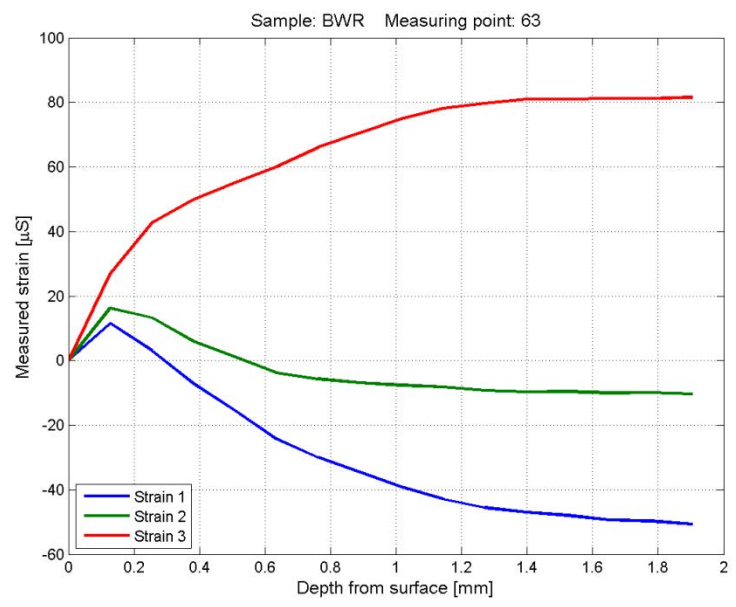


Figure A3:25 Raw data from measurement point 63 on the BWR sample

Depth mm	Gage 1 $\mu\text{m}/\text{m}$	Gage 2 $\mu\text{m}/\text{m}$	Gage 3 $\mu\text{m}/\text{m}$
0.00	-1	-2	-1
0.13	17	21	18
0.25	-14	9	12
0.38	-58	-29	-3
0.51	-104	-47	-13
0.64	-95	-35	-5
0.76	-95	-27	-3
0.89	-98	-25	0
1.02	-99	-23	2
1.14	-104	-23	1
1.27	-105	-25	0
1.40	-105	-22	2
1.52	-103	-19	1
1.65	-102	-18	-2
1.78	-103	-19	-2
1.91	-103	-19	-1

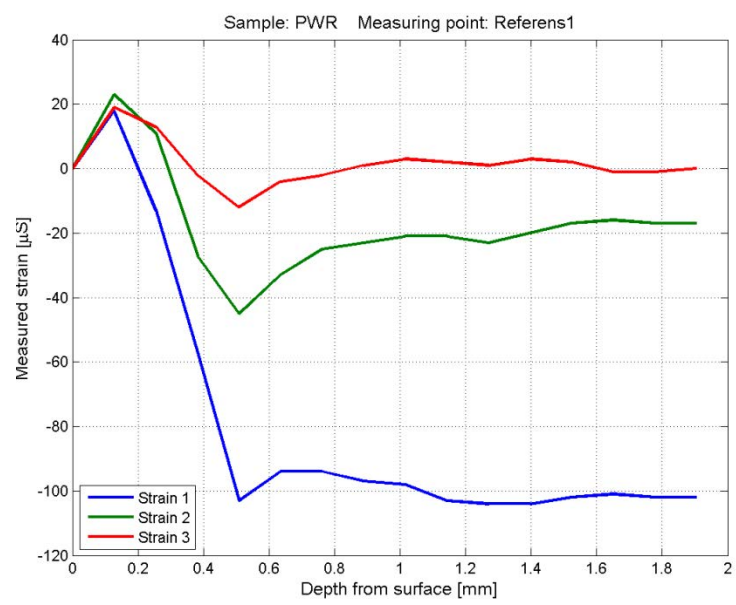


Figure A3:26 Raw data from measurement point RI on the PWR sample

Appendix 3

Depth mm	Gage 1 $\mu\text{m}/\text{m}$	Gage 2 $\mu\text{m}/\text{m}$	Gage 3 $\mu\text{m}/\text{m}$
0.00	0	-1	0
0.13	26	22	24
0.25	39	27	31
0.38	45	24	32
0.51	82	51	38
0.64	87	50	33
0.76	92	51	31
0.89	96	52	30
1.02	98	54	29
1.14	101	54	29
1.27	103	55	27
1.40	104	55	24
1.52	104	54	24
1.65	104	54	25
1.78	105	54	22
1.91	105	54	23

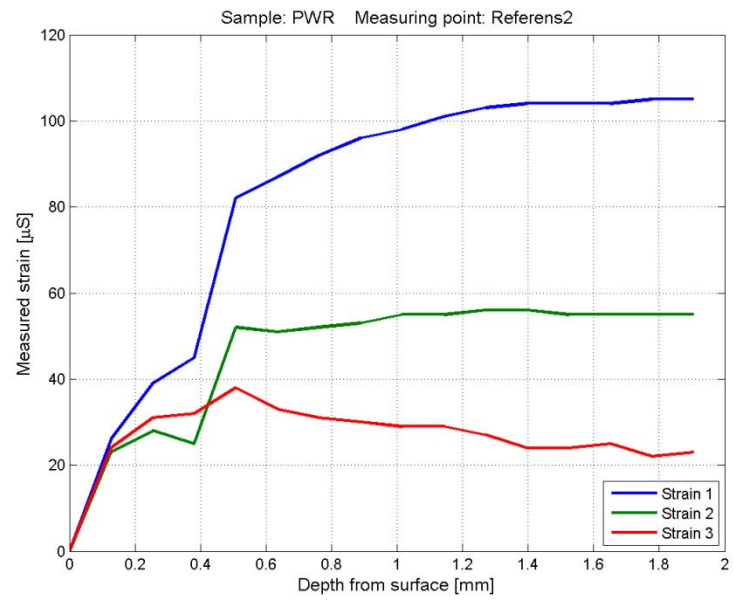


Figure A3:27 Raw data from measurement point $R2$ on the PWR sample

Depth mm	Gage 1 $\mu\text{m}/\text{m}$	Gage 2 $\mu\text{m}/\text{m}$	Gage 3 $\mu\text{m}/\text{m}$
0.00	0	0	0
0.13	24	25	18
0.25	37	37	22
0.38	46	41	19
0.51	6	15	-49
0.64	11	20	-46
0.76	28	34	-43
0.89	41	40	-43
1.02	48	42	-44
1.14	53	46	-45
1.27	55	47	-47
1.40	58	49	-50
1.52	61	51	-52
1.65	60	51	-55
1.78	59	50	-57
1.91			

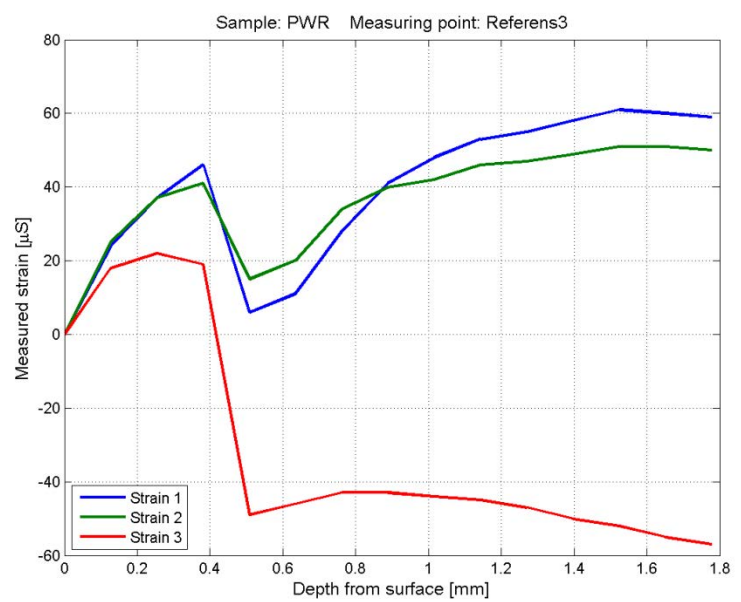


Figure A3:28 Raw data from measurement point $R3$ on the PWR sample

Appendix 3

Depth mm	Gage 1 $\mu\text{m}/\text{m}$	Gage 2 $\mu\text{m}/\text{m}$	Gage 3 $\mu\text{m}/\text{m}$
0.00	0	-1	0
0.13	22	6	21
0.25	42	12	47
0.38	54	11	69
0.51	54	2	85
0.64	42	-1	92
0.76	37	1	92
0.89	24	0	86
1.02	19	1	86
1.14	11	3	86
1.27	9	3	86
1.40	8	3	84
1.52	2	3	82

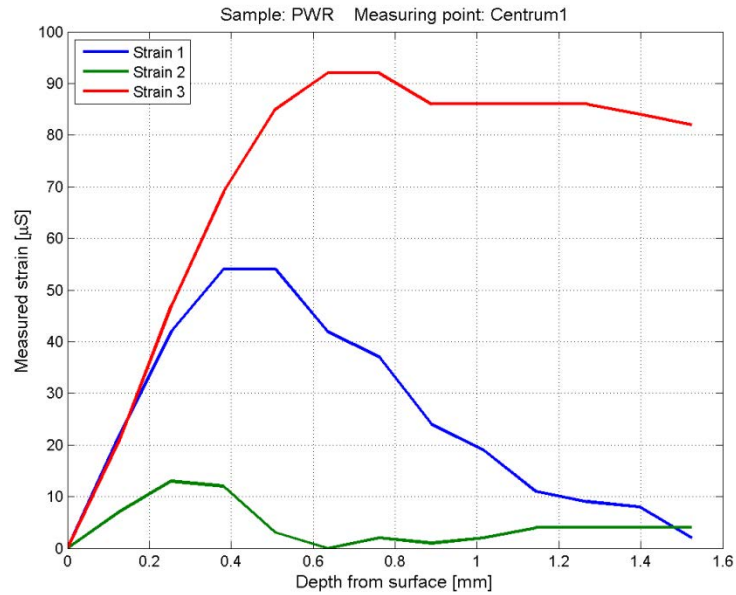


Figure A3:29 Raw data from measurement point C1 on the PWR sample

Depth mm	Gage 1 $\mu\text{m}/\text{m}$	Gage 2 $\mu\text{m}/\text{m}$	Gage 3 $\mu\text{m}/\text{m}$
0.00	0	-1	0
0.13	52	30	36
0.25	105	43	54
0.38	146	46	66
0.51	174	41	70
0.64	190	31	66
0.76	199	22	58
0.89	202	14	47
1.02	201	8	39
1.14	202	4	34
1.27	198	4	29
1.40	198	1	25
1.52	195	1	24
1.65	193	3	25
1.78	192	5	24
1.91	191	6	24

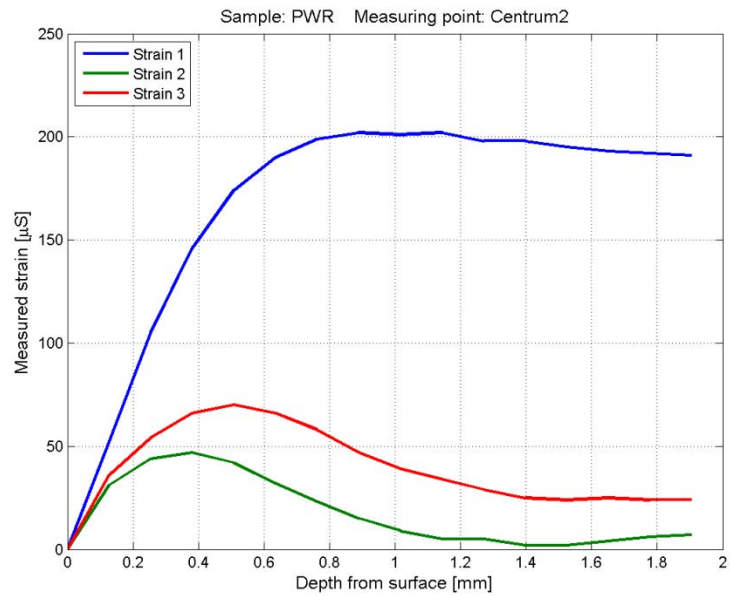


Figure A3:30 Raw data from measurement point C2 on the PWR sample

Appendix 3

Depth mm	Gage 1 μm/m	Gage 2 μm/m	Gage 3 μm/m
0.00	0	-1	0
0.13	14	8	25
0.25	15	5	44
0.38	11	-4	61
0.51	2	-14	73
0.64	-7	-25	77
0.76	-17	-36	81
0.89	-23	-44	86
1.02	-28	-49	90
1.14	-32	-53	92
1.27	-36	-55	95
1.40	-37	-58	97
1.52	-40	-58	98
1.65	-40	-58	99
1.78	-40	-58	100
1.91	-40	-58	102

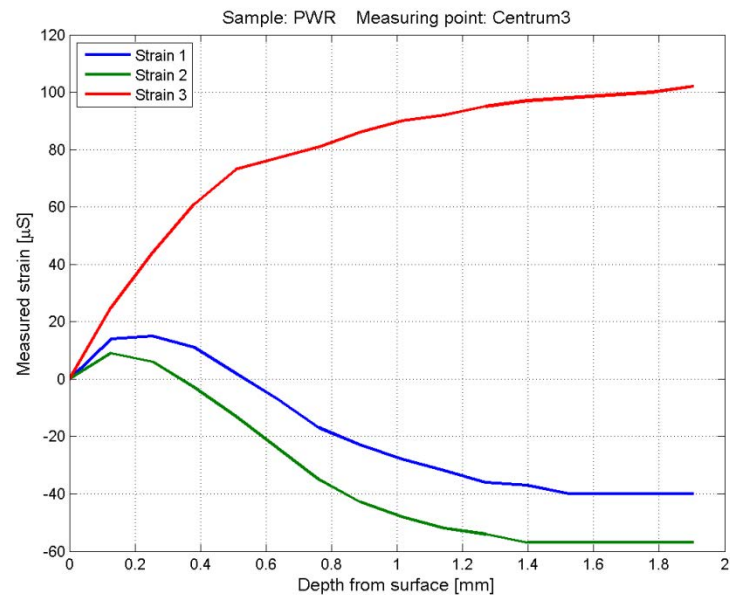


Figure A3:31 Raw data from measurement point C3 on the PWR sample

Depth mm	Gage 1 μm/m	Gage 2 μm/m	Gage 3 μm/m
0.00	-1	-1	0
0.13	27	23	33
0.25	52	45	66
0.38	68	59	97
0.51	77	68	122
0.64	86	73	142
0.76	89	75	151
0.89	88	73	160
1.02	87	72	165
1.14	83	70	167
1.27	81	69	170
1.40	81	71	172
1.52	80	71	173
1.65	80	72	175
1.78	80	72	176
1.91	79	72	177

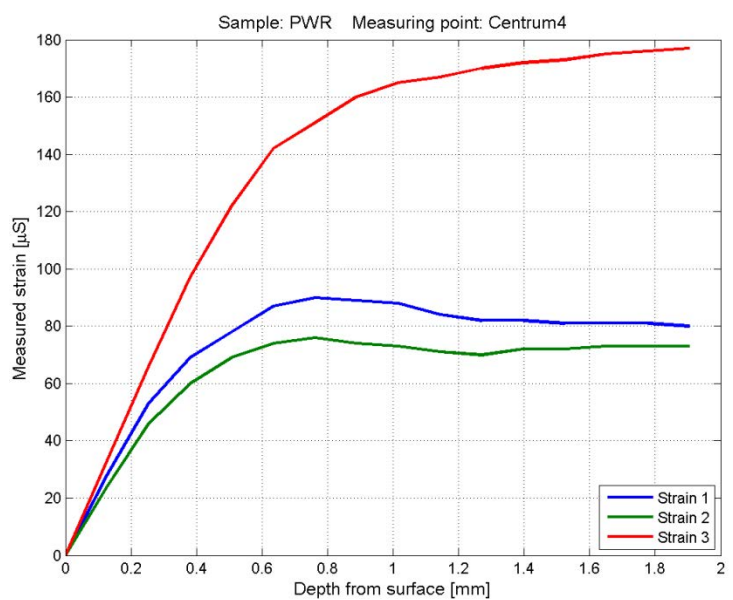


Figure A3:32 Raw data from measurement point C4 on the PWR sample

Appendix 3

Depth mm	Gage 1 $\mu\text{m}/\text{m}$	Gage 2 $\mu\text{m}/\text{m}$	Gage 3 $\mu\text{m}/\text{m}$
0.00	-1	-1	0
0.13	23	22	43
0.25	33	40	87
0.38	31	52	116
0.51	25	62	145
0.64	14	69	162
0.76	1	74	176
0.89	-10	76	188
1.02	-15	80	196
1.14	-20	81	203
1.27	-23	84	207
1.40	-24	84	209
1.52	-25	85	210
1.65	-27	85	215
1.78	-27	86	215
1.91	-27	87	216

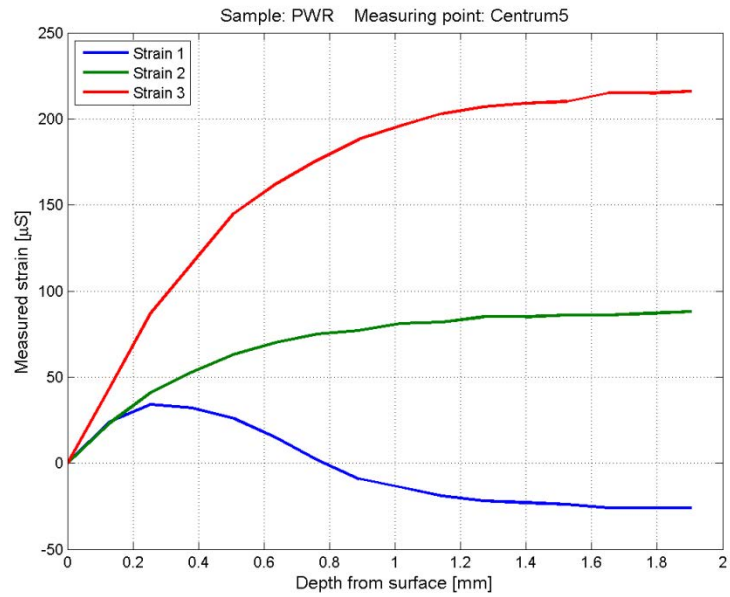


Figure A3:33 Raw data from measurement point C5 on the PWR sample

Depth mm	Gage 1 $\mu\text{m}/\text{m}$	Gage 2 $\mu\text{m}/\text{m}$	Gage 3 $\mu\text{m}/\text{m}$
0.00	-1	-1	0
0.13	25	24	28
0.25	37	33	41
0.38	42	35	51
0.51	45	35	58
0.64	44	36	67
0.76	42	38	80
0.89	40	40	91
1.02	35	40	103
1.14	30	40	113
1.27	27	41	120
1.40	23	42	124
1.52	20	42	127
1.65	19	41	131
1.78	16	41	133
1.91	13	40	134

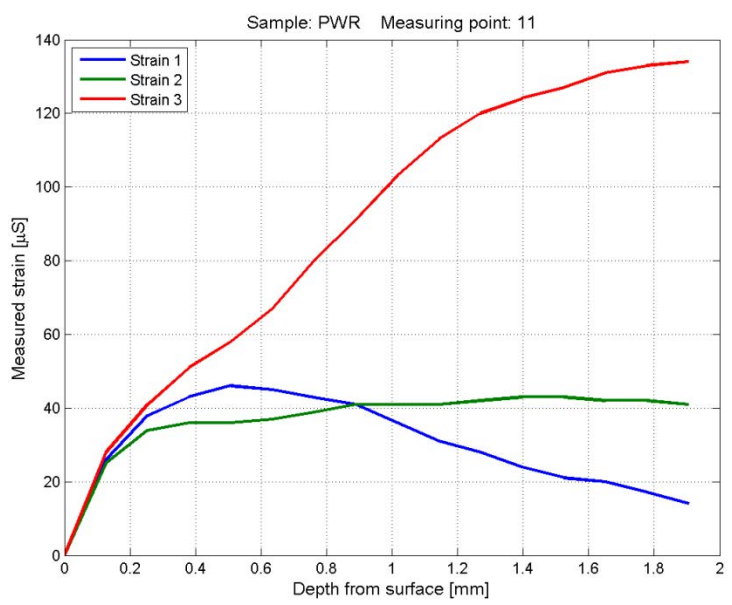


Figure A3:34 Raw data from measurement point 11 on the PWR sample

Appendix 3

Depth mm	Gage 1 μm/m	Gage 2 μm/m	Gage 3 μm/m
0.00	0	-1	0
0.13	28	32	27
0.25	39	47	43
0.38	45	55	56
0.51	47	60	66
0.64	49	67	82
0.76	48	71	96
0.89	44	72	108
1.02	43	76	119
1.14	41	78	126
1.27	38	78	129
1.40	35	78	132
1.52	34	78	134
1.65	30	77	135
1.78	29	76	137
1.91	29	75	139

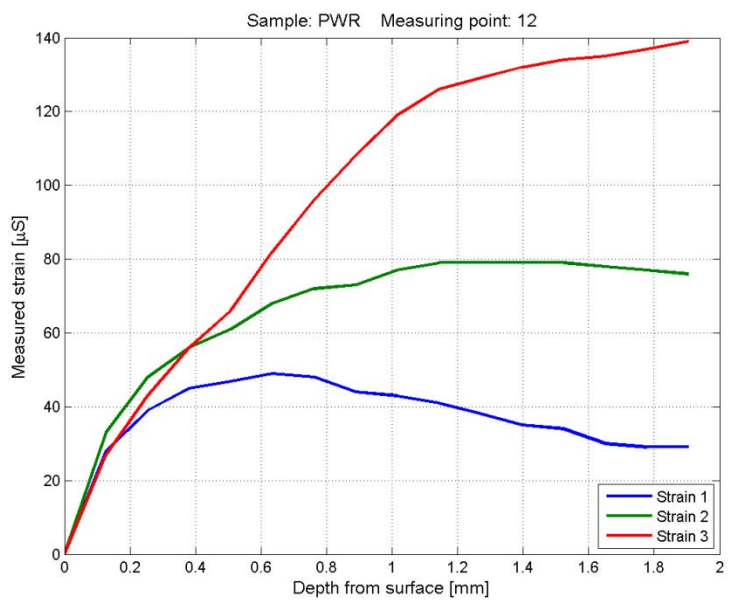


Figure A3:35 Raw data from measurement point 12 on the PWR sample

Depth mm	Gage 1 μm/m	Gage 2 μm/m	Gage 3 μm/m
0.00	0	-1	0
0.13	28	26	33
0.25	36	32	45
0.38	40	38	54
0.51	41	41	59
0.64	46	46	71
0.76	46	52	82
0.89	42	54	89
1.02	34	57	92
1.14	40	58	101
1.27	40	59	102
1.40	38	58	105
1.52	35	60	106
1.65	34	59	106
1.78	34	57	107
1.91	33	54	107

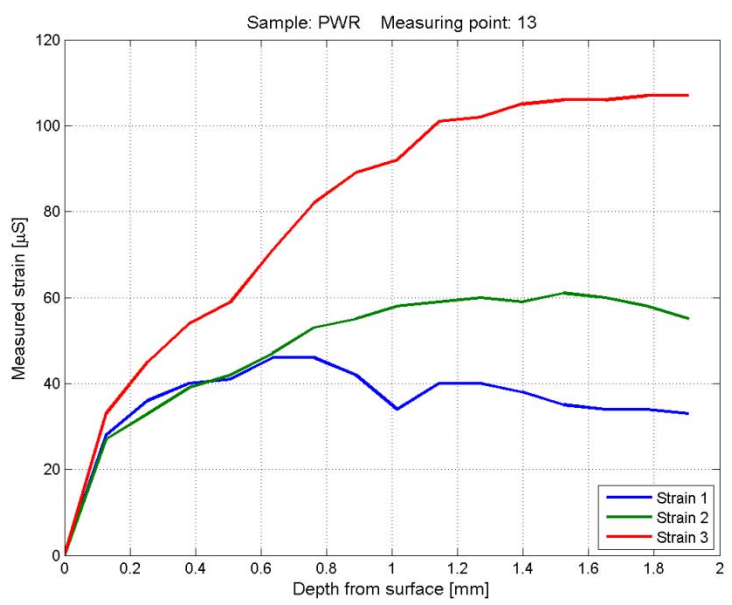


Figure A3:36 Raw data from measurement point 13 on the PWR sample

Appendix 3

Depth mm	Gage 1 $\mu\text{m}/\text{m}$	Gage 2 $\mu\text{m}/\text{m}$	Gage 3 $\mu\text{m}/\text{m}$
0.00	0	-1	0
0.13	23	14	19
0.25	37	15	25
0.38	36	4	17
0.51	41	-3	13
0.64	39	-15	12
0.76	43	-21	13
0.89	43	-29	14
1.02	44	-35	16
1.14	44	-40	20
1.27	43	-39	24
1.40	42	-41	26
1.52	40	-42	26
1.65	39	-43	28
1.78	38	-44	28
1.91	37	-44	29

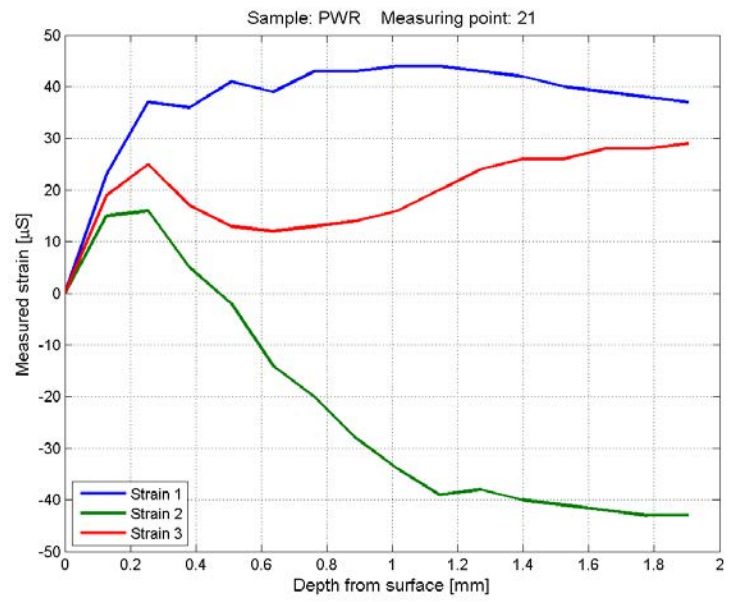


Figure A3:37 Raw data from measurement point 21 on the PWR sample

Depth mm	Gage 1 $\mu\text{m}/\text{m}$	Gage 2 $\mu\text{m}/\text{m}$	Gage 3 $\mu\text{m}/\text{m}$
0.00	0	0	0
0.13	21	21	23
0.25	26	20	29
0.38	31	17	33
0.51	35	15	38
0.64	32	7	42
0.76	34	3	49
0.89	33	1	55
1.02	32	-1	61
1.14	30	-4	65
1.27	28	-7	68
1.40	28	-8	71
1.52	26	-9	72
1.65	24	-11	73
1.78	23	-11	73
1.91	20	-13	72

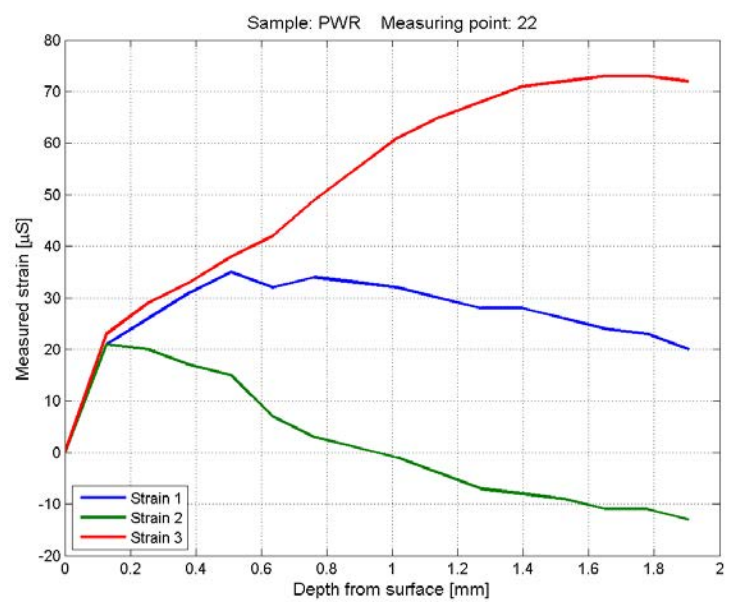


Figure A3:38 Raw data from measurement point 22 on the PWR sample

Appendix 3

Depth mm	Gage 1 μm/m	Gage 2 μm/m	Gage 3 μm/m
0.00	0	-1	-1
0.13	19	15	25
0.25	28	17	36
0.38	32	15	40
0.51	32	12	41
0.64	34	11	47
0.76	33	7	52
0.89	33	5	56
1.02	31	3	60
1.14	30	1	63
1.27	28	-1	67
1.40	27	-2	68
1.52	26	-4	68
1.65	25	-4	68
1.78	24	-5	68
1.91	24	-6	68

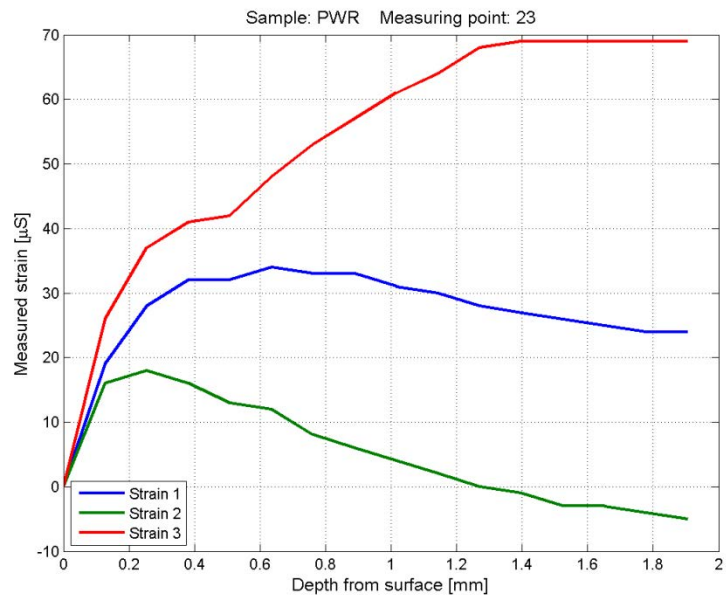


Figure A3:39 Raw data from measurement point 23 on the PWR sample

Depth mm	Gage 1 μm/m	Gage 2 μm/m	Gage 3 μm/m
0.00	0	0	0
0.13	18	12	15
0.25	24	14	23
0.38	26	14	30
0.51	26	14	36
0.64	26	15	42
0.76	25	17	49
0.89	24	19	56
1.02	23	22	63
1.14	22	25	69
1.27	21	26	74
1.40	19	27	76
1.52	17	27	78
1.65	16	27	79
1.78	15	27	80
1.91	13	26	80

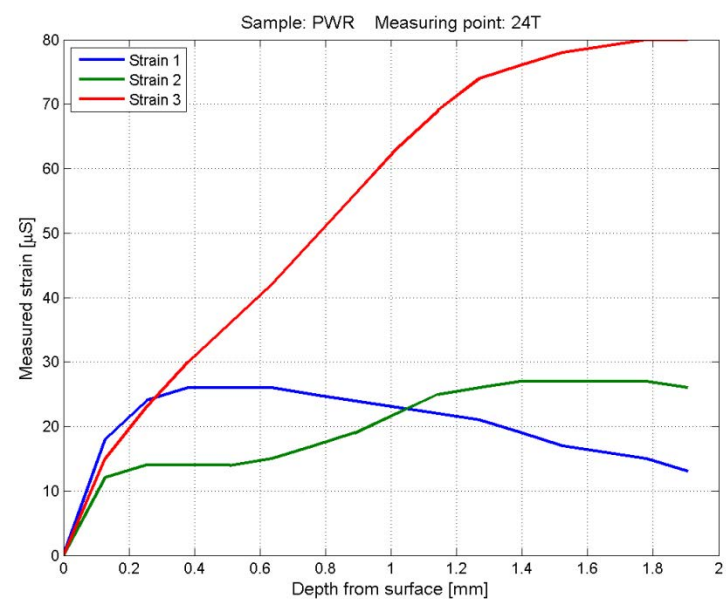


Figure A3:40 Raw data from measurement point 24T on the PWR sample

Appendix 3

Depth mm	Gage 1 $\mu\text{m}/\text{m}$	Gage 2 $\mu\text{m}/\text{m}$	Gage 3 $\mu\text{m}/\text{m}$
0.00	-1	-1	0
0.13	15	9	8
0.25	22	6	9
0.38	28	3	8
0.51	29	-1	5
0.64	33	-2	4
0.76	39	-3	8
0.89	41	-5	9
1.02	41	-6	11
1.14	39	-8	12
1.27	39	-9	14
1.40	37	-10	16
1.52	36	-11	16
1.65	33	-13	16
1.78	33	-13	18
1.91	31	-14	17

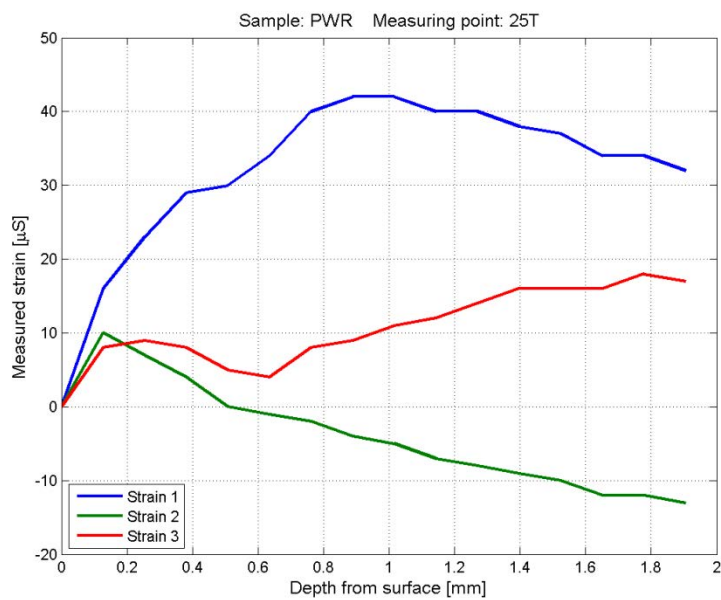


Figure A3:41 Raw data from measurement point 25T on the PWR sample

Depth mm	Gage 1 $\mu\text{m}/\text{m}$	Gage 2 $\mu\text{m}/\text{m}$	Gage 3 $\mu\text{m}/\text{m}$
0.00	0	0	0
0.13	10	18	19
0.25	3	27	37
0.38	-5	30	53
0.51	-16	28	62
0.64	-21	30	75
0.76	-26	31	87
0.89	-31	33	97
1.02	-35	36	103
1.14	-39	38	109
1.27	-40	40	114
1.40	-44	41	117
1.52	-46	40	118
1.65	-46	41	120
1.78	-46	41	121
1.91	-48	40	121

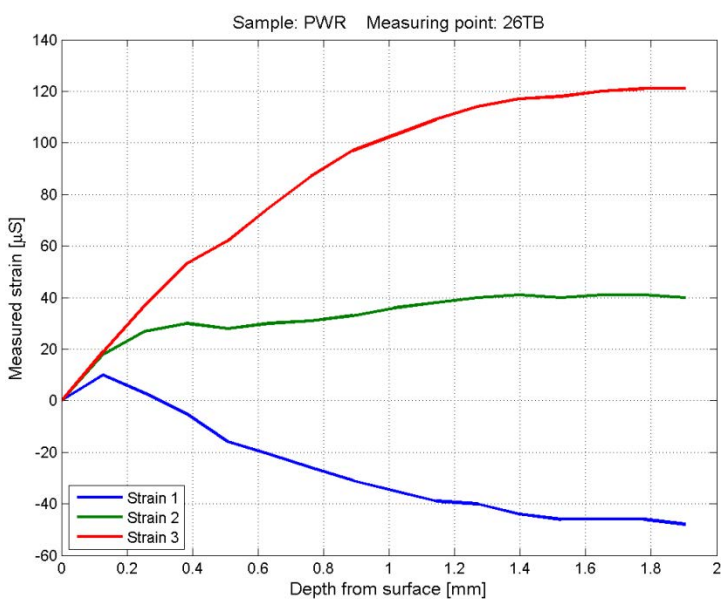


Figure A3:42 Raw data from measurement point 26TB on the PWR sample

Appendix 3

Depth mm	Gage 1 $\mu\text{m}/\text{m}$	Gage 2 $\mu\text{m}/\text{m}$	Gage 3 $\mu\text{m}/\text{m}$
0.00	0	0	0
0.13	11	11	19
0.25	6	2	34
0.38	-4	-11	46
0.51	-13	-24	54
0.64	-24	-37	64
0.76	-34	-46	74
0.89	-41	-53	85
1.02	-46	-55	96
1.14	-50	-57	104
1.27	-52	-57	109
1.40	-57	-56	113
1.52	-59	-56	116
1.65	-61	-56	118
1.78	-63	-56	121
1.91	-64	-55	121

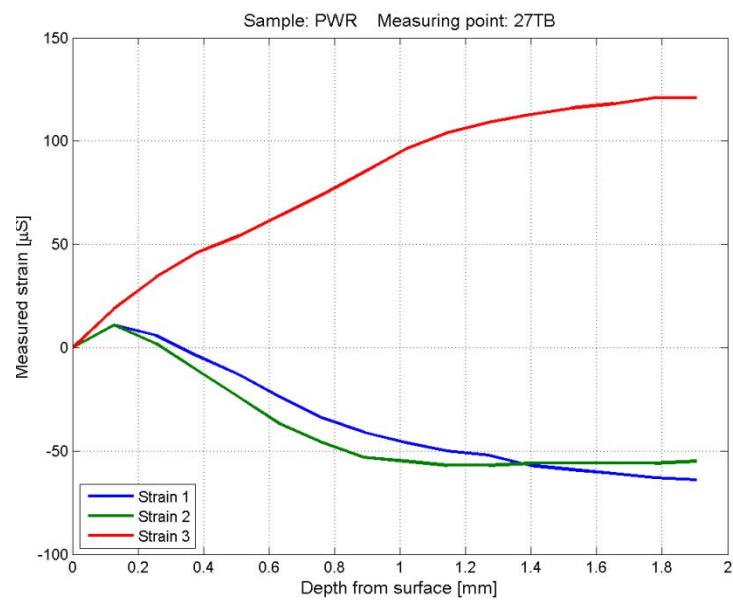


Figure A3:43 Raw data from measurement point 27TB on the PWR sample

Depth mm	Gage 1 $\mu\text{m}/\text{m}$	Gage 2 $\mu\text{m}/\text{m}$	Gage 3 $\mu\text{m}/\text{m}$
0.00	1	0	-1
0.13	15	13	18
0.25	25	8	31
0.38	30	-6	39
0.51	33	-20	43
0.64	35	-38	46
0.76	34	-55	53
0.89	33	-70	60
1.02	30	-82	69
1.14	27	-89	75

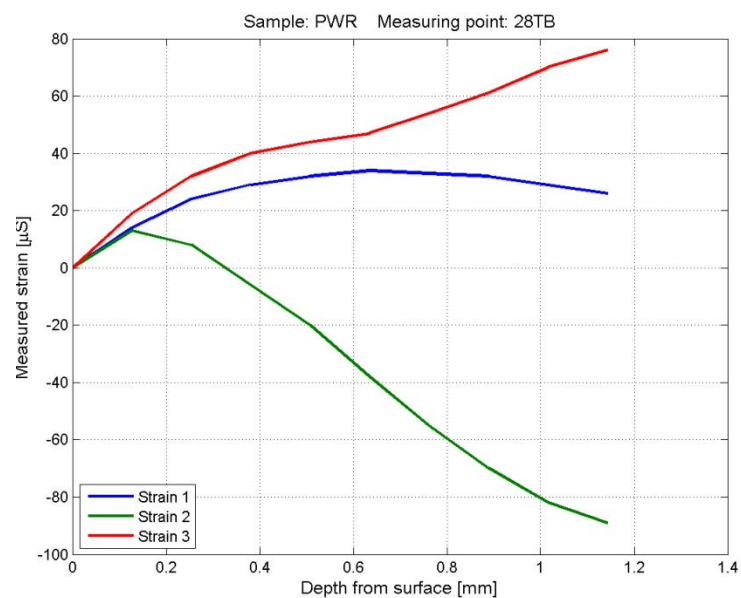


Figure A3:44 Raw data from measurement point 28TB on the PWR sample

Appendix 3

Depth mm	Gage 1 $\mu\text{m}/\text{m}$	Gage 2 $\mu\text{m}/\text{m}$	Gage 3 $\mu\text{m}/\text{m}$
0.00	1	0	0
0.13	16	15	18
0.25	17	10	35
0.38	13	-6	44
0.51	10	-21	51
0.64	7	-35	58
0.76	-3	-51	65
0.89	-4	-58	73
1.02	-11	-66	82
1.14	-15	-69	90
1.27	-19	-71	94
1.40	-22	-72	100
1.52	-25	-74	104
1.65	-27	-74	107
1.78	-29	-76	108
1.91	-32	-78	108

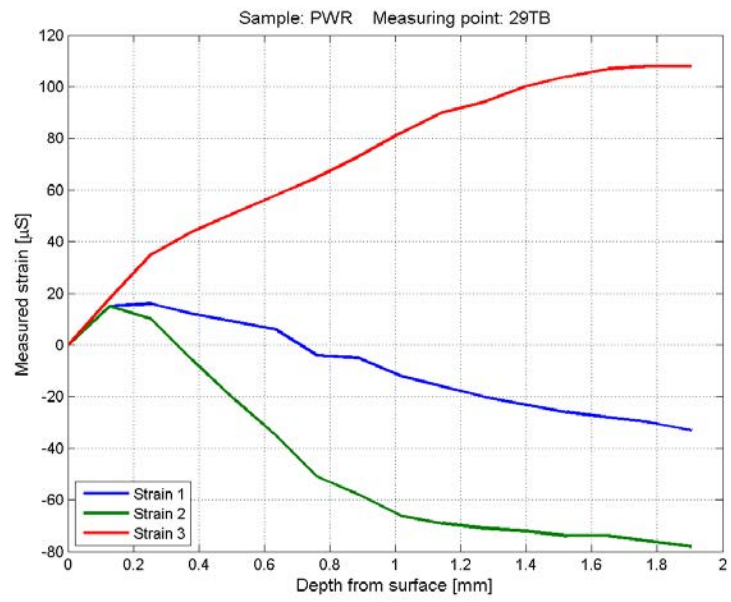


Figure A3:45 Raw data from measurement point 29TB on the PWR sample

Depth mm	Gage 1 $\mu\text{m}/\text{m}$	Gage 2 $\mu\text{m}/\text{m}$	Gage 3 $\mu\text{m}/\text{m}$
0.00	0	-1	0
0.13	19	22	21
0.25	26	24	28
0.38	30	23	34
0.51	34	24	40
0.64	36	24	49
0.76	34	25	57
0.89	35	27	66
1.02	31	29	75
1.14	28	30	83
1.27	26	32	88
1.40	23	32	93
1.52	21	32	96
1.65	20	32	97
1.78	18	32	98
1.91	15	32	99

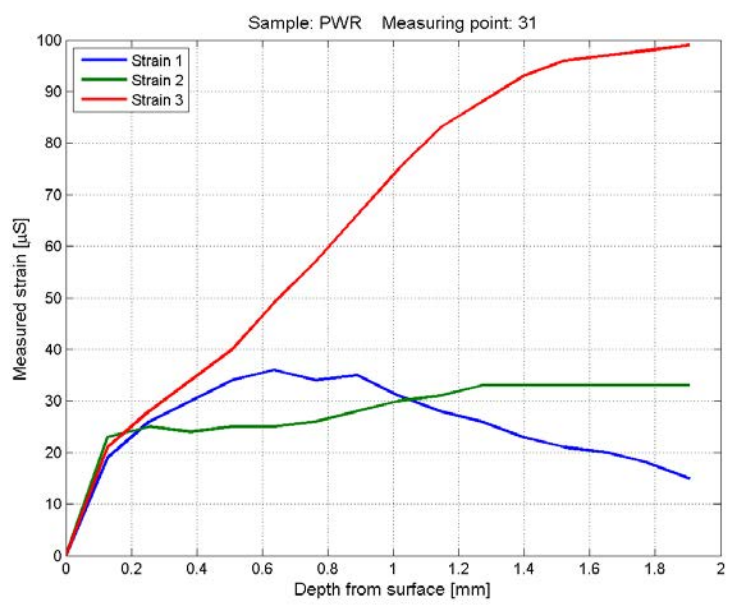


Figure A3:46 Raw data from measurement point 31 on the PWR sample

Appendix 3

Depth mm	Gage 1 $\mu\text{m}/\text{m}$	Gage 2 $\mu\text{m}/\text{m}$	Gage 3 $\mu\text{m}/\text{m}$
0.00	0	0	0
0.13	20	18	24
0.25	30	26	38
0.38	34	30	48
0.51	37	34	58
0.64	39	37	68
0.76	42	41	82
0.89	41	44	94
1.02	41	48	107
1.14	39	50	113
1.27	37	50	119
1.40	35	50	122
1.52	32	49	124
1.65	32	49	127
1.78	30	47	127
1.91	28	47	129

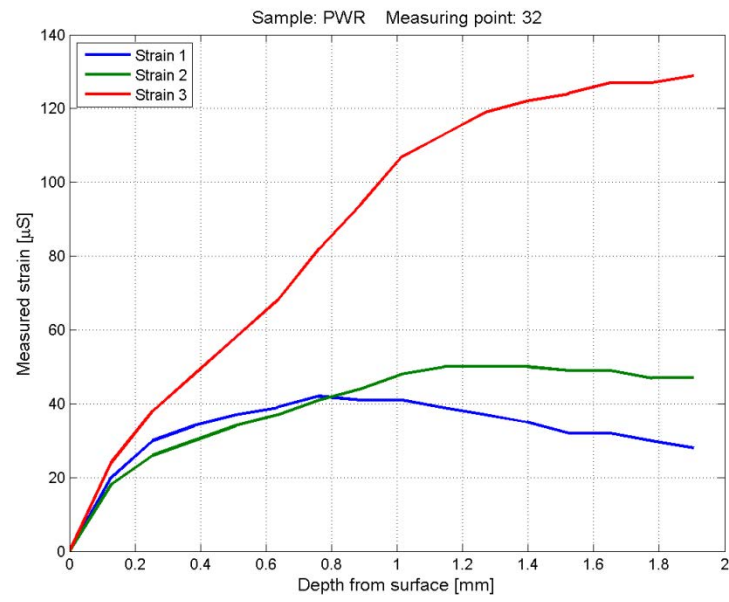


Figure A3:47 Raw data from measurement point 32 on the PWR sample

Depth mm	Gage 1 $\mu\text{m}/\text{m}$	Gage 2 $\mu\text{m}/\text{m}$	Gage 3 $\mu\text{m}/\text{m}$
0.00	0	-1	0
0.13	22	19	27
0.25	31	27	38
0.38	35	29	41
0.51	38	30	44
0.64	41	32	49
0.76	42	33	53
0.89	41	33	56
1.02	41	34	62
1.14	41	35	64
1.27	40	35	66
1.40	39	34	67
1.52	38	35	68
1.65	39	35	68
1.78	38	35	69
1.91	37	34	69

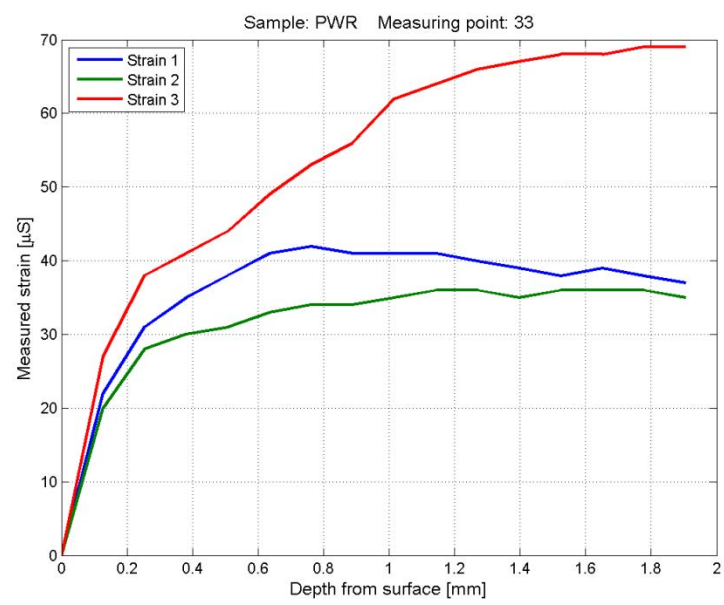


Figure A3:48 Raw data from measurement point 33 on the PWR sample

Appendix 3

Depth mm	Gage 1 μm/m	Gage 2 μm/m	Gage 3 μm/m
0.00	3	3	1
0.13	40	51	36
0.28	39	62	44
0.38	40	60	48
0.51	37	19	34
0.64	40	27	40
0.76	42	25	40
0.89	40	26	41
1.02	39	25	46
1.14	31	32	58
1.27	30	35	61
1.40	29	31	62
1.52	28	30	60
1.65	24	31	68

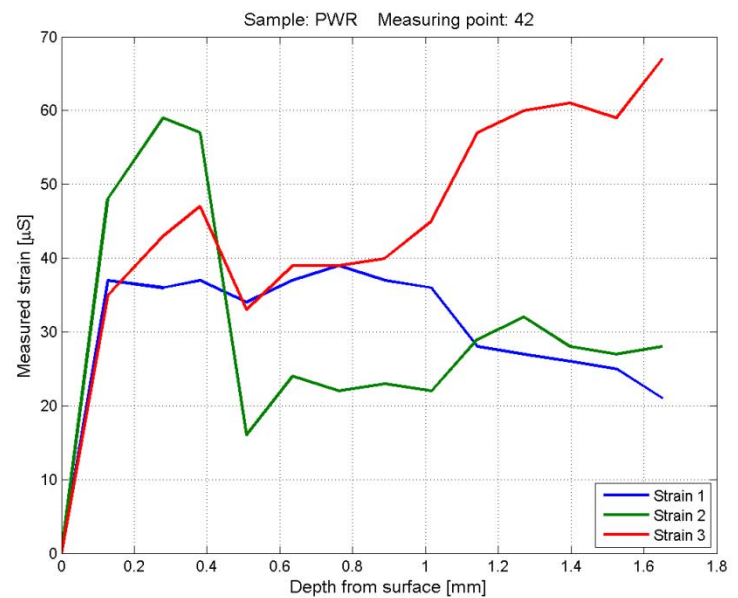


Figure A3:49 Raw data from measurement point 42 on the PWR sample

Depth mm	Gage 1 μm/m	Gage 2 μm/m	Gage 3 μm/m
0.00	-1	-4	-3
0.13	25	25	28
0.28	38	39	40
0.38	40	43	48
0.51	38	42	54
0.64	44	52	66
0.76	43	57	78
0.89	43	60	85
1.02	40	63	91
1.14	41	64	92
1.27	41	63	94
1.40	42	61	89
1.52	40	67	99
1.65	39	67	97
1.78	39	66	98
1.91	35	68	103

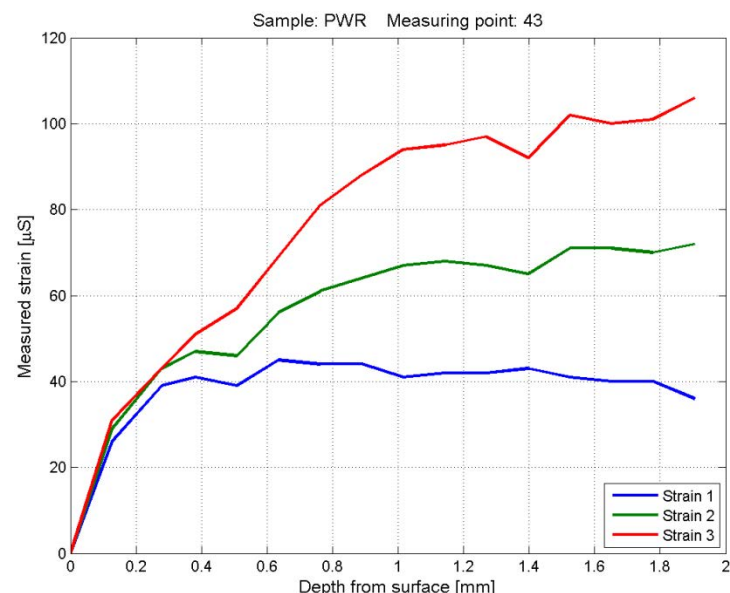


Figure A3:50 Raw data from measurement point 43 on the PWR sample

Appendix 3

Depth mm	Gage 1 $\mu\text{m}/\text{m}$	Gage 2 $\mu\text{m}/\text{m}$	Gage 3 $\mu\text{m}/\text{m}$
0.00	0	-1	-1
0.13	19	25	20
0.38	33	57	44
0.51	38	69	53
0.64	39	77	60
0.76	42	81	63
0.89	40	84	67
1.02	39	85	67
1.14	39	85	67

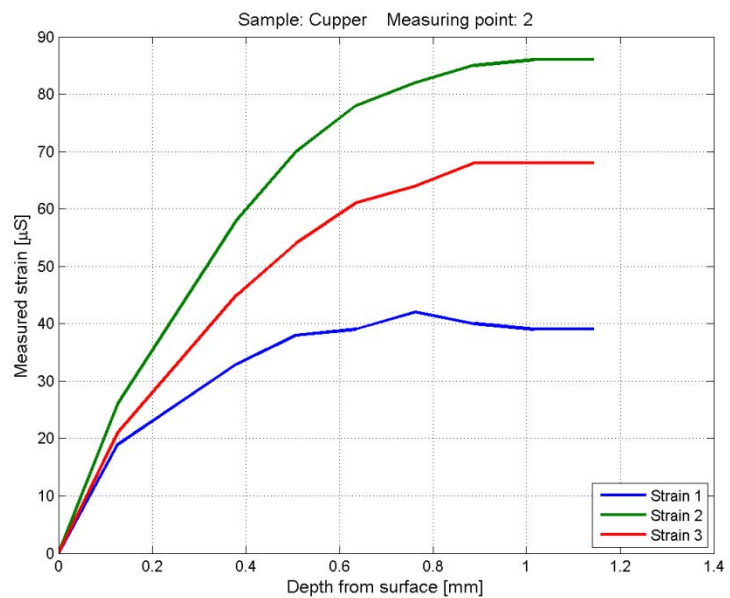


Figure A3:51 Raw data from measurement point 2 on the Copper sample

Depth mm	Gage 1 $\mu\text{m}/\text{m}$	Gage 2 $\mu\text{m}/\text{m}$	Gage 3 $\mu\text{m}/\text{m}$
0.00	0	-1	0
0.13	15	22	26
0.28	23	41	48
0.38	25	52	59
0.51	28	62	70
0.64	26	65	74
0.76	29	69	74
0.89	27	70	76
1.02	27	69	76
1.14	24	69	77
1.27	24	70	76
1.40	23	69	75
1.52	23	69	76
1.65	19	68	73
1.78	19	65	71
1.91	19	66	72

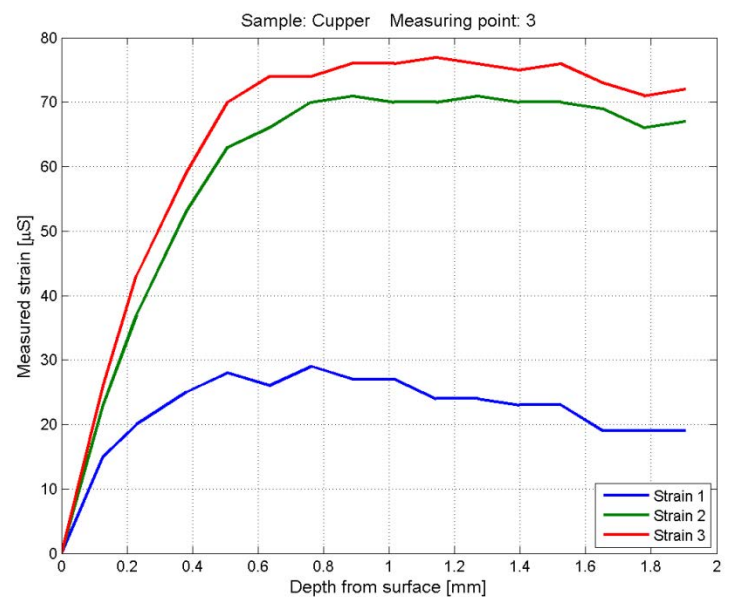


Figure A3:52 Raw data from measurement point 3 on the Copper sample

Appendix 3

Depth mm	Gage 1 μm/m	Gage 2 μm/m	Gage 3 μm/m
0.00	0	-1	0
0.13	13	17	24
0.28	30	38	53
0.38	43	53	72
0.51	47	62	84
0.64	48	67	93
0.76	54	71	102
0.89	54	73	105
1.02	55	73	107
1.14	54	74	109
1.27	54	73	110
1.40	53	71	111
1.52	52	71	112
1.65	53	72	113
1.78	52	70	112

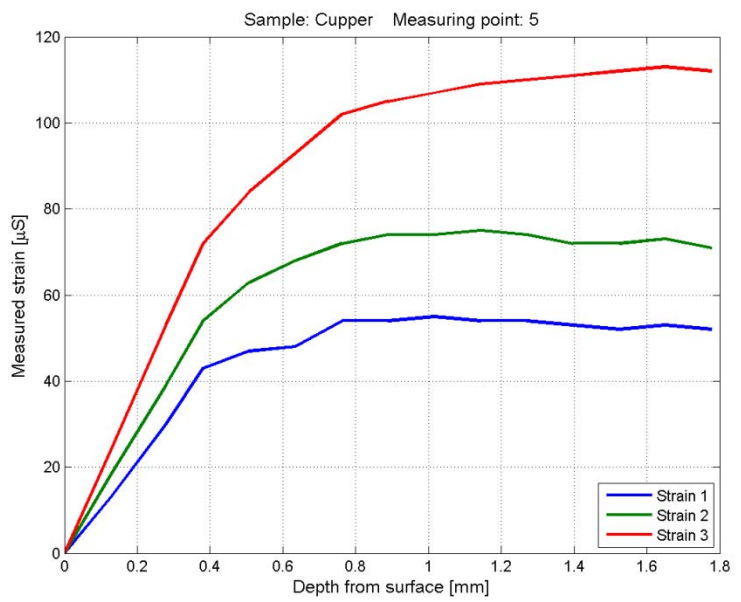


Figure A3:53 Raw data from measurement point 5 on the Copper sample

Appendix 4

Max / min principal stresses calculated by the Integral method

This appendix contains max / min principal stresses ¹⁾ calculated by the *Integral method*.

For each measuring point one table and two graphs are supplied. All calculated stresses and angles are shown in the table. The first graph shows the maximum and minimum principal stress and the second graph shows the orientation of the principal stress direction (the clockwise angle between the Strain Gage 1 and the axis of the maximum principal stress) see *Figure A4:1*.

All graphs show large compressive stresses close to the surface. These stresses are with a high degree of probability caused by the machining when the samples were cut out from the inserts. I.e. the high compressive stresses are not representative for the insets and therefore they are plotted with dashed curves.

Calculated stresses are considered to be not reliable if the corresponding von Mises effective stress is larger than 70% of the yield stress. In those cases the calculated stress values are shaded.

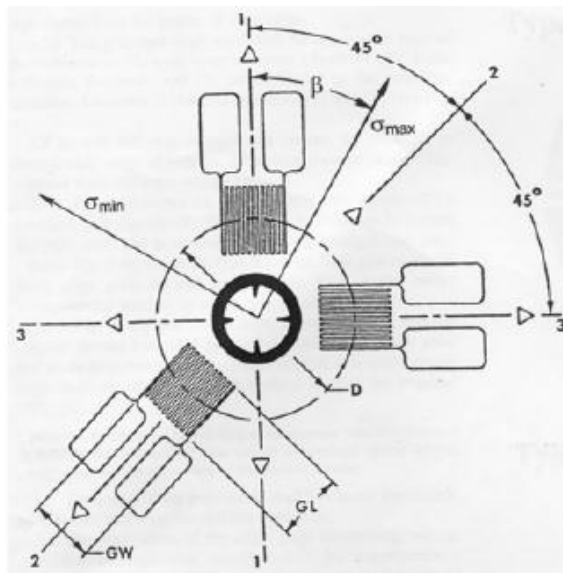


Figure A4:1 A sketch showing the orientations of the three strain gages and the definition of the angle β

¹⁾ At every point in a stressed body there are at least one rectangular coordinate system where the corresponding sheer stresses are zero. The corresponding stresses are called principal stresses. On a surface where the normal stress is zero there are two such principal stresses.

Appendix 4

Table 1: Figures with max / min principal stresses in the BWR sample

Measuring point	Figure	Measuring point	Figure	Measuring point	Figure
R1	Fig: A4:2	R2	Fig: A4:3	---	---
11	Fig: A4:4	12	Fig: A4:5	13	Fig: A4:6
21	Fig: A4:7	22	Fig: A4:8	23	Fig: A4:9
31	Fig: A4:10	32	Fig: A4:11	33	Fig: A4:12
34T	Fig: A4:13	35T	Fig: A4:14	---	---
36TB	Fig: A4:15	37TB	Fig: A4:16	38TB	Fig: A4:17
41	Fig: A4:18	42	Fig: A4:19	43	Fig: A4:20
51	Fig: A4:21	52	Fig: A4:22	53	Fig: A4:23
61	Fig: A4:24	62	Fig: A4:25	63	Fig: A4:26

Table 2: Figures with max / min principal stresses in the PWR sample

Measuring point	Figure	Measuring point	Figure	Measuring point	Figure
R1	Fig: A4:27	R2	Fig: A4:28	R3	Fig: A4:29
C1	Fig: A4:30	C2	Fig: A4:31	C3	Fig: A4:32
C4	Fig: A4:33	C5	Fig: A4:34	---	---
11	Fig: A4:35	12	Fig: A4:36	13	Fig: A4:37
21	Fig: A4:38	22	Fig: A4:39	23	Fig: A4:40
24T	Fig: A4:41	25T	Fig: A4:42	---	---
26TB	Fig: A4:43	27TB	Fig: A4:44	28TB	Fig: A4:45
29TB	Fig: A4:46	---	---	---	---
31	Fig: A4:47	32	Fig: A4:48	33	Fig: A4:49
41	---	42	Fig: A4:50	43	Fig: A4:51

Table 3: Figures with max / min principal stresses in the Copper sample

Measuring point	Figure	Measuring point	Figure	Measuring point	Figure
2	Fig: A4:52	3	Fig: A4:53	5	Fig: A4:54

Appendix 4

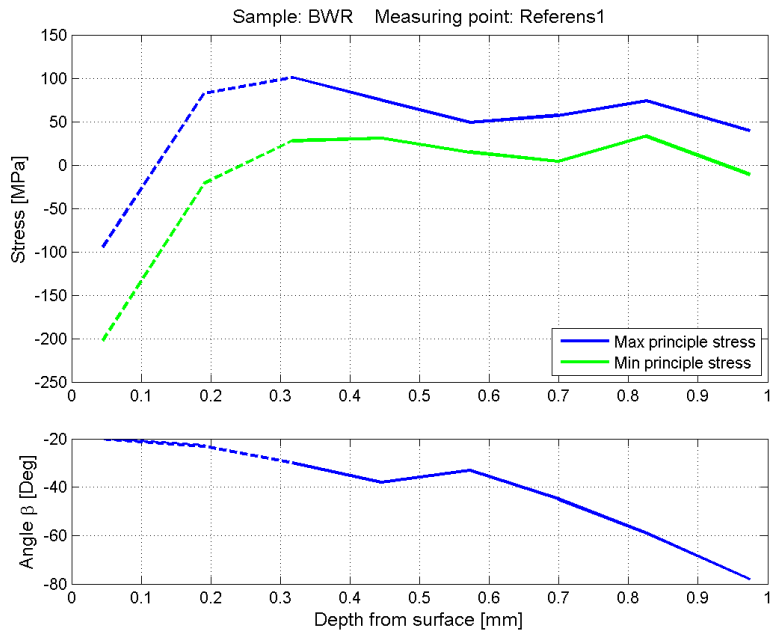


Figure A4:2 Principal stresses calculated for Measuring point *R1* on the BWR sample.

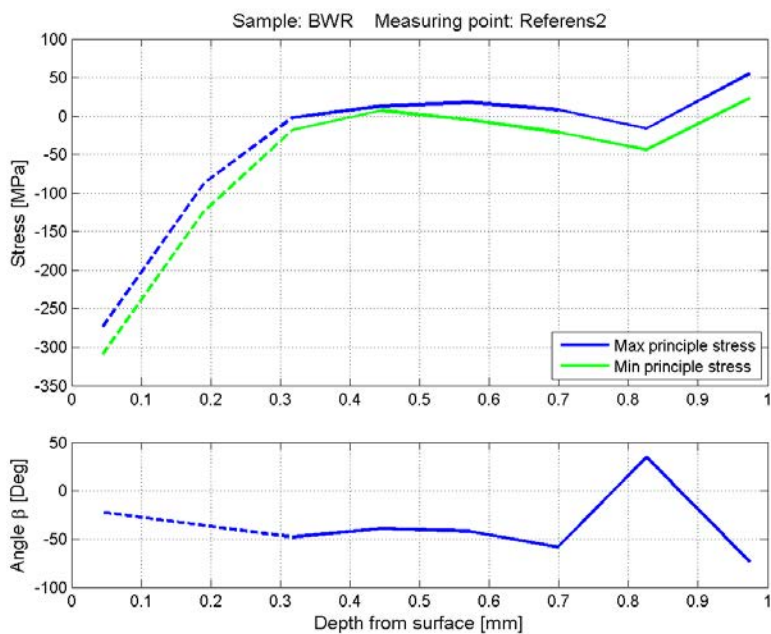
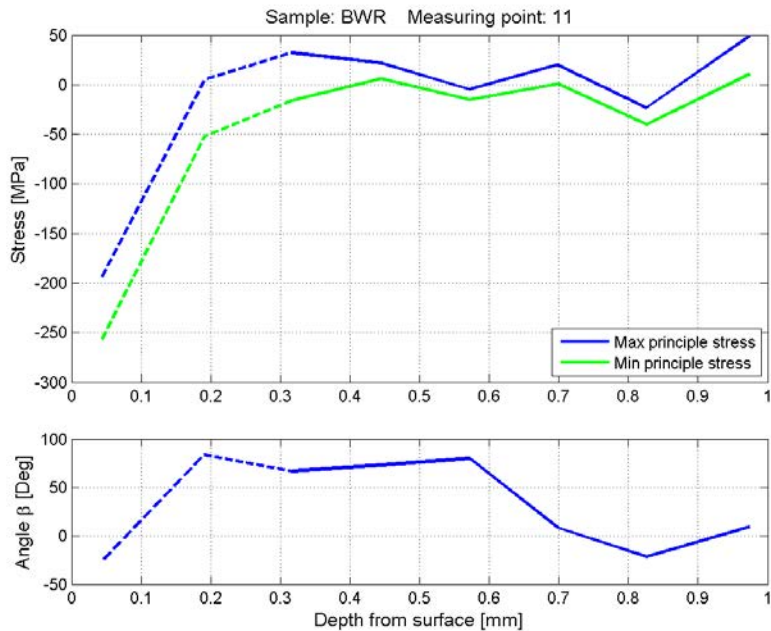
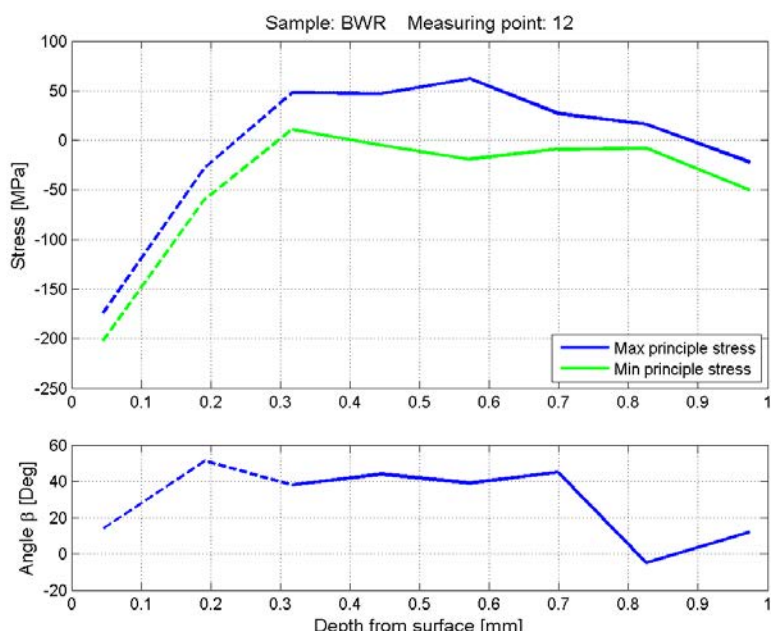


Figure A4:3 Principal stresses calculated for Measuring point *R2* on the BWR sample. For the shaded stresses the von Mises effective stress is larger than 70% of the yield stress and therefore they are not reliable.

Appendix 4

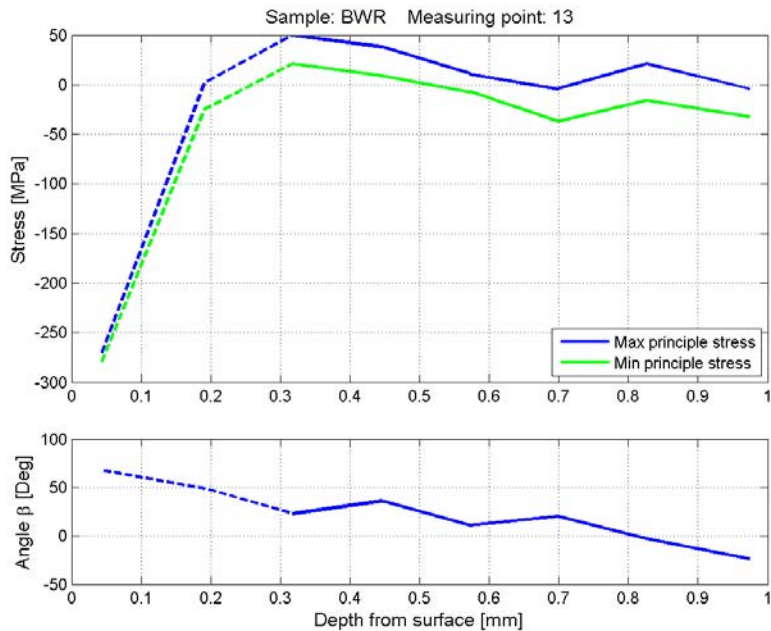
Figure A4:4

Principal stresses calculated for Measuring point 11 on the BWR sample. For the shaded stresses the von Mises effective stress is larger than 70% of the yield stress and therefore they are not reliable.

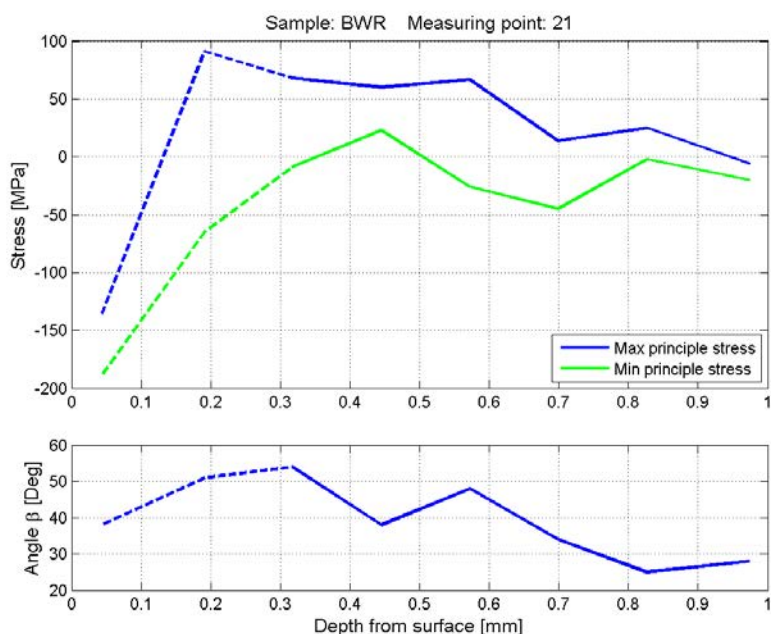
Figure A4:5

Principal stresses calculated for Measuring point 12 on the BWR sample. For the shaded stresses the von Mises effective stress is larger than 70% of the yield stress and therefore they are not reliable.

Appendix 4

Figure A4:6

Principal stresses calculated for Measuring point 13 on the BWR sample. For the shaded stresses the von Mises effective stress is larger than 70% of the yield stress and therefore they are not reliable.

Figure A4:7

Principal stresses calculated for Measuring point 21 on the BWR sample

Appendix 4

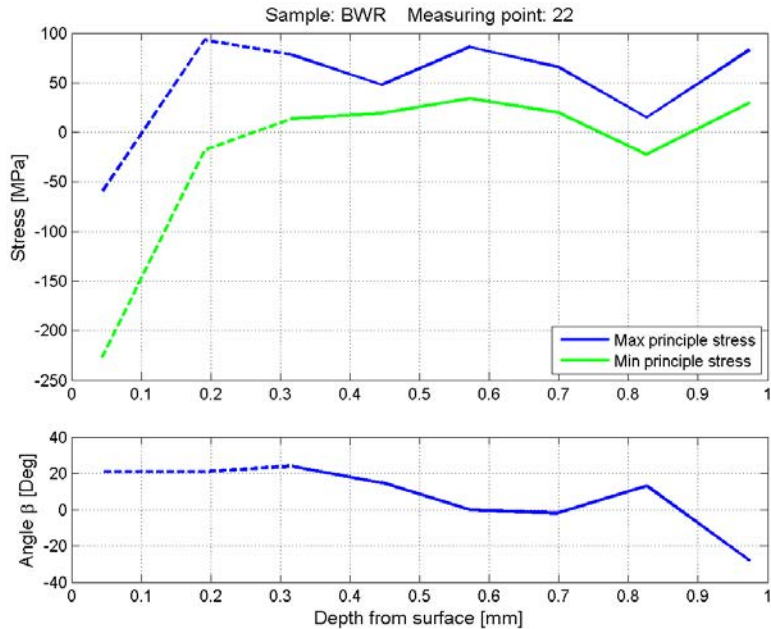


Figure A4:8 Principal stresses calculated for Measuring point 22 on the BWR sample.

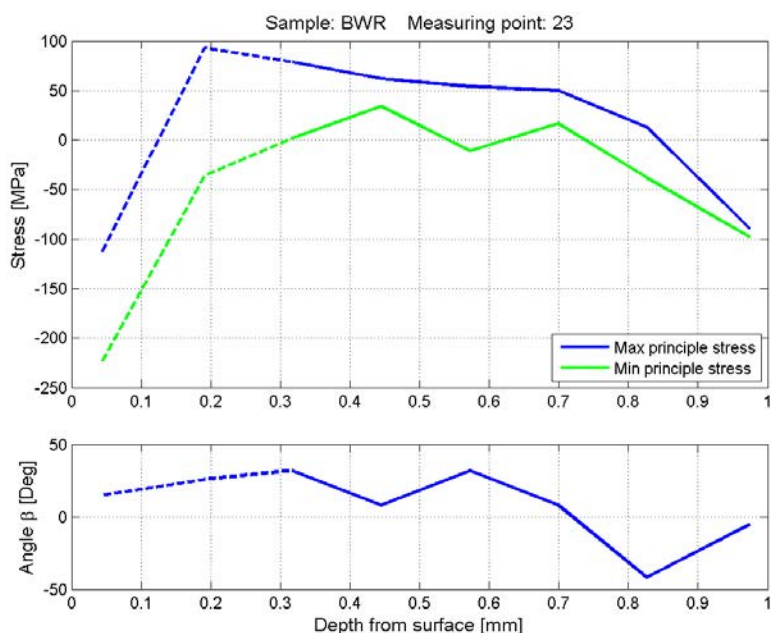


Figure A4:9 Principal stresses calculated for Measuring point 23 on the BWR sample.

Appendix 4

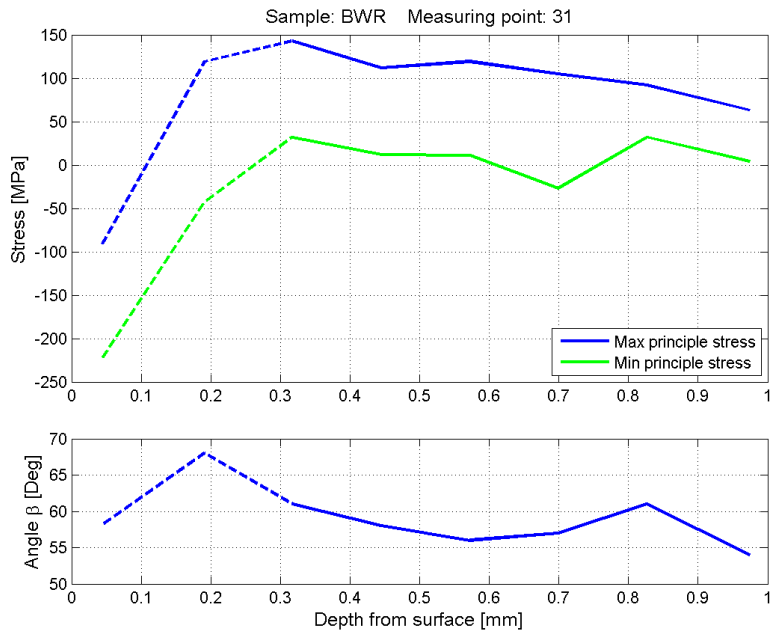


Figure A4:10 Principal stresses calculated for Measuring point 31 on the BWR sample.

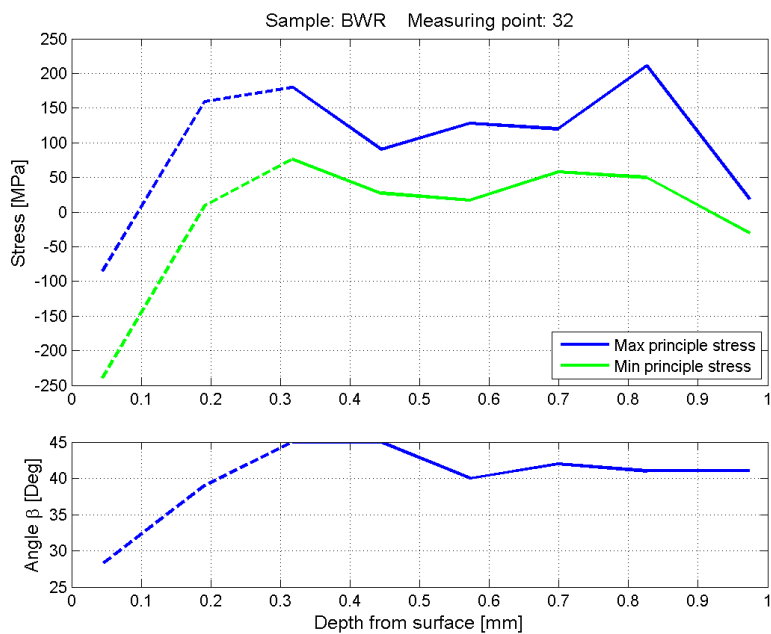


Figure A4:11 Principal stresses calculated for Measuring point 32 on the BWR sample.

Appendix 4

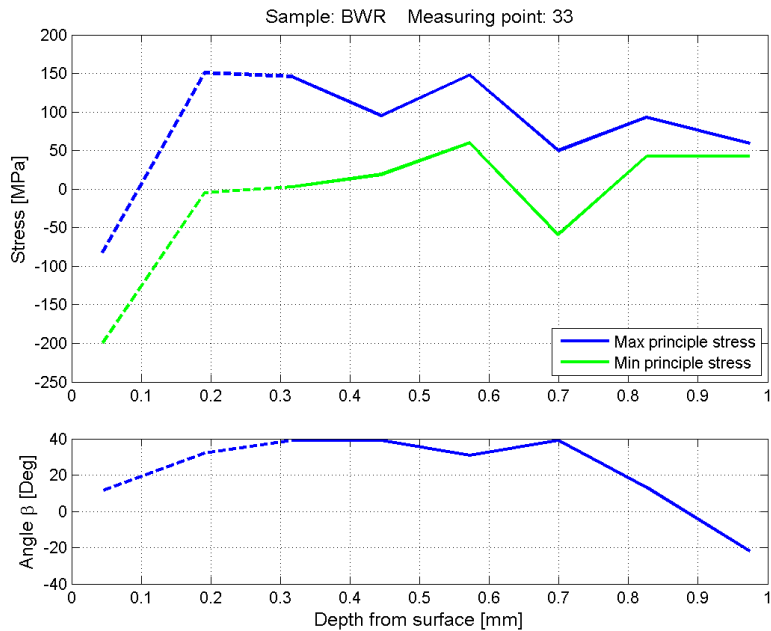


Figure A4:12 Principal stresses calculated for Measuring point 33 on the BWR sample

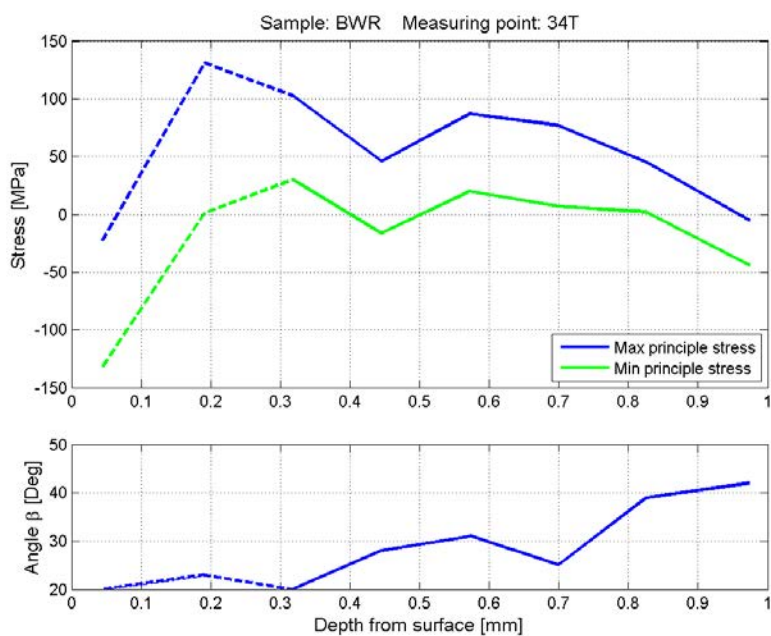


Figure A4:13 Principal stresses calculated for Measuring point 34T on the BWR sample

Appendix 4

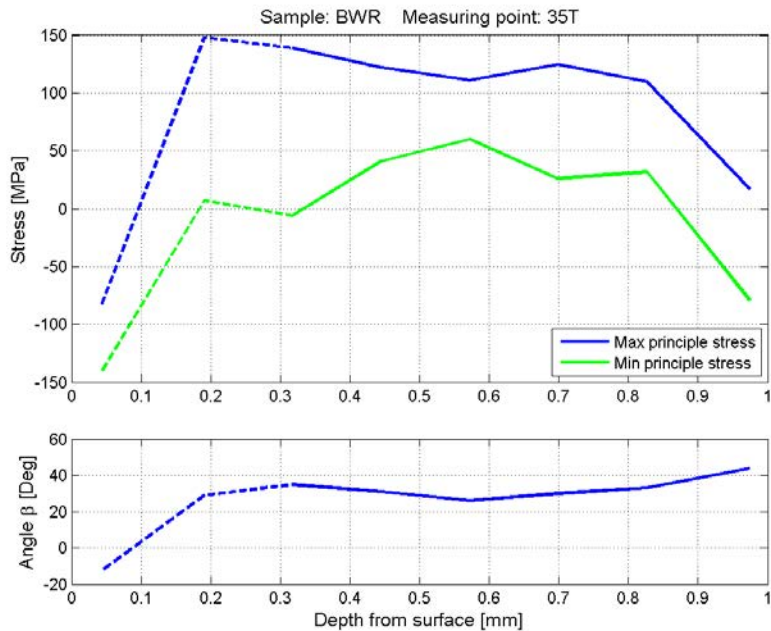


Figure A4:14 Principal stresses calculated for Measuring point 35T on the BWR sample

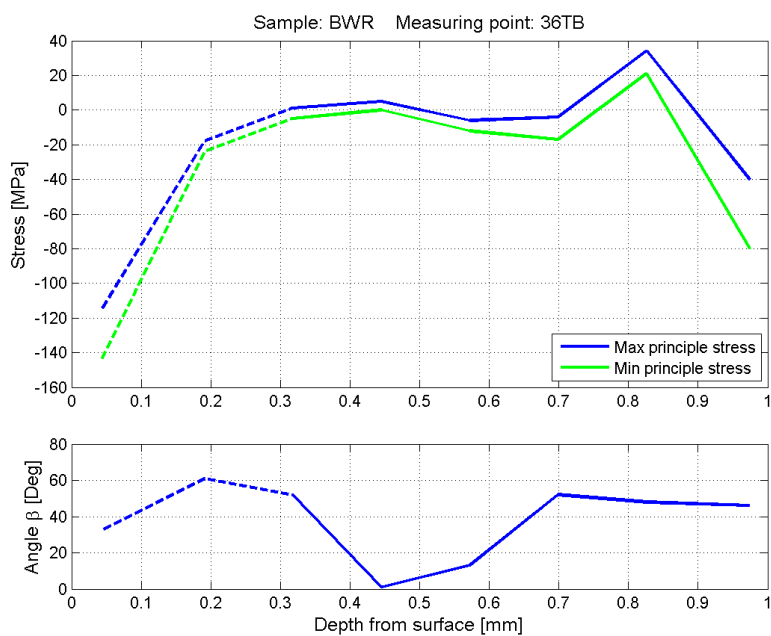


Figure A4:15 Principal stresses calculated for Measuring point 36TB on the BWR sample

Appendix 4

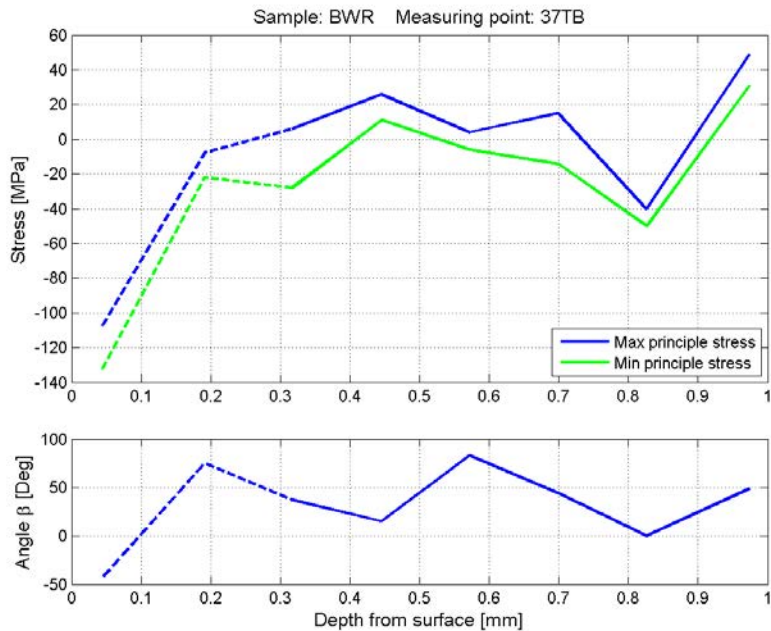


Figure A4:16 Principal stresses calculated for Measuring point 37TB on the BWR sample

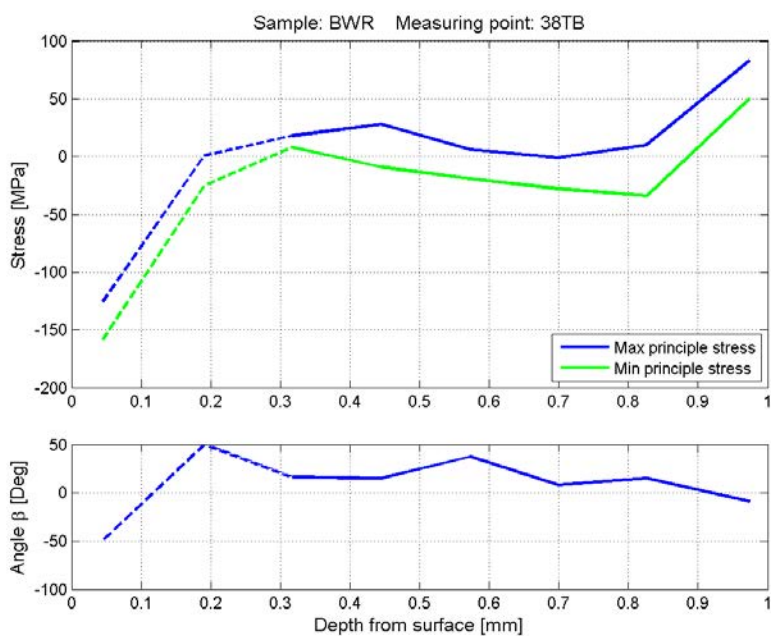


Figure A4:17 Principal stresses calculated for Measuring point 38TB on the BWR sample

Appendix 4

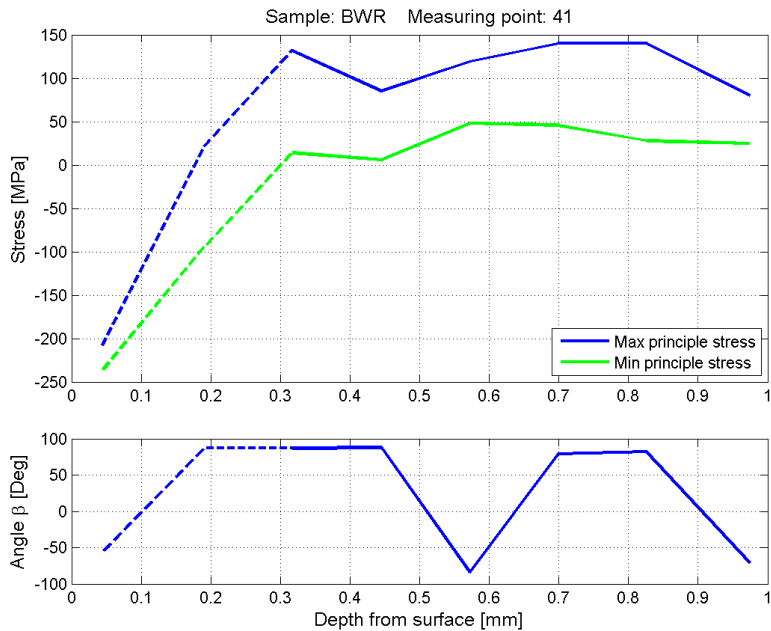


Figure A4:18 Principal stresses calculated for Measuring point 41 on the BWR sample. For the shaded stresses the von Mises effective stress is larger than 70% of the yield stress and therefore they are not reliable.

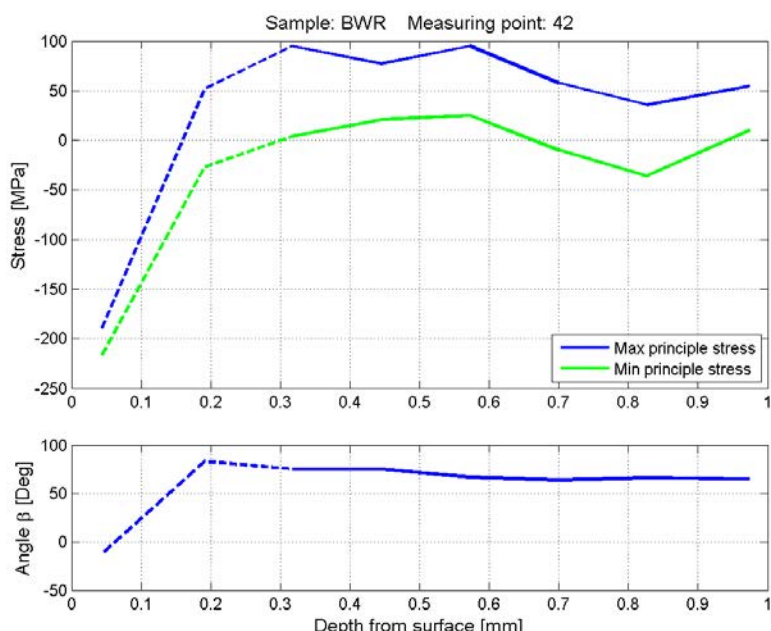


Figure A4:19 Principal stresses calculated for Measuring point 42 on the BWR sample. For the shaded stresses the von Mises effective stress is larger than 70% of the yield stress and therefore they are not reliable.

Appendix 4

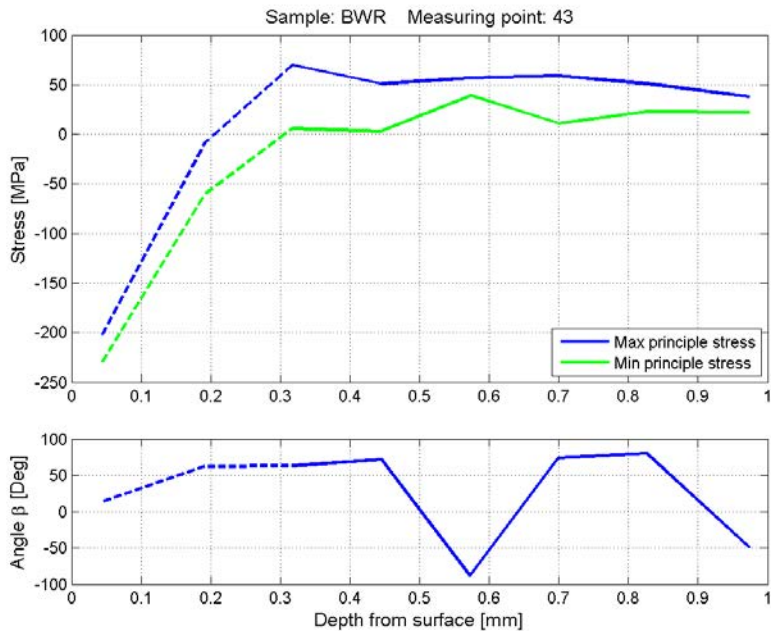


Figure A4:20 Principal stresses calculated for Measuring point 43 on the BWR sample. For the shaded stresses the von Mises effective stress is larger than 70% of the yield stress and therefore they are not reliable.

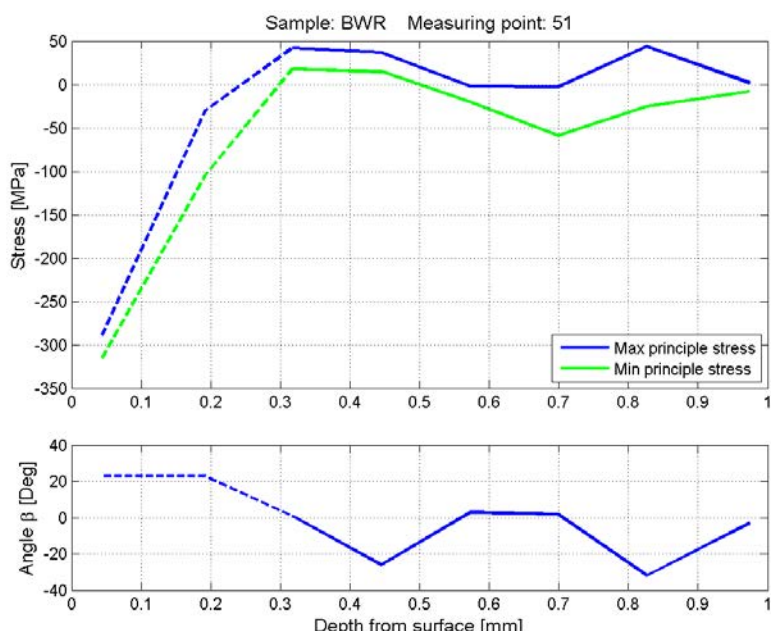


Figure A4:21 Principal stresses calculated for Measuring point 51 on the BWR sample. For the shaded stresses the von Mises effective stress is larger than 70% of the yield stress and therefore they are not reliable.

Appendix 4

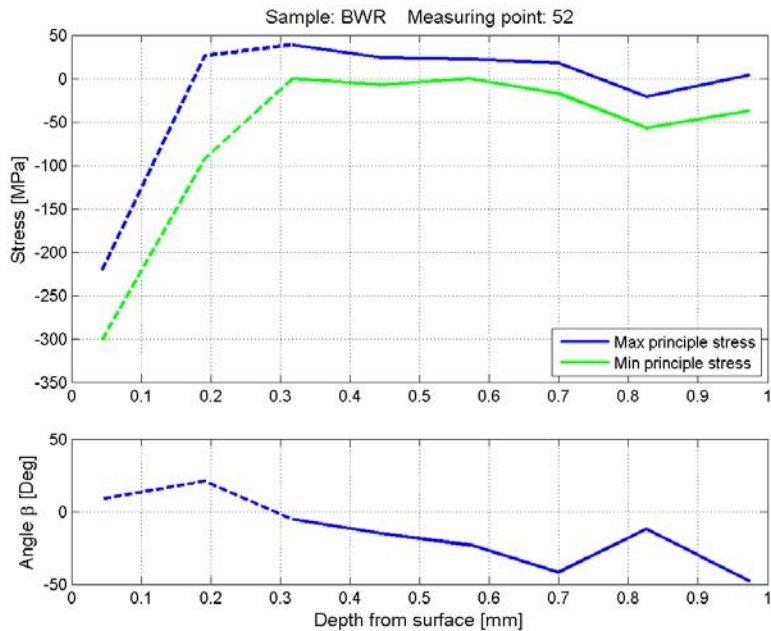


Figure A4:22 Principal stresses calculated for Measuring point 52 on the BWR sample. For the shaded stresses the von Mises effective stress is larger than 70% of the yield stress and therefore they are not reliable.

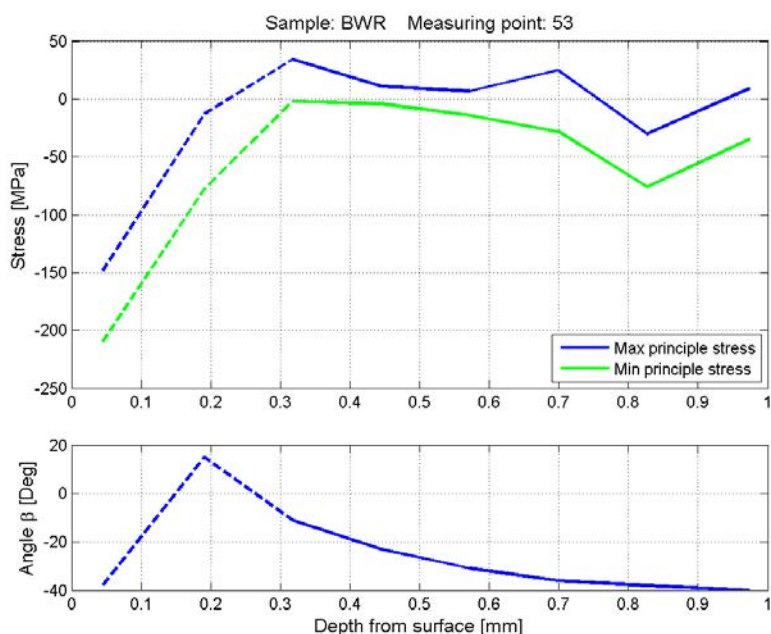


Figure A4:23 Principal stresses calculated for Measuring point 53 on the BWR sample..

Appendix 4

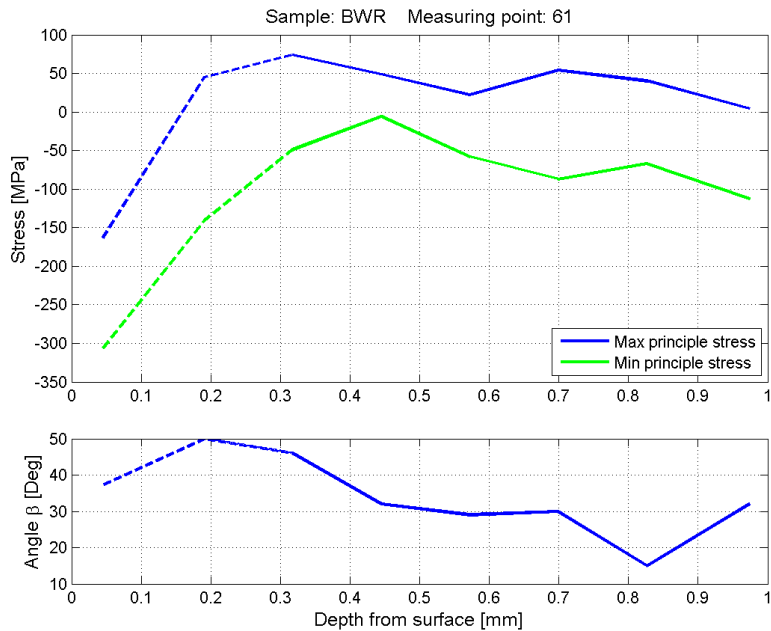


Figure A4:24 Principal stresses calculated for Measuring point 61 on the BWR sample. For the shaded stresses the von Mises effective stress is larger than 70% of the yield stress and therefore they are not reliable.

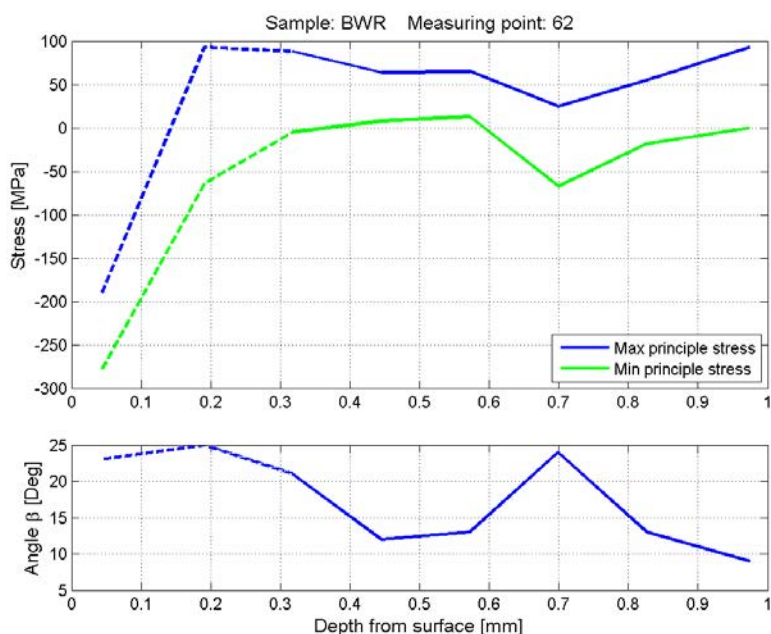


Figure A4:25 Principal stresses calculated for Measuring point 62 on the BWR sample. For the shaded stresses the von Mises effective stress is larger than 70% of the yield stress and therefore they are not reliable.

Appendix 4

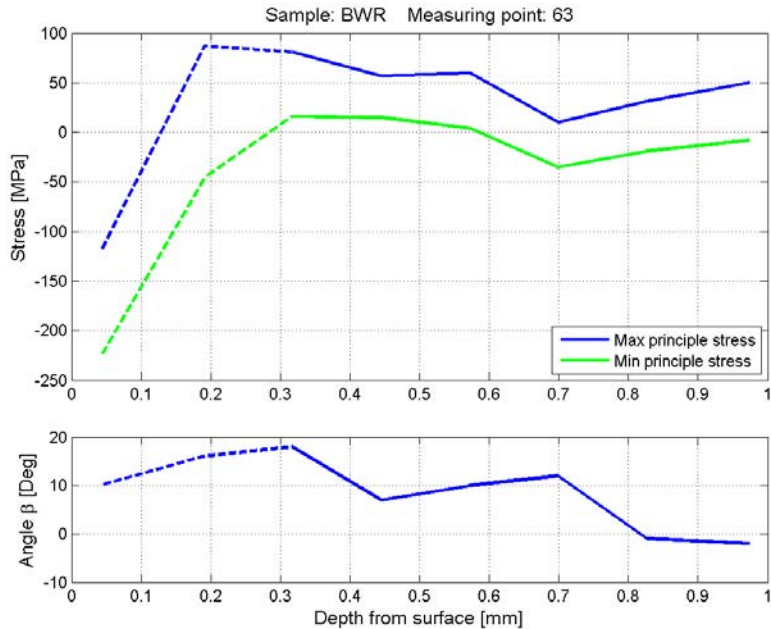


Figure A4:26 Principal stresses calculated for Measuring point 63 on the BWR sample. For the shaded stresses the von Mises effective stress is larger than 70% of the yield stress and therefore they are not reliable.

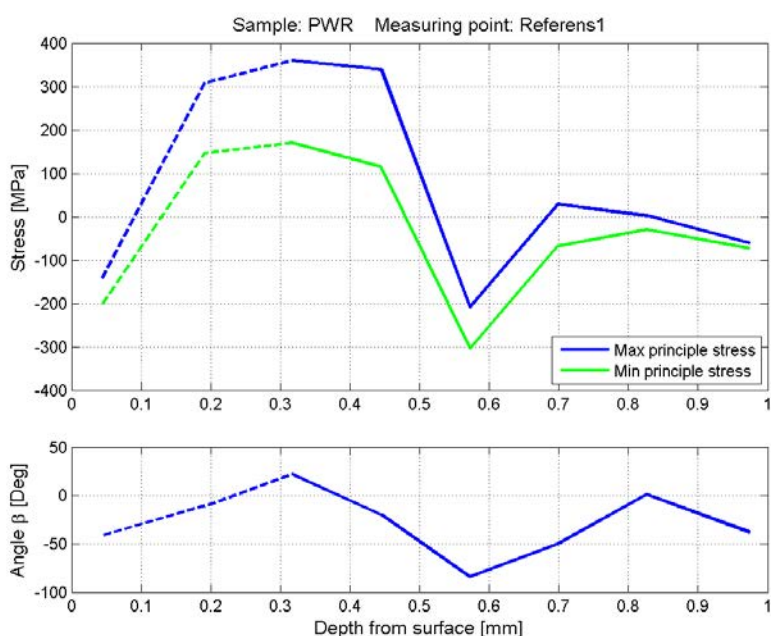


Figure A4:27 Principal stresses calculated for Measuring point R1 on the PWR sample. For the shaded stresses the von Mises effective stress is larger than 70% of the yield stress and therefore they are not reliable.

Appendix 4

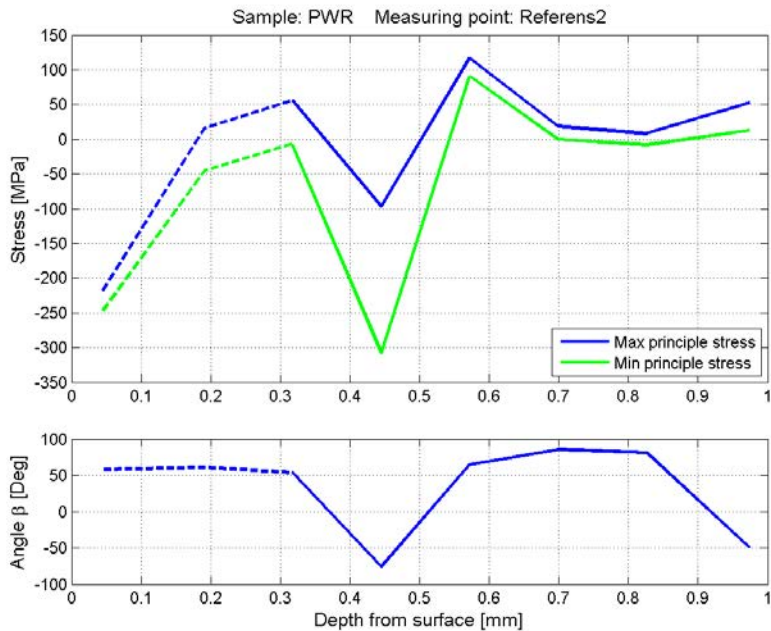


Figure A4:28 Principal stresses calculated for Measuring point *R2* on the PWR sample. For the shaded stresses the von Mises effective stress is larger than 70% of the yield stress and therefore they are not reliable.

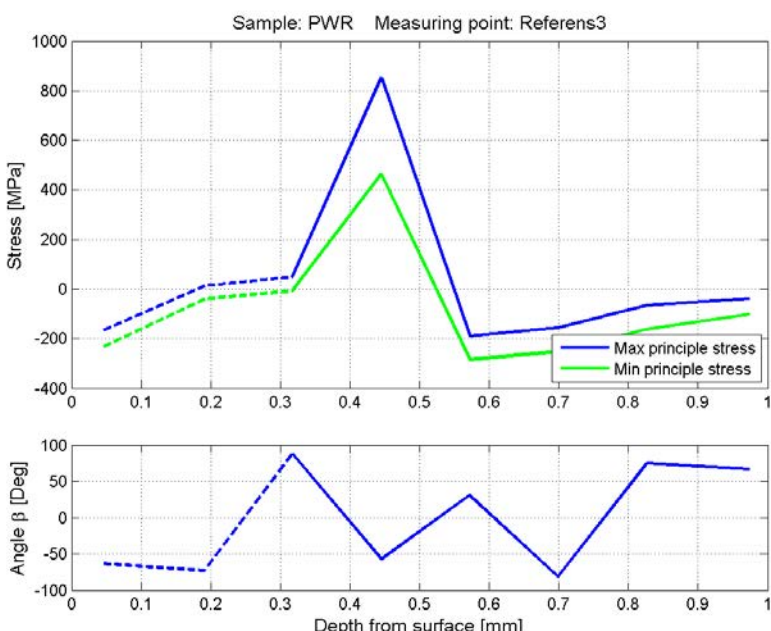


Figure A4:29 Principal stresses calculated for Measuring point *R3* on the PWR sample. For the shaded stresses the von Mises effective stress is larger than 70% of the yield stress and therefore they are not reliable.

Appendix 4

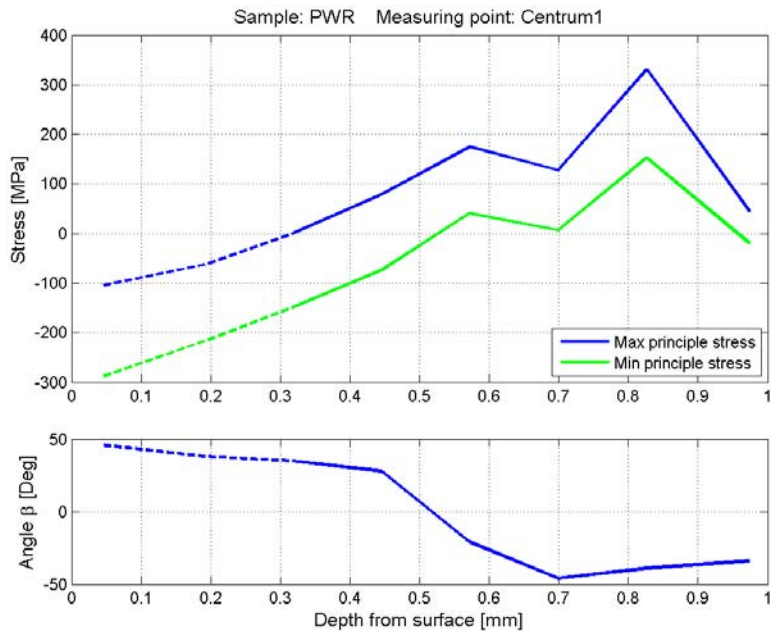


Figure A4:30 Principal stresses calculated for Measuring point *C1* on the PWR sample. For the shaded stresses the von Mises effective stress is larger than 70% of the yield stress and therefore they are not reliable.

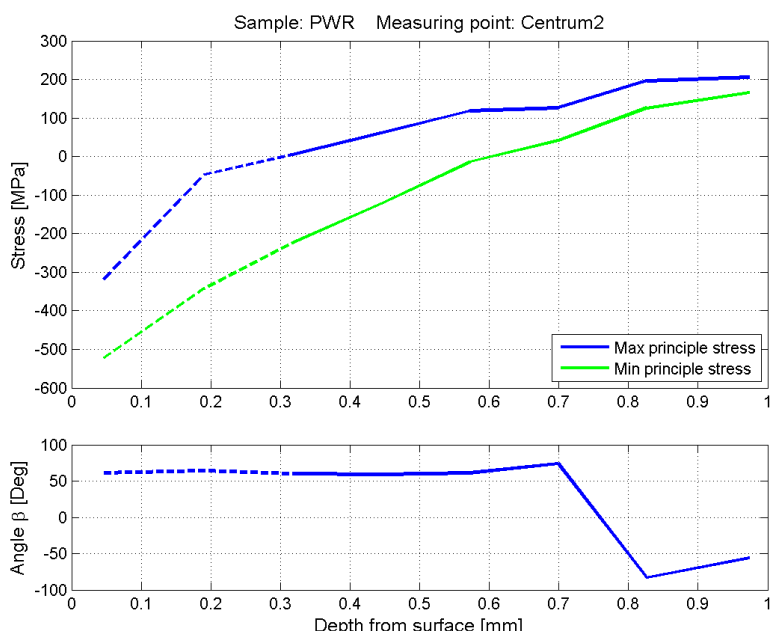


Figure A4:31 Principal stresses calculated for Measuring point *C2* on the PWR sample. For the shaded stresses the von Mises effective stress is larger than 70% of the yield stress and therefore they are not reliable.

Appendix 4

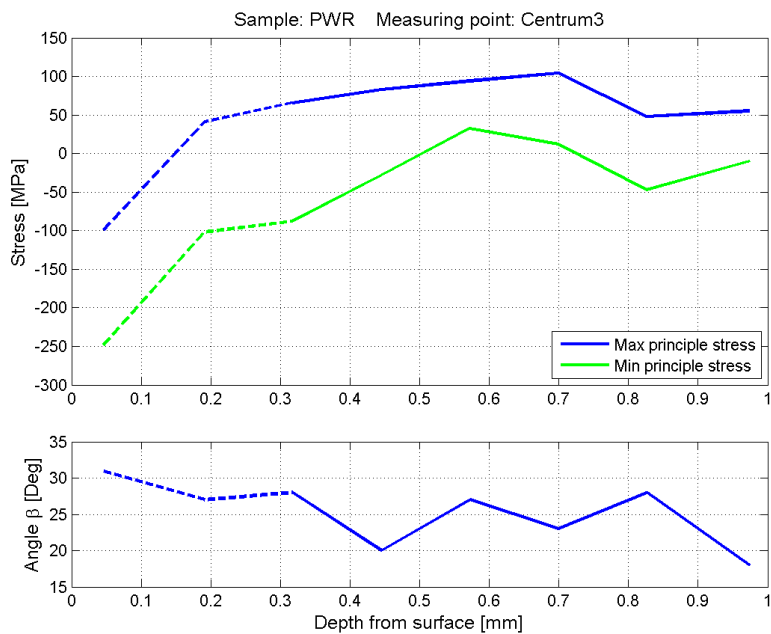


Figure A4:32 Principal stresses calculated for Measuring point C3 on the PWR sample.

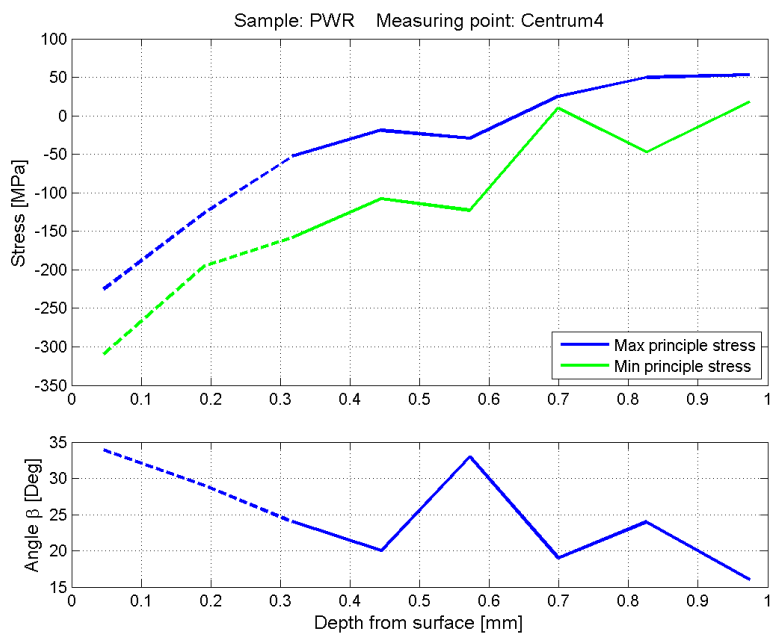


Figure A4:33 Principal stresses calculated for Measuring point C4 on the PWR sample. For the shaded stresses the von Mises effective stress is larger than 70% of the yield stress and therefore they are not reliable.

Appendix 4

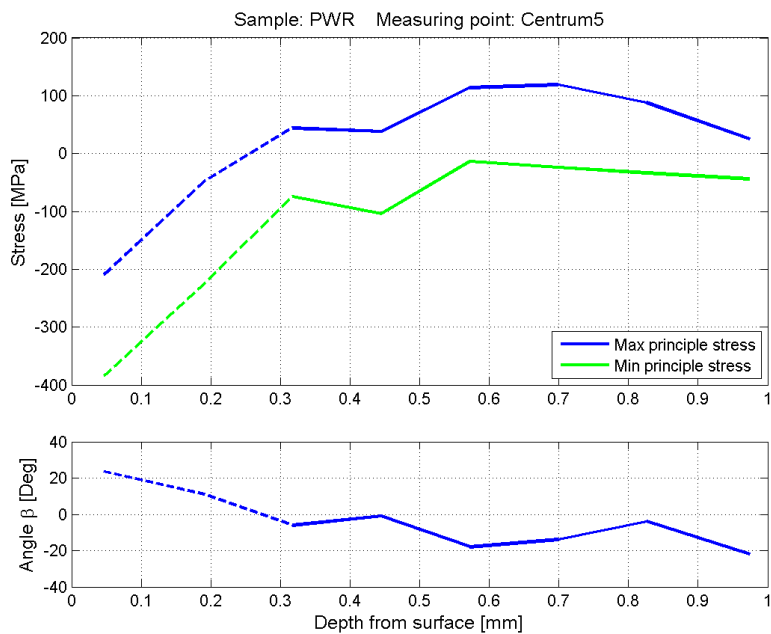


Figure A4:34 Principal stresses calculated for Measuring point *C5* on the PWR sample. For the shaded stresses the von Mises effective stress is larger than 70% of the yield stress and therefore they are not reliable.

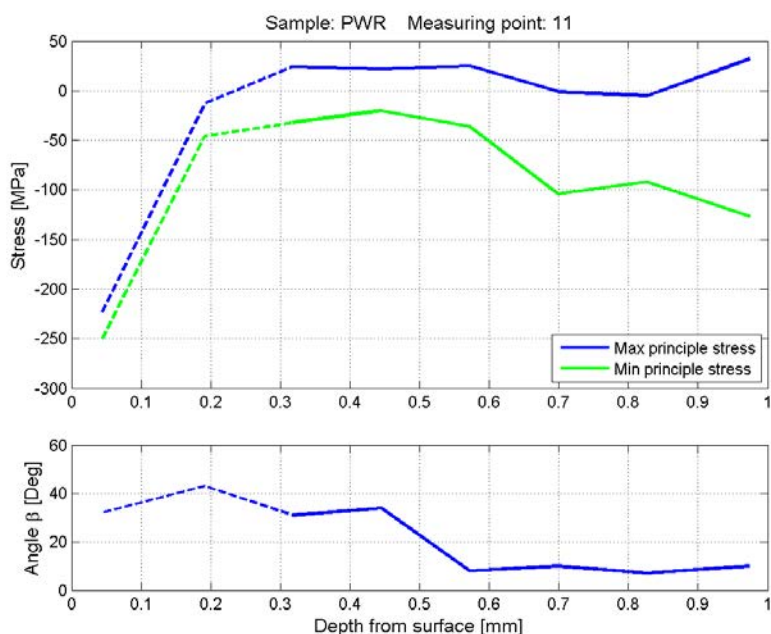


Figure A4:35 Principal stresses calculated for Measuring point *11* on the PWR sample. For the shaded stresses the von Mises effective stress is larger than 70% of the yield stress and therefore they are not reliable.

Appendix 4

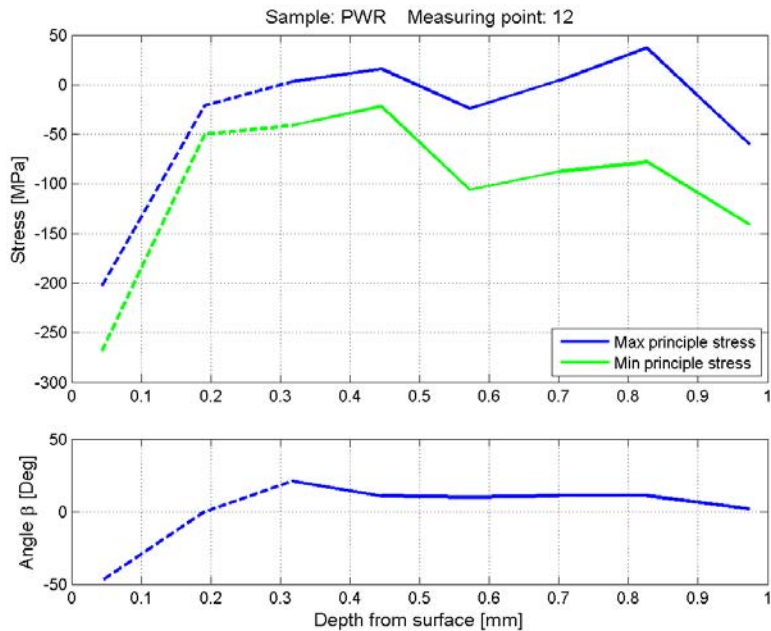


Figure A4:36 Principal stresses calculated for Measuring point 12 on the PWR sample. For the shaded stresses the von Mises effective stress is larger than 70% of the yield stress and therefore they are not reliable.

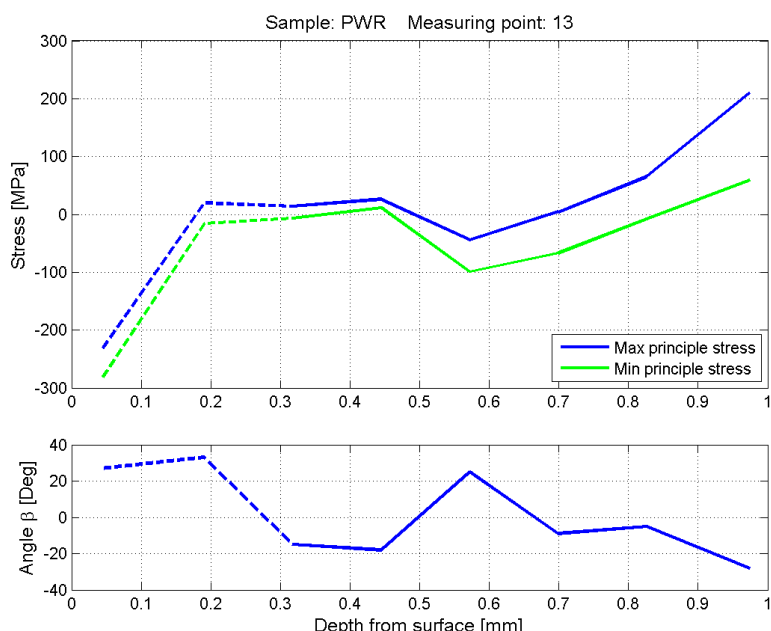


Figure A4:37 Principal stresses calculated for Measuring point 13 on the PWR sample. For the shaded stresses the von Mises effective stress is larger than 70% of the yield stress and therefore they are not reliable.

Appendix 4

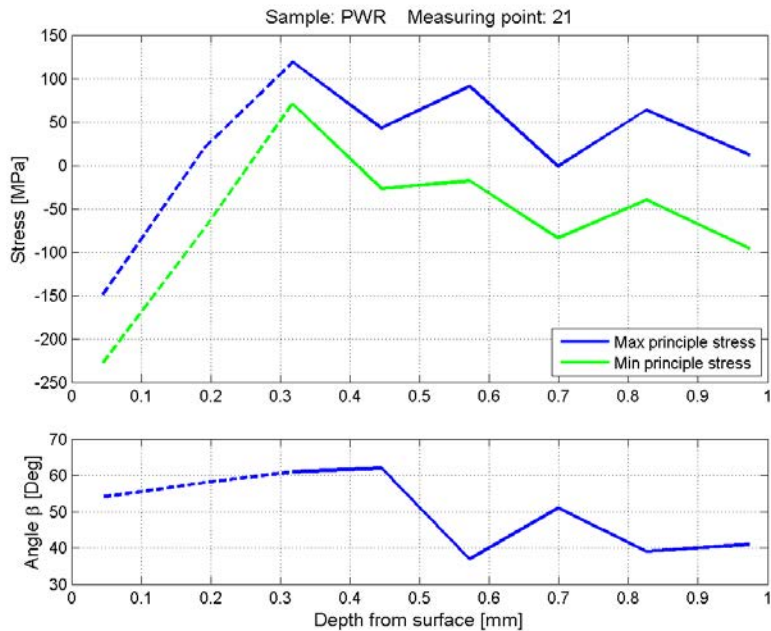


Figure A4:38 Principal stresses calculated for Measuring point 21 on the PWR sample.

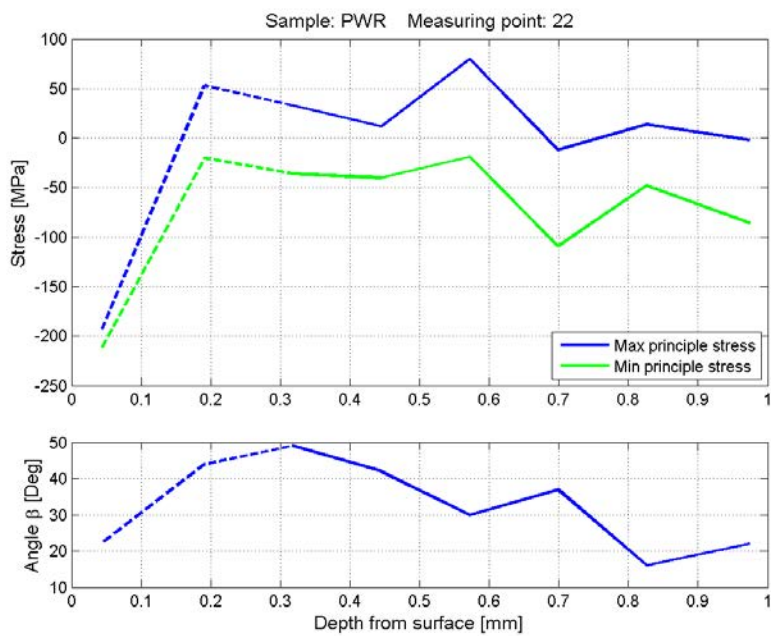
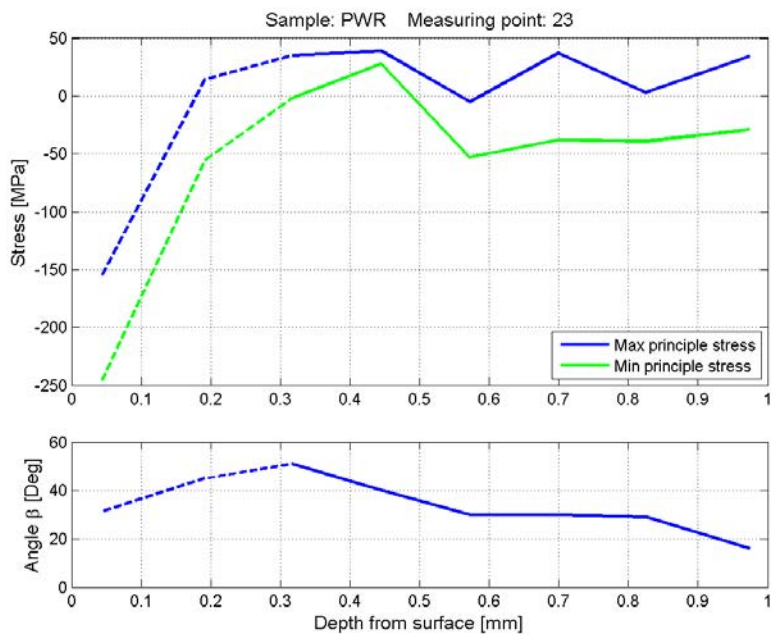


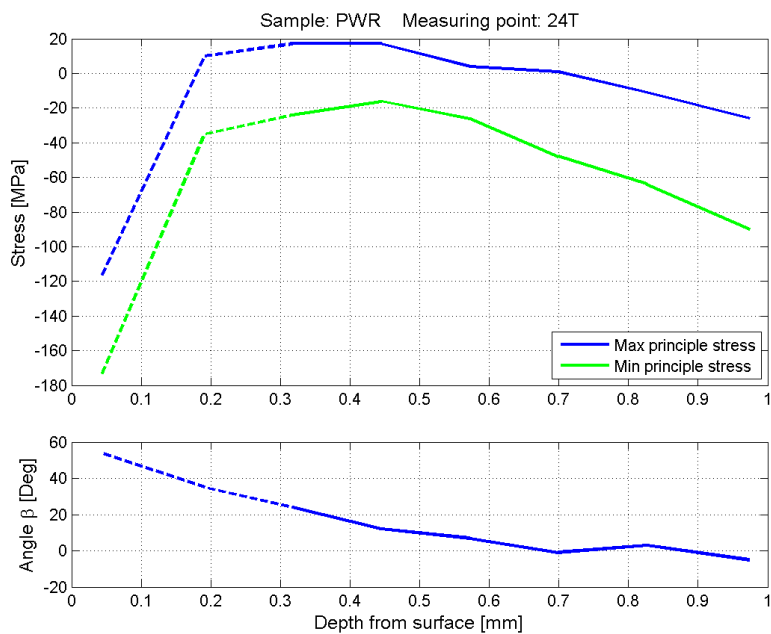
Figure A4:39 Principal stresses calculated for Measuring point 22 on the PWR sample

Appendix 4



Depth mm	σ_{Max} MPa	σ_{Min} MPa	β Deg
0.04	-157	-248	31
0.19	14	-56	45
0.32	35	-2	51
0.45	39	28	40
0.57	-5	-53	30
0.70	37	-38	30
0.83	3	-39	29
0.97	34	-29	16

Figure A4:40 Principal stresses calculated for Measuring point 23 on the PWR sample.



Depth mm	σ_{Max} MPa	σ_{Min} MPa	β Deg
0.04	-118	-175	54
0.19	10	-35	35
0.32	17	-24	24
0.45	17	-16	12
0.57	4	-26	7
0.70	1	-48	-1
0.83	-11	-64	3
0.97	-26	-90	-5

Figure A4:41 Principal stresses calculated for Measuring point 24T on the PWR sample

Appendix 4

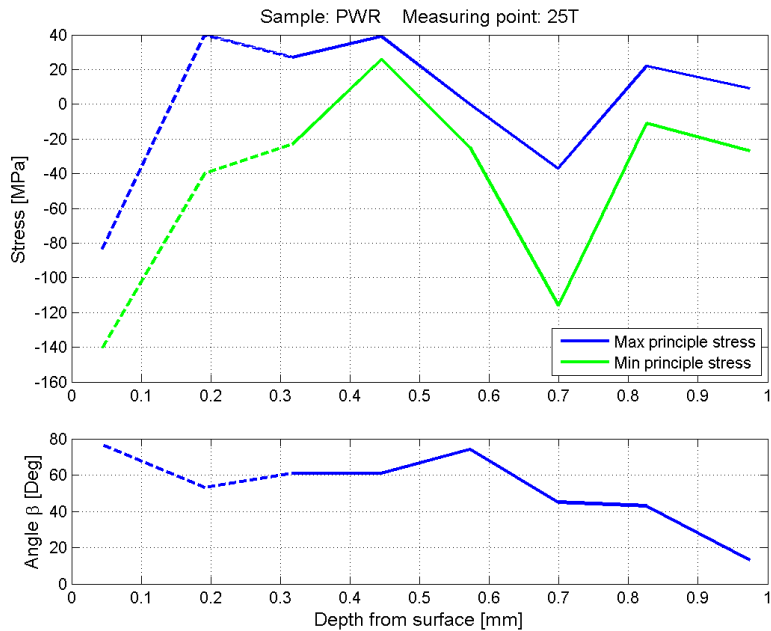


Figure A4:42 Principal stresses calculated for Measuring point 25T on the PWR sample

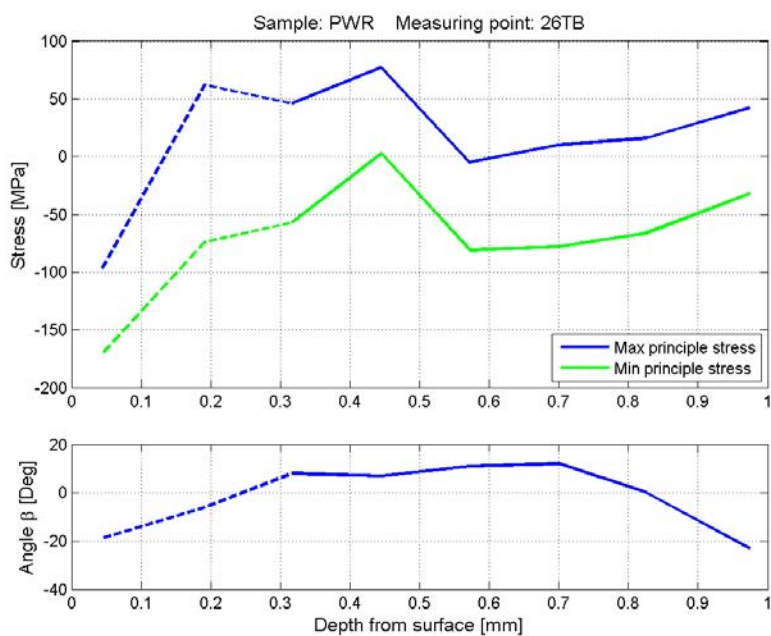
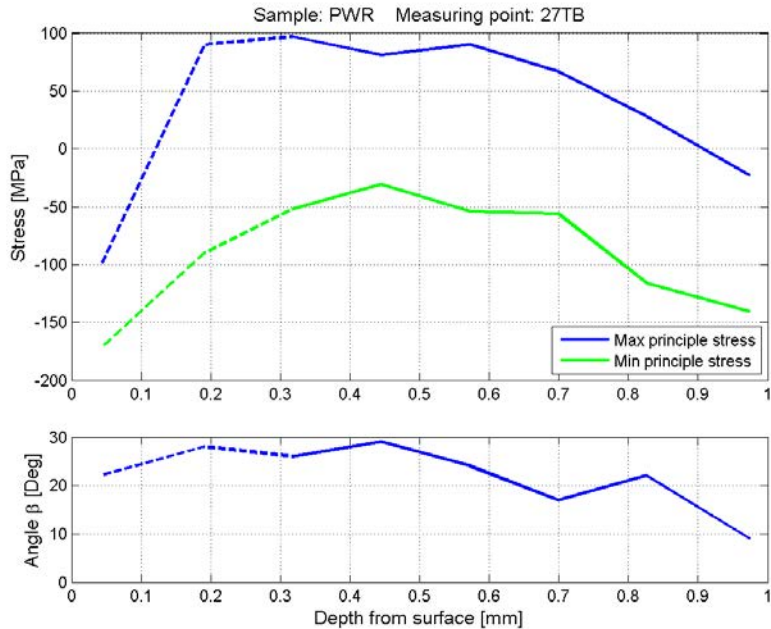


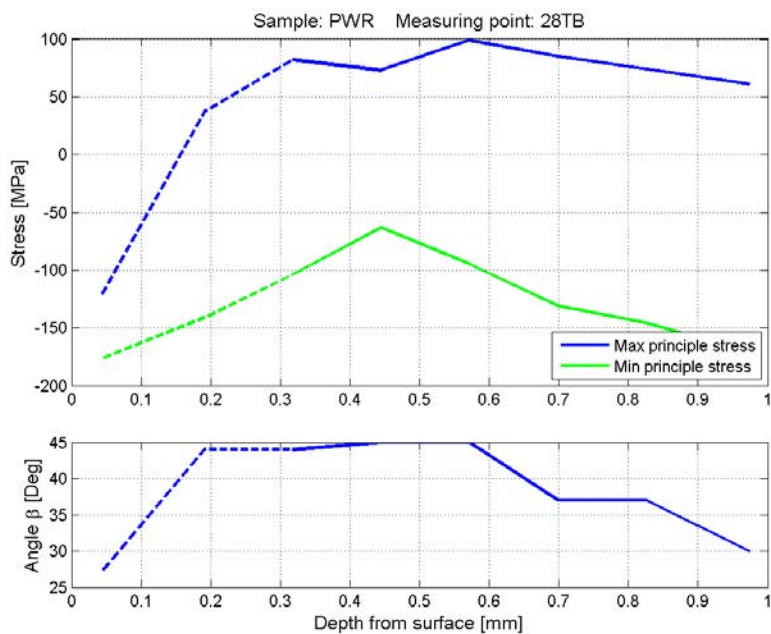
Figure A4:43 Principal stresses calculated for Measuring point 26TB on the PWR sample

Appendix 4



Depth mm	σ_{Max} MPa	σ_{Min} MPa	β Deg
0.04	-101	-172	22
0.19	90	-90	28
0.32	97	-52	26
0.45	81	-31	29
0.57	90	-54	24
0.70	67	-56	17
0.83	28	-116	22
0.97	-23	-141	9

Figure A4:44 Principal stresses calculated for Measuring point 27TB on the PWR sample



Depth mm	σ_{Max} MPa	σ_{Min} MPa	β Deg
0.04	-123	-177	27
0.19	37	-141	44
0.32	82	-104	44
0.45	73	-63	45
0.57	99	-95	45
0.70	85	-131	37
0.83	74	-146	37
0.97	61	-172	30

Figure A4:45 Principal stresses calculated for Measuring point 28TB on the PWR sample

Appendix 4

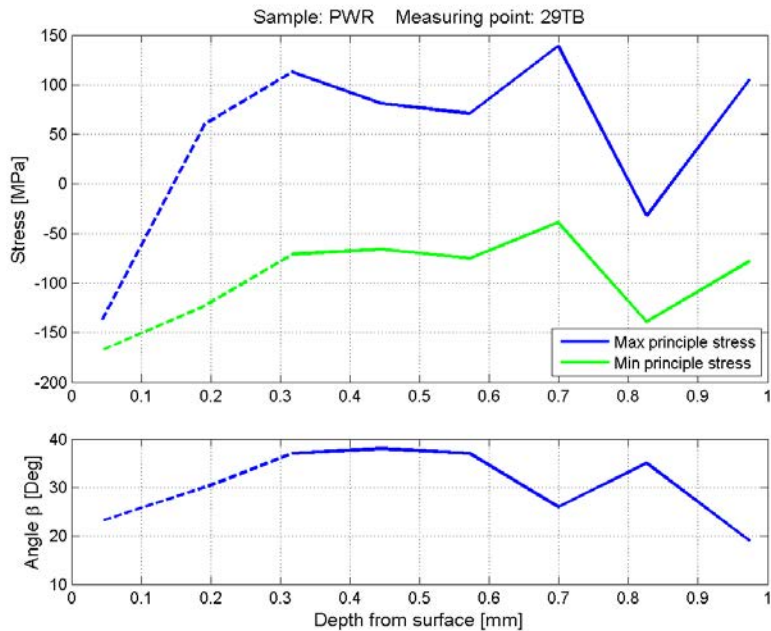


Figure A4:46 Principal stresses calculated for Measuring point 29TB on the PWR sample

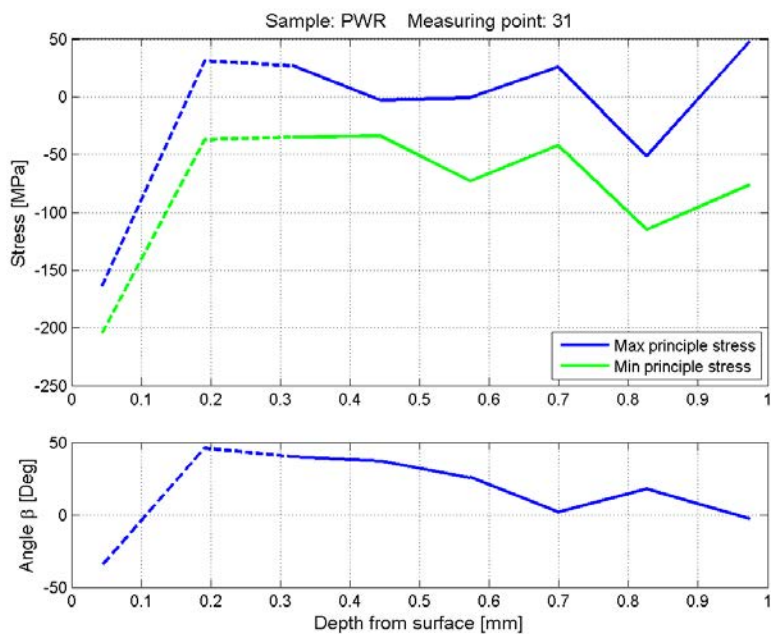


Figure A4:47 Principal stresses calculated for Measuring point 31 on the PWR sample

Appendix 4

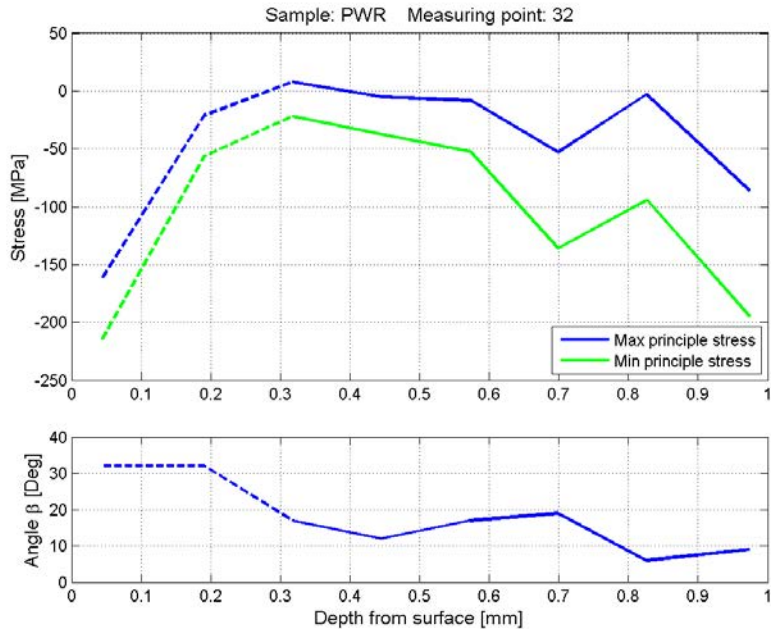


Figure A4:48 Principal stresses calculated for Measuring point 32 on the PWR sample.

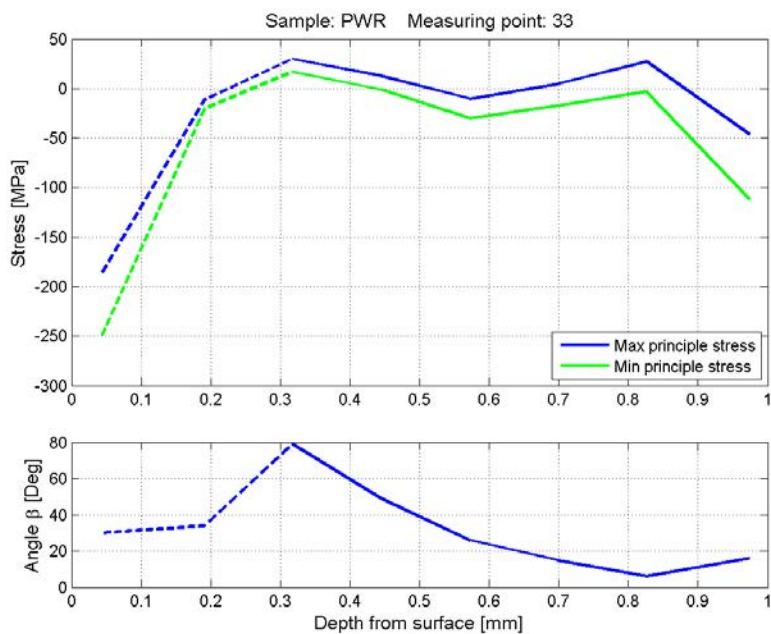


Figure A4:49 Principal stresses calculated for Measuring point 33 on the PWR sample. For the shaded stresses the von Mises effective stress is larger than 70% of the yield stress and therefore they are not reliable.

Appendix 4

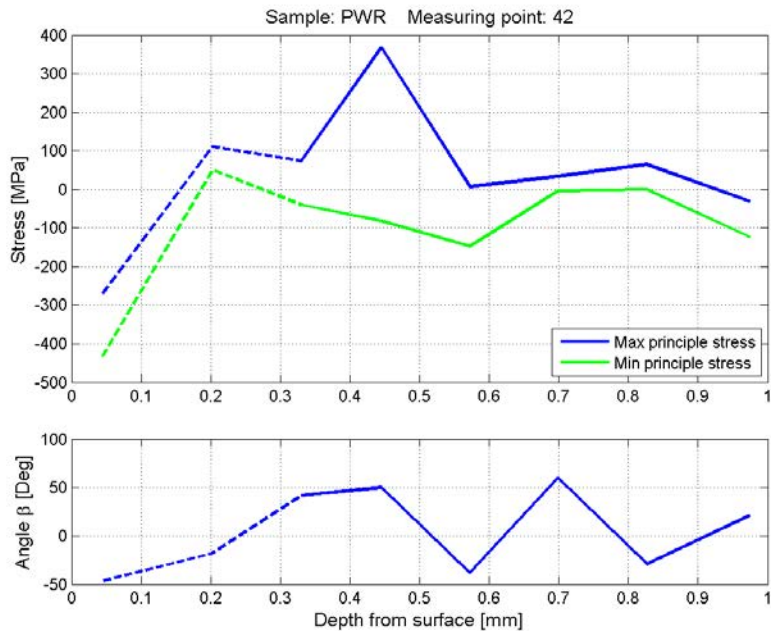


Figure A4:50 Principal stresses calculated for Measuring point 42 on the PWR sample. For the shaded stresses the von Mises effective stress is larger than 70% of the yield stress and therefore they are not reliable.

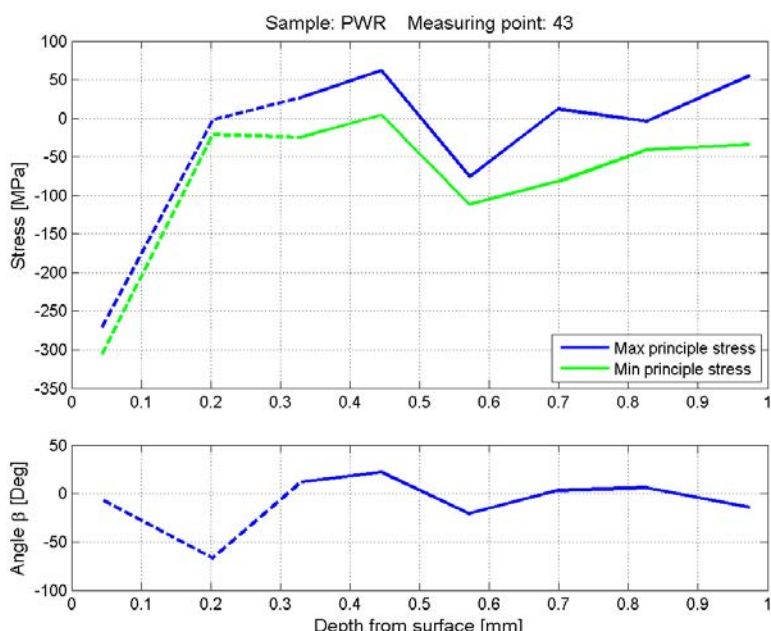


Figure A4:51 Principal stresses calculated for Measuring point 43 on the PWR sample. For the shaded stresses the von Mises effective stress is larger than 70% of the yield stress and therefore they are not reliable.

Appendix 4

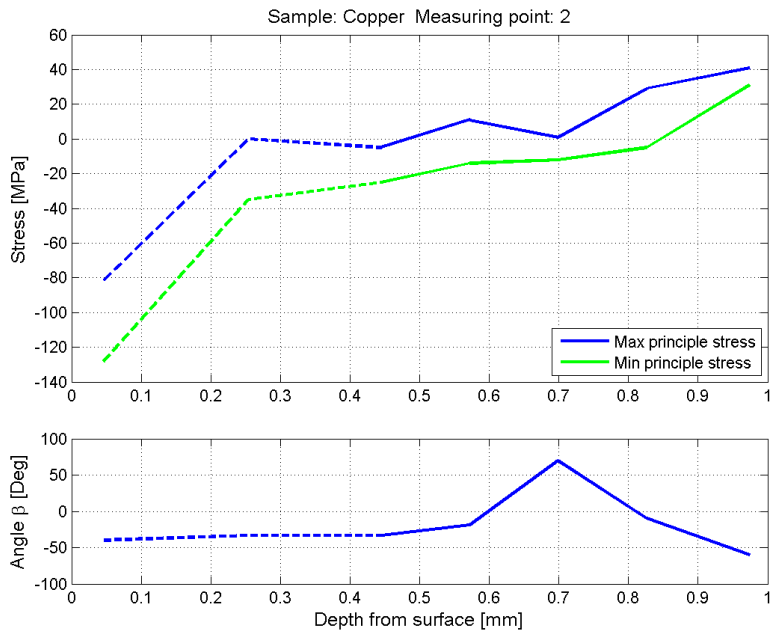


Figure A4:52 Principal stresses calculated for Measuring point 2 on the Copper sample. For the shaded stresses the von Mises effective stress is larger than 70% of the yield stress and therefore they are not reliable.

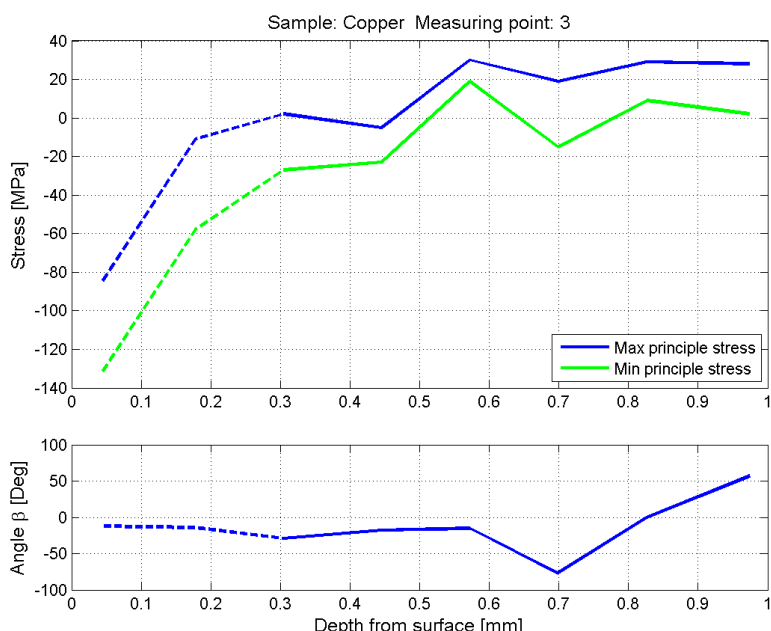


Figure A4:53 Principal stresses calculated for Measuring point 3 on the Copper sample. For the shaded stresses the von Mises effective stress is larger than 70% of the yield stress and therefore they are not reliable.

Appendix 4

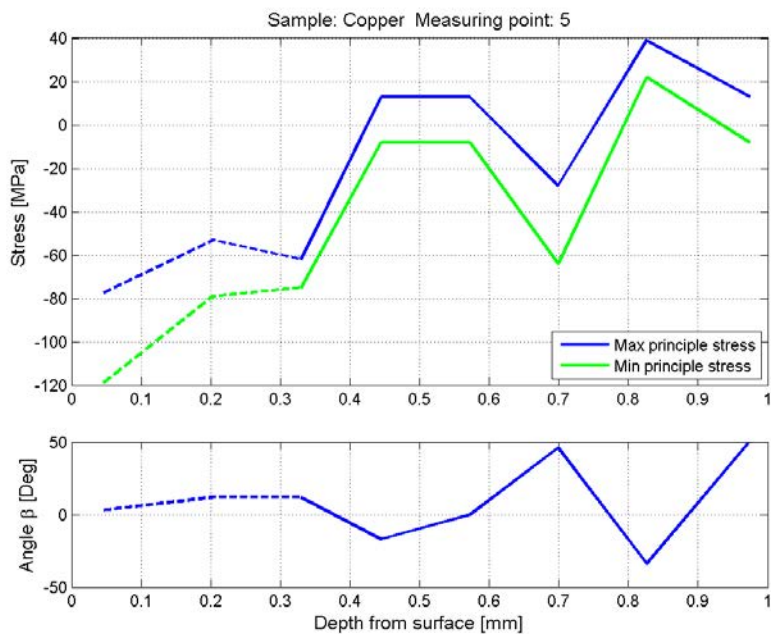
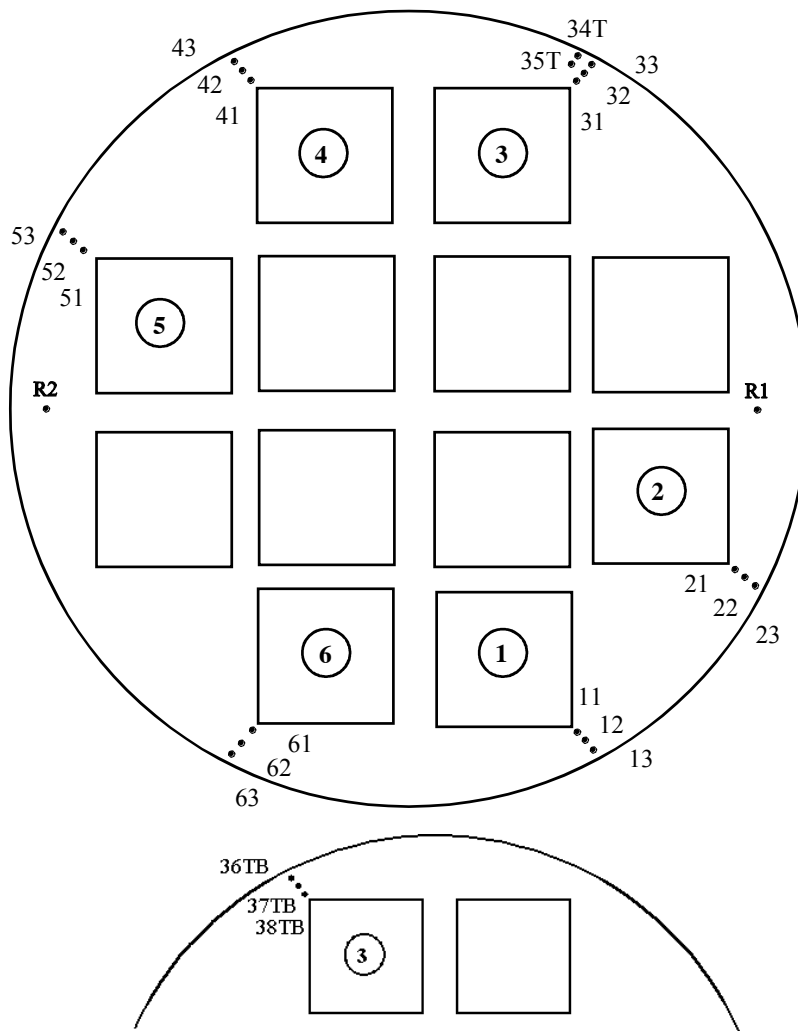


Figure A4:54 Principal stresses calculated for Measuring point 5 on the Copper sample. For the shaded stresses the von Mises effective stress is larger than 70% of the yield stress and therefore they are not reliable.

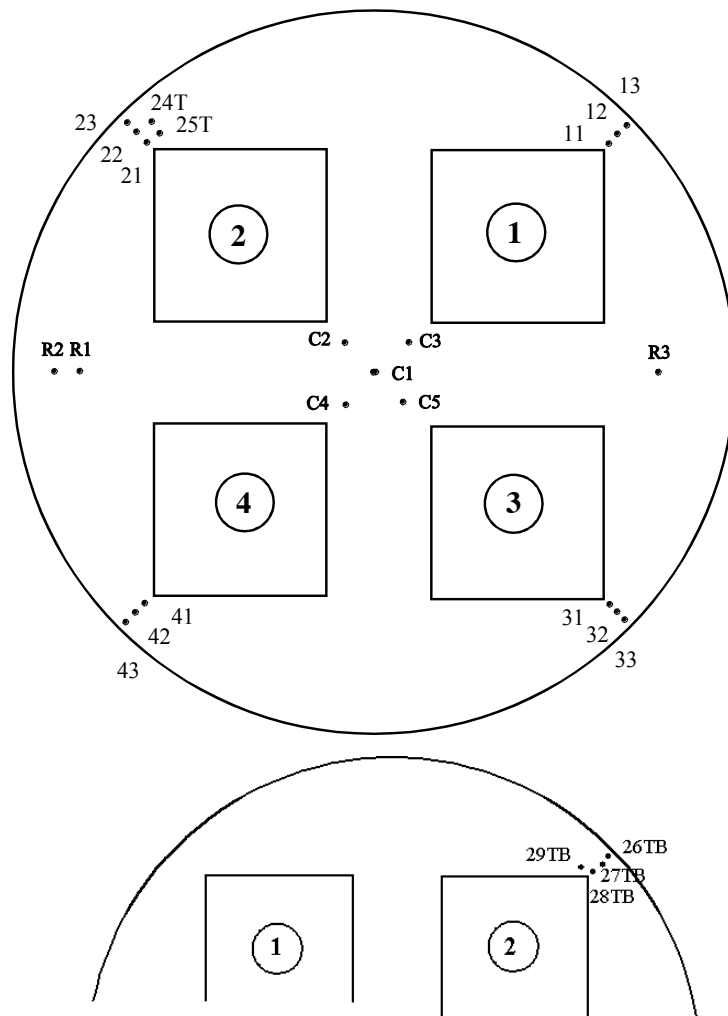
Appendix 4



Point	Max stress	Point	Max stress	Point	Max stress
R1	101 MPa	R2	55 MPa	---	---
11	49 MPa	12	62 MPa	13	50 MPa
21	91 MPa	22	93 MPa	23	93 MPa
31	143 MPa	32	211 MPa	33	151 MPa
34T	131 MPa	35T	148 MPa	---	---
36TB	34 MPa	37TB	49 MPa	38TB	83 MPa
41T	140 MPa	42	95 MPa	43	70 MPa
51	44 MPa	52	39 MPa	53	34 MPa
61	74 MPa	62	93 MPa	63	87 MPa

Figure A4:55 A summary of the results from the measurement on BWR sample. For each measurement point the maximum calculated tensile stress value is given. The aim of this table is to give a quick view of the results and it will not replace the results given in the previous figures. According to the main report the uncertainty in the reported values is less than 20%

Appendix 4



Point	Max stress	Point	Max stress	Point	Max stress
R1	360 MPa	R2	117 MPa	R3	853 MPa
C1	331 MPa	C2	205 MPa	C3	104 MPa
C4	53 MPa	C5	119 MPa	---	---
11	25 MPa	12	37 MPa	13	210 MPa
21	119 MPa	22	80 MPa	23	39 MPa
24T	17MPa	25T	40MPa	---	---
26TB	77MPa	27TB	97MPa	28TB	99MPa
29TB	139MPa	---	---	---	---
31	48 MPa	32	8 MPa	33	30 MPa
41	---	42	368 MPa	43	62 MPa

Figure A4:56

A summary of the results from the measurement on PWR sample. For each measurement point the maximum calculated tensile stress value is given. The aim of this table is to give a quick view of the results and it will not replace the results given in the previous figures. The shaded values are above 70% of the yield stress and therefore not reliable. According to the main report the uncertainty in the reported values is less than 20%

Appendix 5

Normal and shear stresses in a global coordinate system

In Appendix 4 the principle stresses are calculated from the measured strains and calculated by the integral method. In this appendix these stresses are expressed in the local coordinate system referring to the gages and in a global coordinate system referring to the directions in the insert tube. A summary of the results, i.e. the hoop stresses are given in Table A5: 6 - Table A5: 15

The gages in the rosette are named Strain gage 1, Strain gage 2 and Strain gage 3 according to Figure A5: 1.

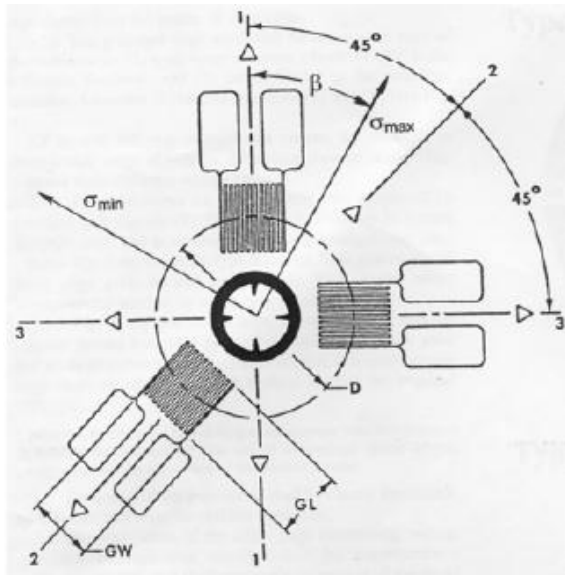


Figure A5: 1 A sketch showing the orientations of the three strain gages and the definition of the angle β .

In this report the X-direction is the direction of Strain gage 1 and the Y-direction is the direction of Strain gage 3. The angle β is the clockwise angle between Strain gage 1 and the maximum principle stress. With this directions the stresses in the local coordinate system can be calculated from Figure A5: 2

For each measuring point one table and one graph are supplied. All calculated stresses are shown in the table.

All graphs show large compressive stresses close to the surface. These stresses are with a high degree of probability caused by the machining when the samples were cut out from the inserts. I.e. the high compressive stresses are not representative for the insets and therefore they are plotted with dashed curves.

Calculated stresses are considered to be not reliable if the corresponding von Mises effective stress is larger than 70% of the yield stress. In those cases the calculated stress values are shaded.

Appendix 5

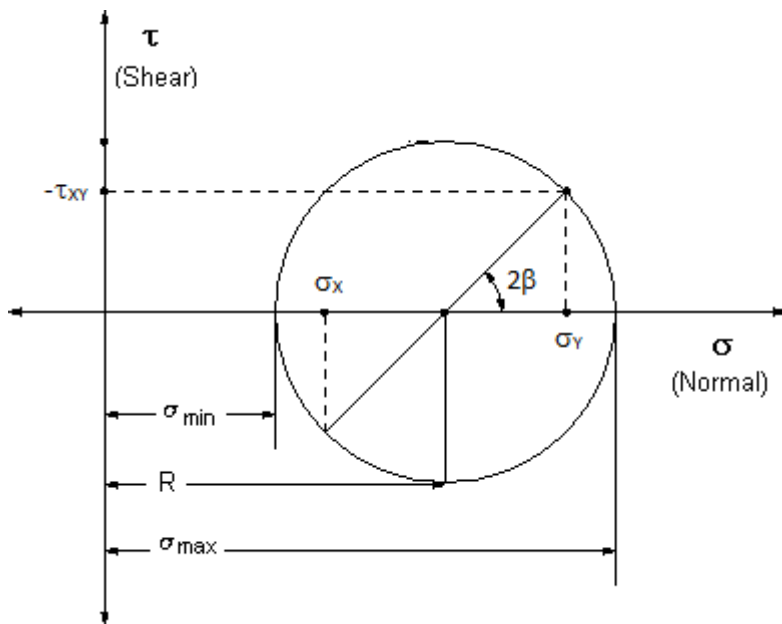


Figure A5: 2 Mohrs circle, with the directions and angles defined in Figure A5: 1. Mohrs circle is used for calculating the stresses in the local coordinate system.

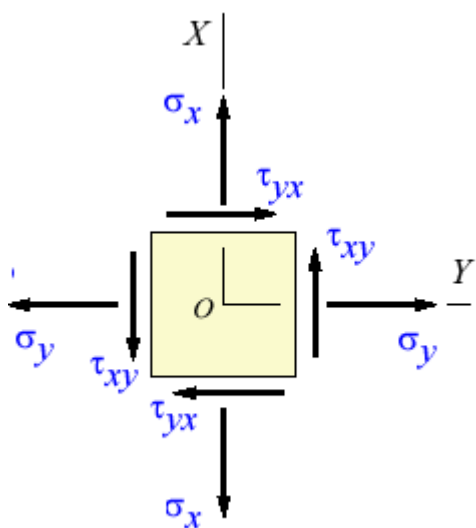


Figure A5: 3 Definition of the directions for the local stresses

Appendix 5

As global coordinate system for the insert tube, cylindrical coordinates (r, θ, z) are used, see Figure A5: 4.

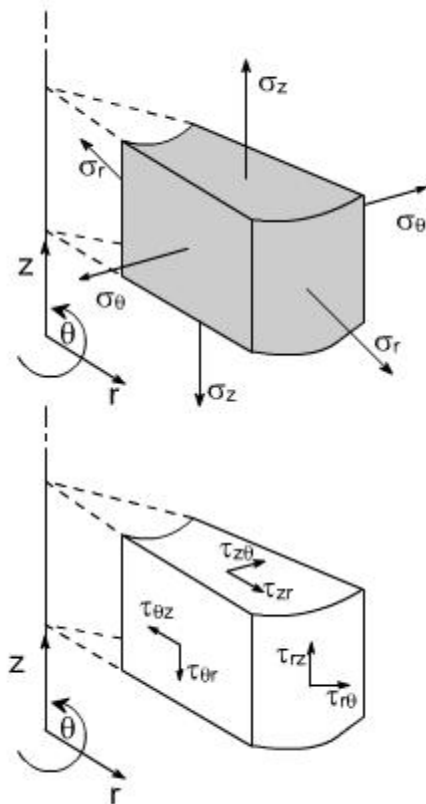


Figure A5: 4 The global coordinate referring to the insert tube, The hoop direction is named θ , the axial z and the radial r .

At the measurements done at SP, a 75 mm thick specimens cut in parallel with the end surfaces of the insert tube were used. The surface of the specimen is in the (r, θ) plane. Then the stresses σ_r , σ_θ and $\tau_{r\theta}$ can be determined. VEQTER, Ref [10], used an insert tube and the drilling was done from the mantle surface in the (r, θ) plane. Then σ_θ , σ_z , and $\tau_{\theta z}$ can be determined. That is, only the hoop stress (σ_θ) is common and can be compared.

For the BWR sample none of the local coordinates is consistent with the hoop direction, so the hoop stress must be calculate, which can be done with a standard formula. But for the PWR sample all gages were oriented so that the hoop stress corresponds to either the X- or the Y-direction (gage C1 was placed at a singular point in the cylindrical coordinate system).

Appendix 5

Table A5: 1 The angle between the Y-direction and the hoop direction for the measuring points at the BWR sample

Measuring point	Angle to Y-direction	Measuring point	Angle to Y-direction	Measuring point	Angle to Y-direction
R1	-45	R2	-45	---	---
11	-15	12	-15	13	-15
21	+15	22	+15	23	+15
31	+15	32	+15	33	+15
34T	+15	35T	+15	---	
36TB	-15	37TB	-15	38TB	-15
41	-15	42	-15	43	-15
51	+15	52	+15	53	+15
61	+15	62	+15	63	+15

Table A5: 2 The hoop direction for the PWR sample as a local coordinate

Measuring point	Local direc-tion	Measuring point	Local direc-tion	Measuring point	Local direc-tion
R1	X	R2	X	R3	X
C1	--	C2	Y	C3	Y
C4		C5		---	
11	Y	12	Y	13	Y
21	Y	22	Y	23	Y
24T	Y	25T	Y	---	
26TB	Y	27TB	Y	28TB	Y
29TB	Y	---		---	
31	Y	32	Y	33	Y
41	---	42	Y	43	Y

Appendix 5

Table A5: 3 Figures with local / global stresses in the BWR sample

Measuring point	Figure	Measuring point	Figure	Measuring point	Figure
R1	Fig: A5:5	R2	Fig: A5:6	---	---
11	Fig: A5:7	12	Fig: A5:8	13	Fig: A5:9
21	Fig: A5:10	22	Fig: A5:11	23	Fig: A5:12
31	Fig: A5:13	32	Fig: A5:14	33	Fig: A5:15
34T	Fig: A5:16	35T	Fig: A5:17	---	---
36TB	Fig: A5:18	37TB	Fig: A5:19	38TB	Fig: A5:20
41	Fig: A5:21	42	Fig: A5:22	43	Fig: A5:23
51	Fig: A5:24	52	Fig: A5:25	53	Fig: A5:26
61	Fig: A5:27	62	Fig: A5:28	63	Fig: A5:29

Table A5: 4 Figures with local / global stresses in the PWR sample

Measuring point	Figure	Measuring point	Figure	Measuring point	Figure
R1	Fig: A5:30	R2	Fig: A5:31	R3	Fig: A5:32
C1	Fig: A5:33	C2	Fig: A5:34	C3	Fig: A5:35
C4	Fig: A5:36	C5	Fig: A5:37	---	---
11	Fig: A5:38	12	Fig: A5:39	13	Fig: A5:40
21	Fig: A5:41	22	Fig: A5:42	23	Fig: A5:43
24T	Fig: A5:44	25T	Fig: A5:45	---	---
26TB	Fig: A5:46	27TB	Fig: A5:47	28TB	Fig: A5:48
29TB	Fig: A5:49	---	---	---	---
31	Fig: A5:50	32	Fig: A5:51	33	Fig: A5:52
41	---	42	Fig: A5:53	43	Fig: A5:54

Table A5: 5 Figures with local stresses in the Copper sample

Measuring point	Figure	Measuring point	Figure	Measuring point	Figure
2	Fig: A5:55	3	Fig: A5:56	5	Fig: A5:57

Appendix 5

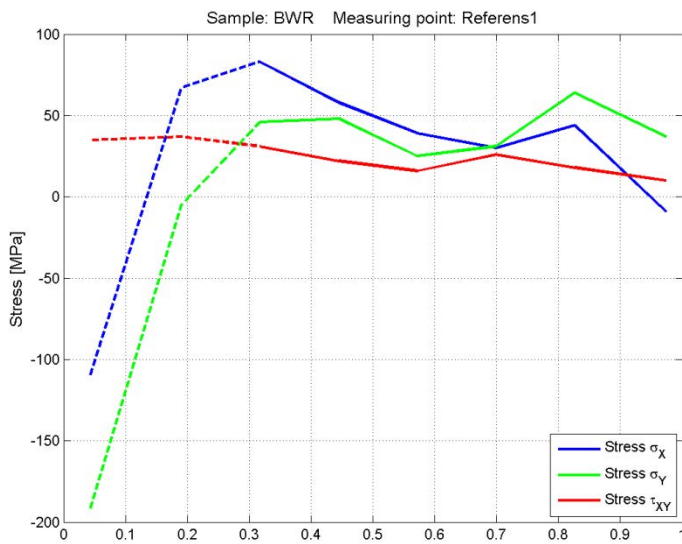


Figure A5: 5 Stresses calculated for Measuring point *R1* on the BWR sample.

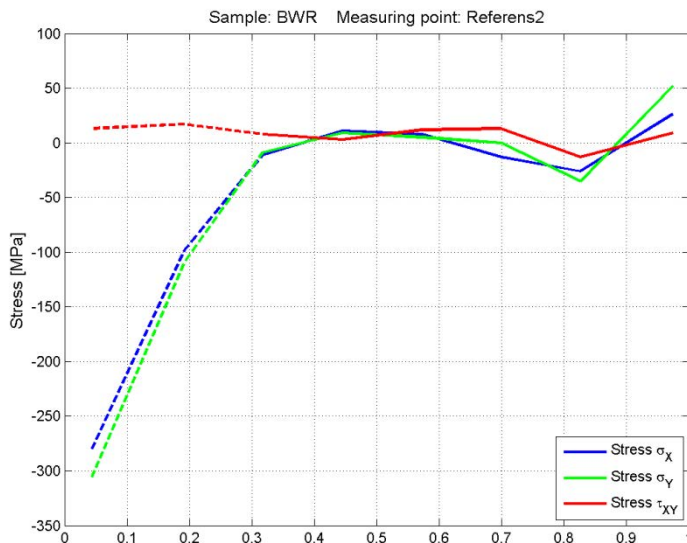
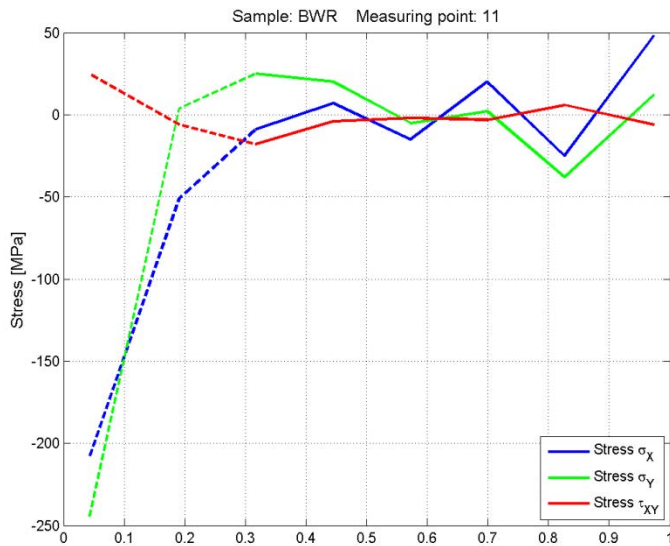


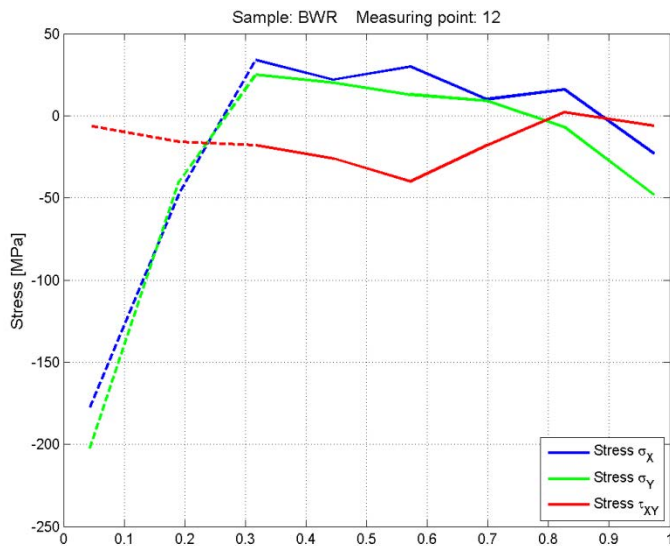
Figure A5: 6 Stresses calculated for Measuring point *R2* on the BWR sample. For the shaded stresses the von Mises effective stress is larger than 70% of the yield stress and therefore they are not reliable

Appendix 5



Depth mm	σ_x MPa	σ_y MPa	τ_{xy} MPa	σ_e MPa	σ_θ MPa
0.04	-209	-246	25	229	-256
0.10	-51	4	-6	52	3
0.32	-9	25	-18	29	31
0.50	7	20	-4	17	21
0.57	-15	-5	-2	13	-4
0.70	20	2	-3	18	4
0.83	-25	-38	6	33	-40
0.97	48	12	-6	43	17

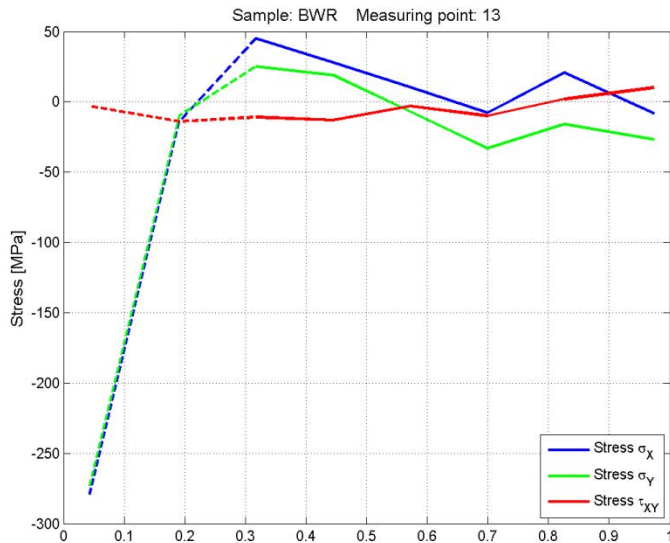
Figure A5: 7 Stresses calculated for Measuring point 11 on the BWR sample. For the shaded stresses the von Mises effective stress is larger than 70% of the yield stress and therefore they are not reliable



Depth mm	σ_x MPa	σ_y MPa	τ_{xy} MPa	σ_e MPa	σ_θ MPa
0.04	-179	-204	-6	192	-199
0.19	-47	-40	-16	43	-32
0.32	34	25	-18	29	34
0.45	22	20	-26	19	33
0.57	30	13	-40	23	34
0.70	10	9	-18	6	18
0.83	16	-7	2	20	-6
0.97	-23	-48	-6	41	-43

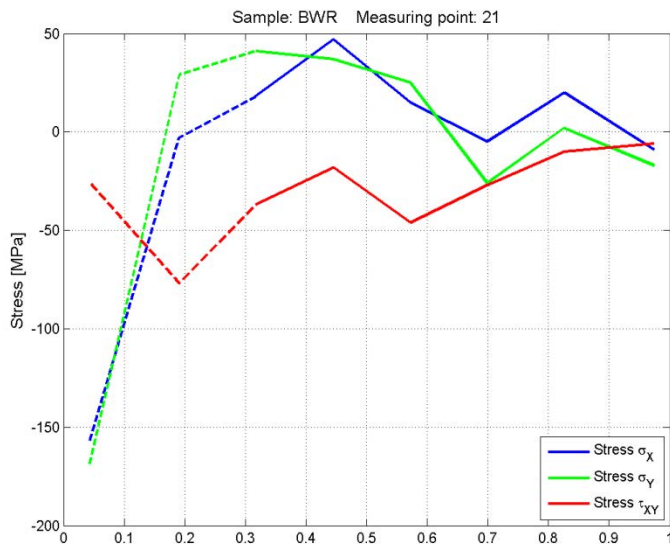
Figure A5: 8 Stresses calculated for Measuring point 12 on the BWR sample. For the shaded stresses the von Mises effective stress is larger than 70% of the yield stress and therefore they are not reliable

Appendix 5



Depth mm	σ_x MPa	σ_y MPa	τ_{xy} MPa	σ_e MPa	σ_θ MPa
0.04	-281	-275	-3	278	-273
0.19	-14	-10	-14	10	-3
0.32	45	25	-11	38	31
0.45	28	19	-13	23	26
0.57	10	-7	-3	14	-4
0.70	-8	-33	-10	29	-26
0.83	21	-16	2	32	-14
0.97	-8	-27	10	24	-30

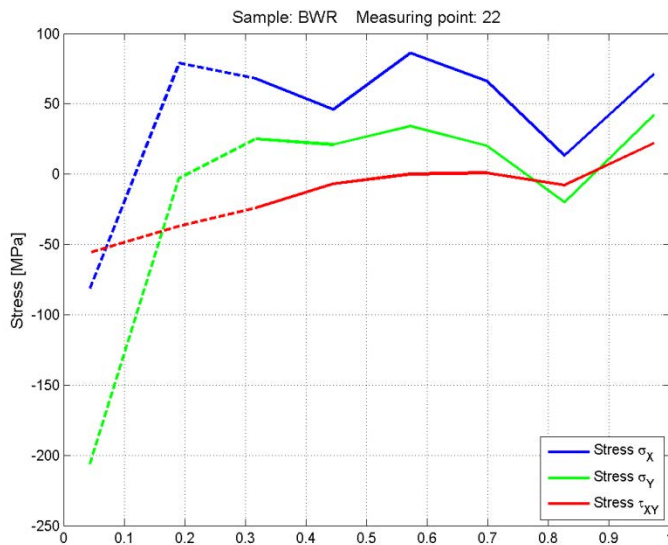
Figure A5: 9 Stresses calculated for Measuring point 13 on the BWR sample. For the shaded stresses the von Mises effective stress is larger than 70% of the yield stress and therefore they are not reliable



Depth mm	σ_x MPa	σ_y MPa	τ_{xy} MPa	σ_e M a	σ_θ Pa
0.04	-158	-170	-25	164	-181
0.19	-3	29	-77	26	-11
0.32	18	41	-37	34	20
0.45	47	37	-18	42	28
0.57	15	25	-46	18	1
0.70	-5	-26	-27	22	-38
0.83	20	2	-10	18	-1
0.97	-9	-17	-6	14	-19

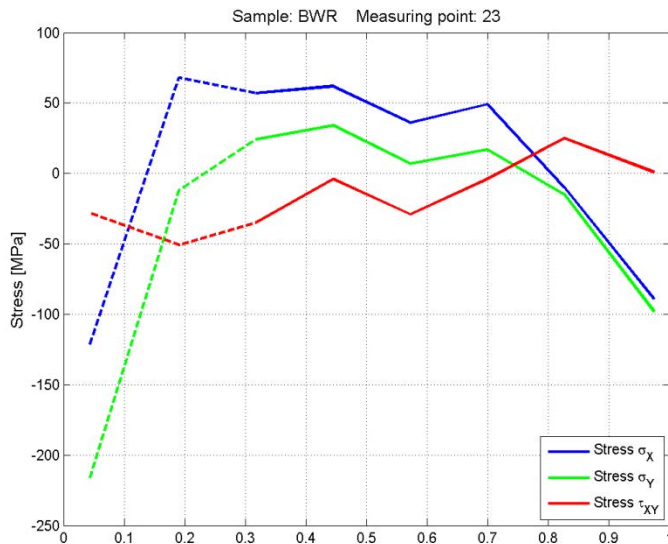
Figure A5: 10 Stresses calculated for Measuring point 21 on the BWR sample

Appendix 5



Depth mm	σ_x MPa	σ_y MPa	τ_{xy} MPa	σ_e MPa	σ_θ MPa
0.04	-83	-208	-56	180	-227
0.19	79	-3	-37	79	-16
0.32	68	25	-24	58	15
0.45	46	21	-7	39	19
0.57	86	34	0	75	37
0.70	66	20	1	58	23
0.83	13	-20	-8	28	-21
0.97	71	42	22	62	54

Figure A5: 11 Stresses calculated for Measuring point 22 on the BWR sample.



Depth mm	σ_x MPa	σ_y MPa	τ_{xy} MPa	σ_e MPa	σ_θ MPa
0.04	-123	-218	-28	189	-225
0.19	68	-12	-51	73	-32
0.32	57	24	-35	48	8
0.45	62	34	-4	53	33
0.57	36	7	-29	31	-5
0.70	49	17	-4	42	17
0.83	-10	-15	25	15	-2
0.97	-89	-98	1	93	-96

Figure A5: 12 Stresses calculated for Measuring point 23 on the BWR sample.

Appendix 5

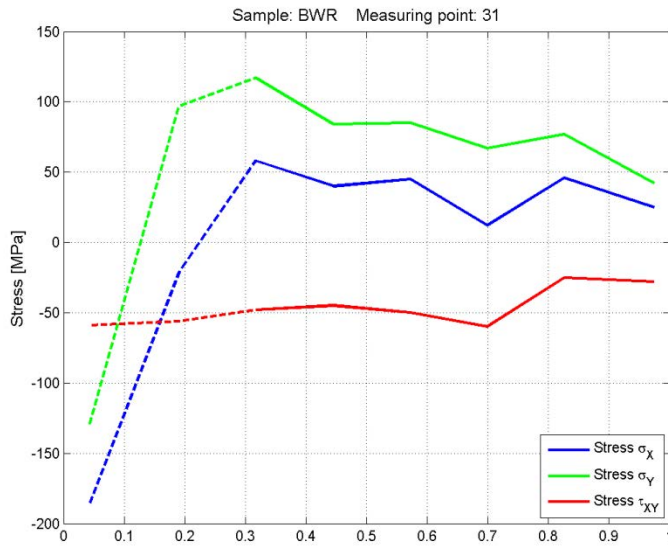


Figure A5: 13 Stresses calculated for Measuring point 31 on the BWR sample.

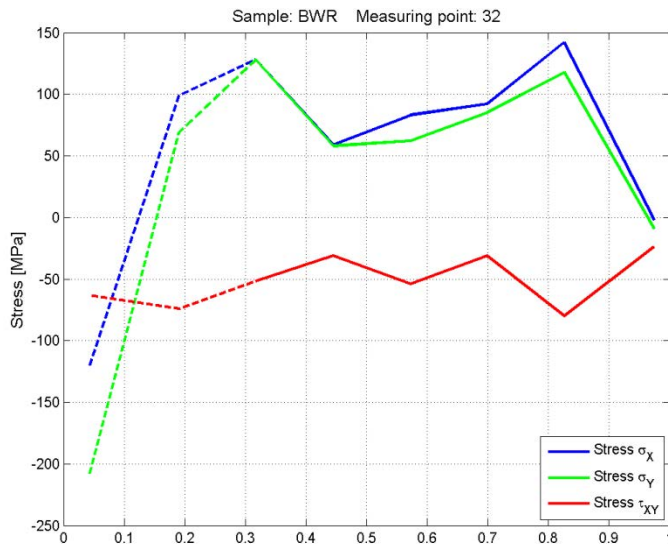


Figure A5: 14 Stresses calculated for Measuring point 32 on the BWR sample.

Appendix 5

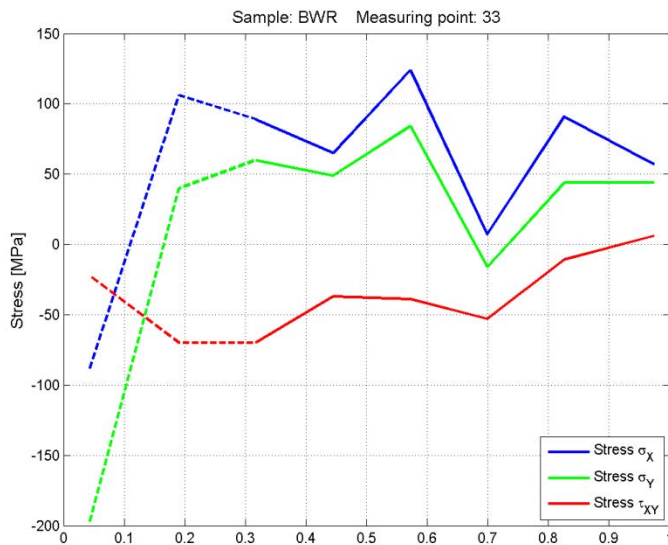


Figure A5: 15 Stresses calculated for Measuring point 33 on the BWR sample.

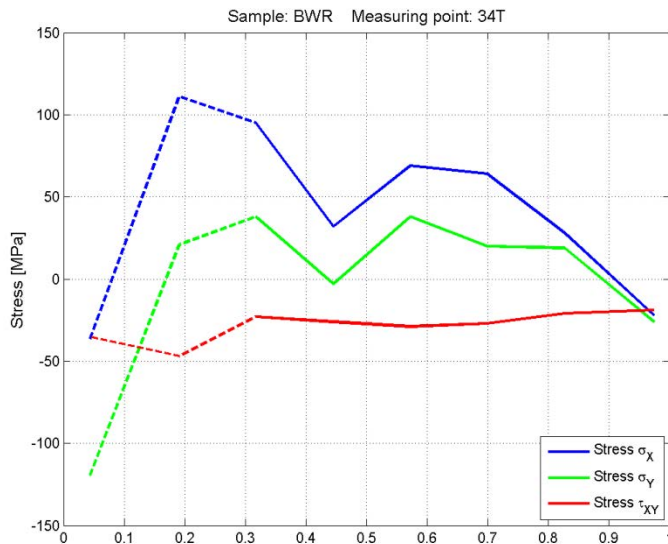
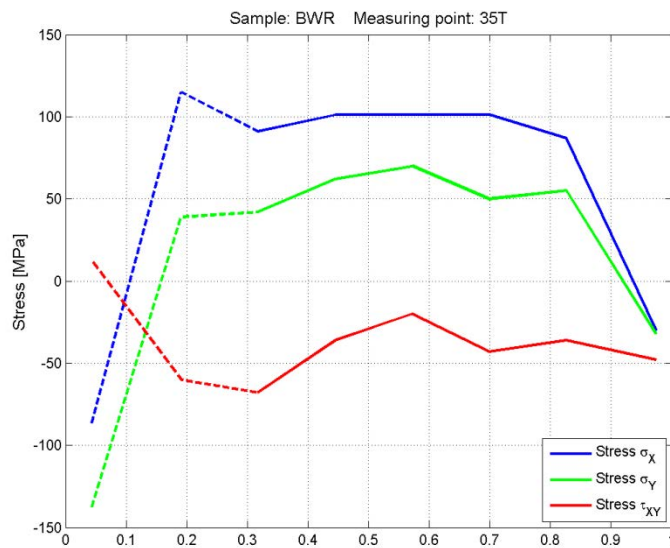


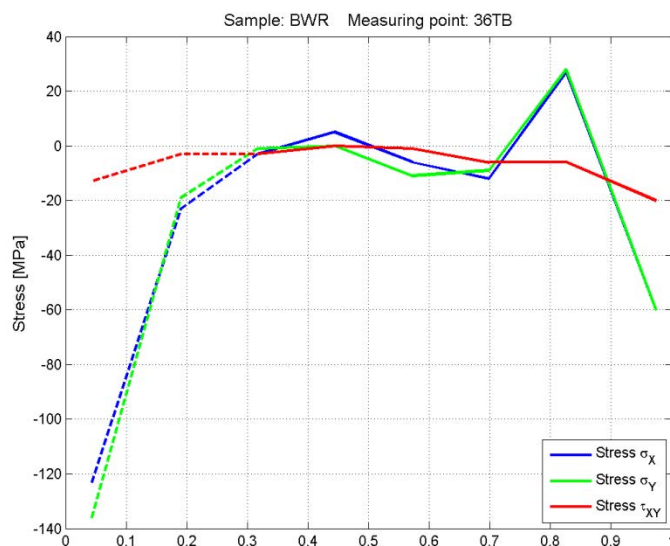
Figure A5: 16 Stresses calculated for Measuring point 34T on the BWR sample

Appendix 5



Depth mm	σ_x MP	σ_y Pa	τ_{xy} MPa	σ_e MPa	σ_θ MPa
0.04	-88	-139	13	121	-129
0.19	115	39	-60	100	14
0.32	91	42	-68	77	11
0.45	101	62	-36	87	46
0.57	101	70	-20	89	62
0.70	101	50	-43	86	31
0.83	87	55	-36	75	39
0.97	-30	-32	-48	28	-55

Figure A5: 17 Stresses calculated for Measuring point 35T on the BWR sample



Depth mm	σ_x MPa	σ_y MPa	τ_{xy} MPa	σ_e MPa	σ_θ MPa
0.04	-124	-137	-13	130	-129
0.1	-23	-19	-3	21	-17
0.32	-3	-1	-3	0	0
0.45	5	0	0	5	0
0.57	-6	-11	-1	9	-10
0.70	-12	-9	-6	9	-6
0.83	27	28	-6	27	30
0.97	-60	-60	-20	59	-50

Figure A5: 18 Stresses calculated for Measuring point 36TB on the BWR sample

Appendix 5

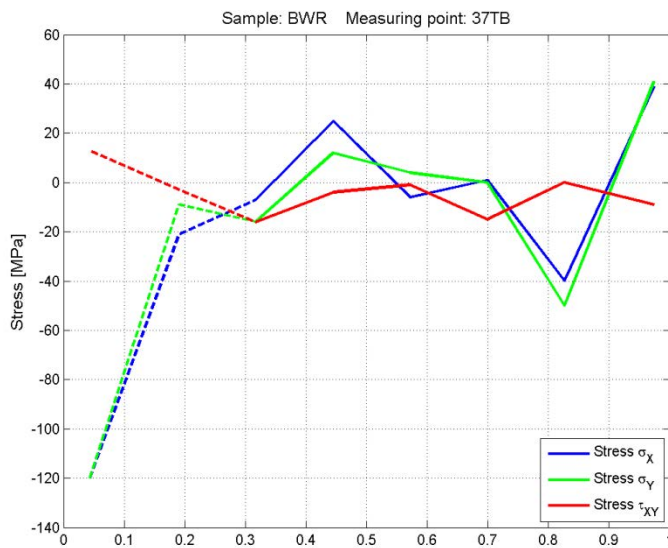


Figure A5: 19 Stresses calculated for Measuring point 37TB on the BWR sample

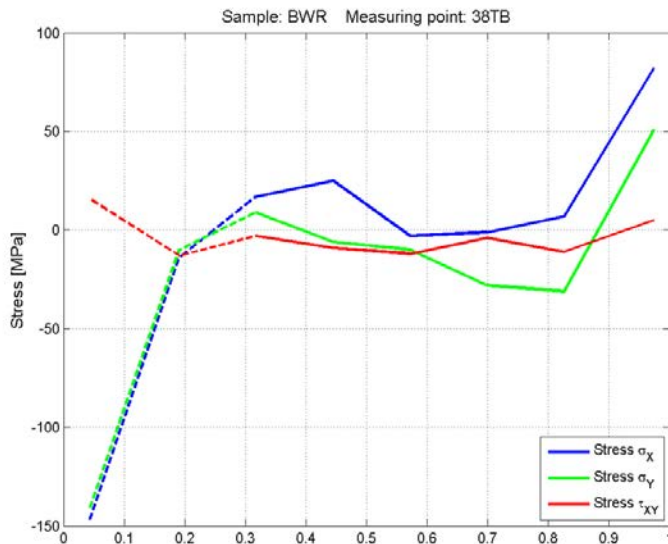


Figure A5: 20 Stresses calculated for Measuring point 38TB on the BWR sample

Appendix 5

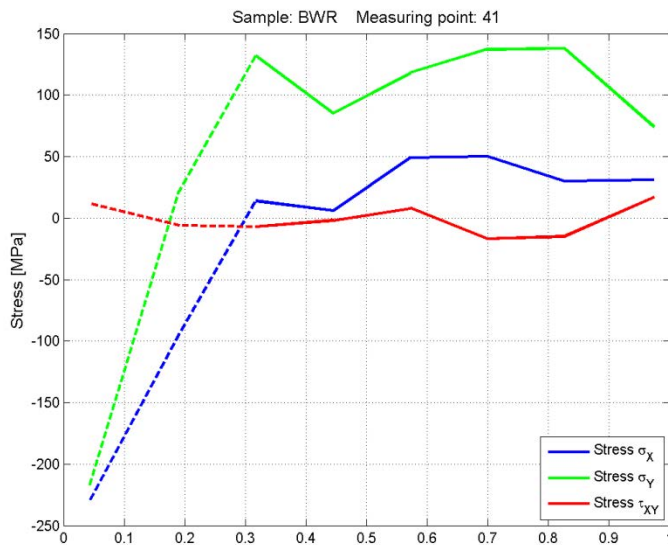


Figure A5: 21 Stresses calculated for Measuring point 41 on the BWR sample. For the shaded stresses the von Mises effective stress is larger than 70% of the yield stress and therefore they are not reliable

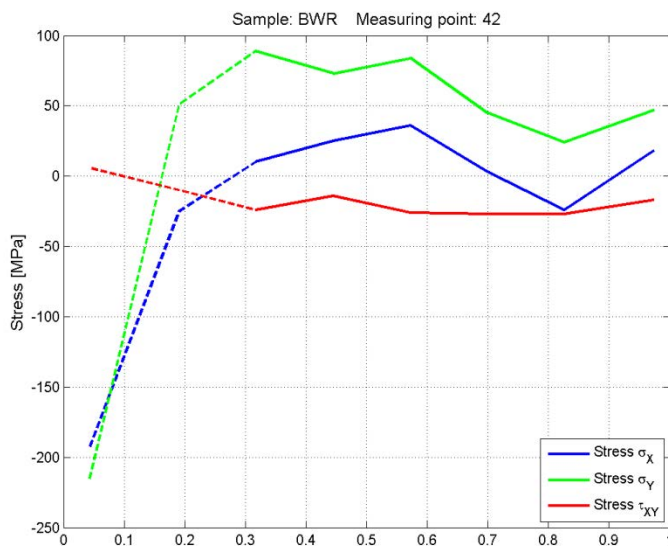
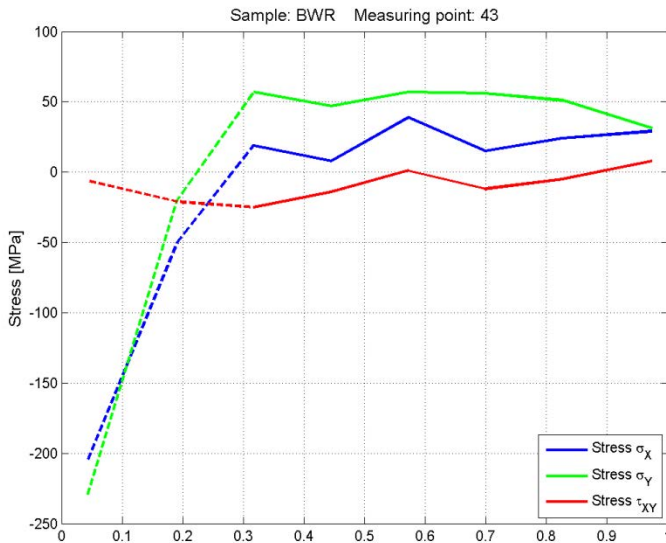


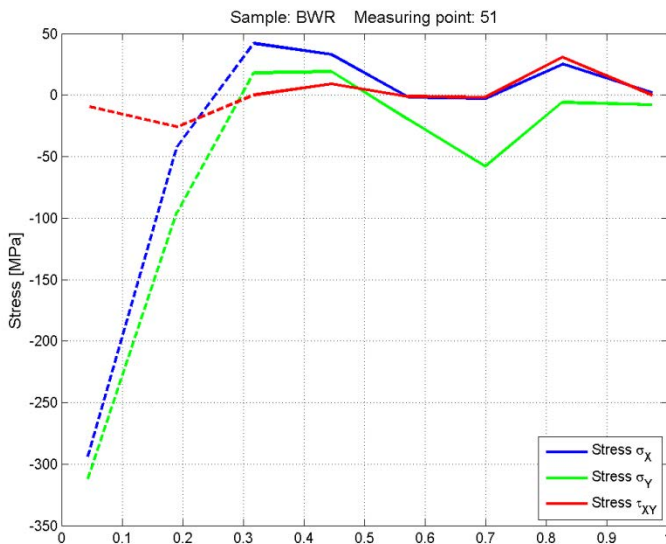
Figure A5: 22 Stresses calculated for Measuring point 42 on the BWR sample. For the shaded stresses the von Mises effective stress is larger than 70% of the yield stress and therefore they are not reliable

Appendix 5



Depth mm	σ_x MPa	σ_y MPa	τ_{xy} MPa	σ_e MPa	σ_θ MPa
0.04	-206	-231	-6	219	-226
0.19	-50	-20	-21	42	-11
0.32	19	57	-25	49	66
0.45	8	47	-14	43	51
0.57	39	57	1	50	55
0.70	15	56	-12	49	59
0.83	24	51	-5	44	51
0.97	29	31	8	30	26

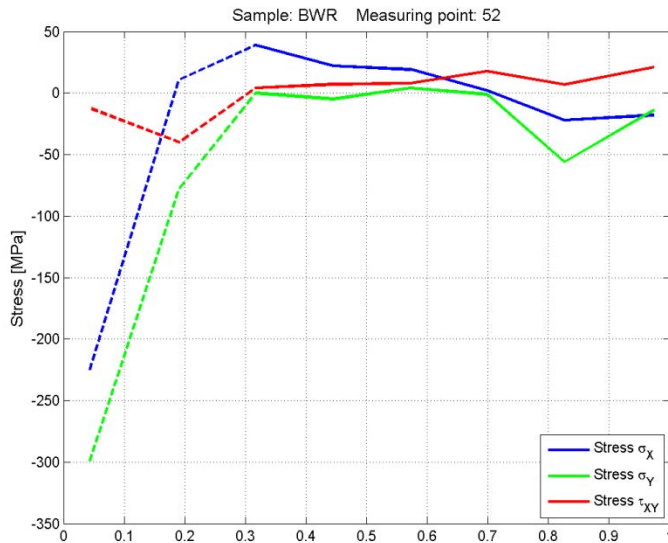
Figure A5: 23 Stresses calculated for Measuring point 43 on the BWR sample. For the shaded stresses the von Mises effective stress is larger than 70% of the yield stress and therefore they are not reliable



Depth mm	σ_x MPa	σ_y MPa	τ_{xy} MPa	σ_e MPa	σ_θ MPa
0.04	-296	-314	-9	305	-317
0.19	-42	-95	-26	81	-104
0.32	42	18	0	36	19
0.45	33	19	9	29	24
0.57	-2	-20	-1	19	-19
0.70	-3	-58	-2	56	-55
0.83	25	-6	31	30	11
0.97	2	-8	0	9	-7

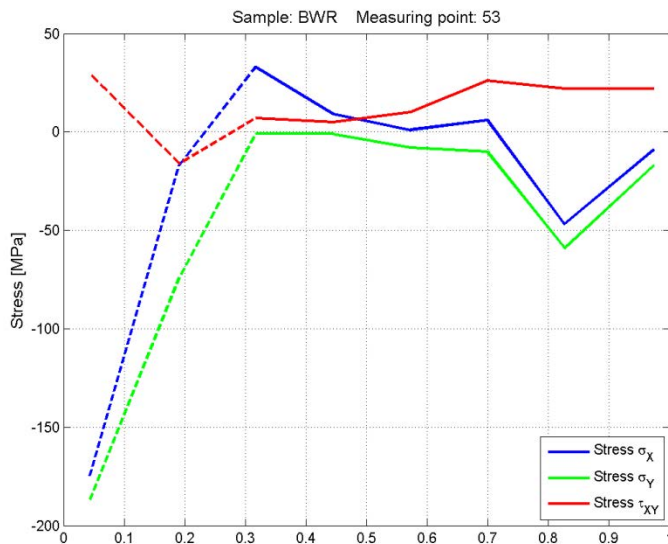
Figure A5: 24 Stresses calculated for Measuring point 51 on the BWR sample. For the shaded stresses the von Mises effective stress is larger than 70% of the yield stress and therefore they are not reliable

Appendix 5



Depth mm	σ_x MPa	σ_y MPa	τ_{xy} MPa	σ_e MPa	σ_θ MPa
0.04	-227	-301	-12	271	-302
0.19	11	-78	-40	83	-92
0.32	39	0	4	39	4
0.45	22	-5	7	25	0
0.57	19	4	8	18	9
0.70	2	-1	18	7	8
0.83	-22	-56	7	49	-50
0.97	-18	-14	21	18	-3

Figure A5: 25 Stresses calculated for Measuring point 52 on the BWR sample. For the shaded stresses the von Mises effective stress is larger than 70% of the yield stress and therefore they are not reliable



Depth mm	σ_x MPa	σ_y MPa	τ_{xy} MPa	σ_e MPa	σ_θ MPa
0.04	-176	-188	30	182	-172
0.19	-17	-74	-16	66	-78
0.32	33	-1	7	33	4
0.45	9	-1	5	10	2
0.57	1	-8	10	10	-2
0.70	6	-10	26	16	4
0.83	-47	-59	22	54	-47
0.97	-9	-17	22	16	-5

Figure A5: 26 Stresses calculated for Measuring point 53 on the BWR sample.

Appendix 5

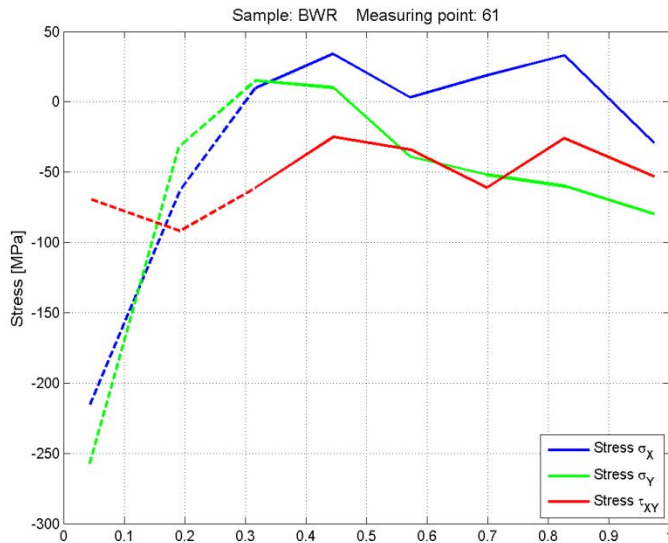


Figure A5: 27 Stresses calculated for Measuring point 61 on the BWR sample. For the shaded stresses the von Mises effective stress is larger than 70% of the yield stress and therefore they are not reliable

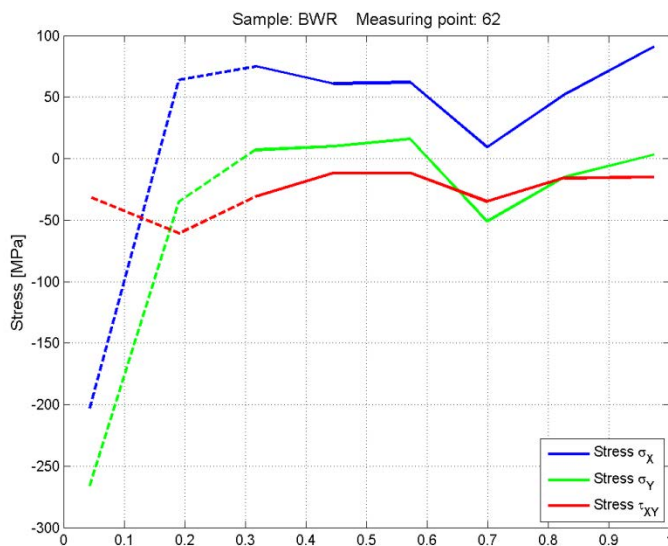
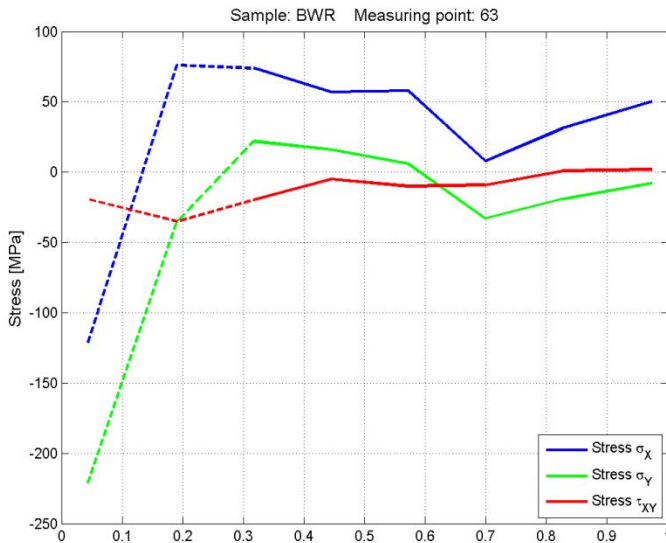


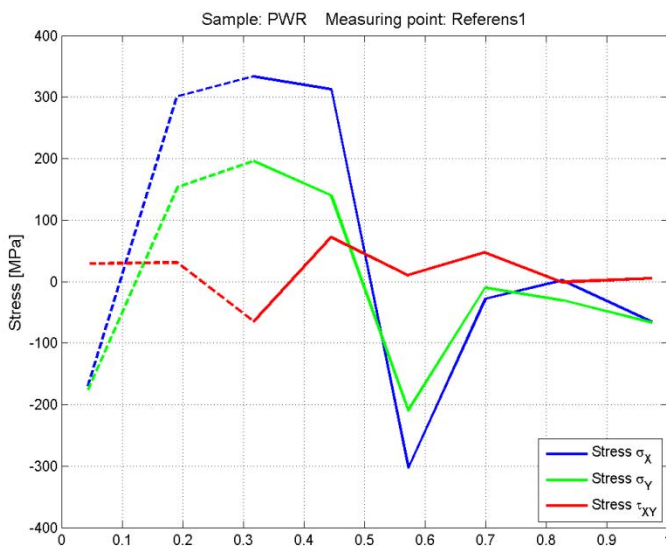
Figure A5: 28 Stresses calculated for Measuring point 62 on the BWR sample. For the shaded stresses the von Mises effective stress is larger than 70% of the yield stress and therefore they are not reliable

Appendix 5



Depth mm	σ_x MPa	σ_y MPa	τ_{xy} MPa	σ_e MPa	σ_θ MPa
0.04	-123	-223	-19	193	-225
0.19	76	-35	-35	97	-45
0.3	74	22	-20	65	15
0.45	57	16	-5	50	16
0.57	58	6	-10	54	4
0.70	8	-33	-9	37	-34
0.83	31	-19	1	43	-15
0.97	50	-8	2	54	-3

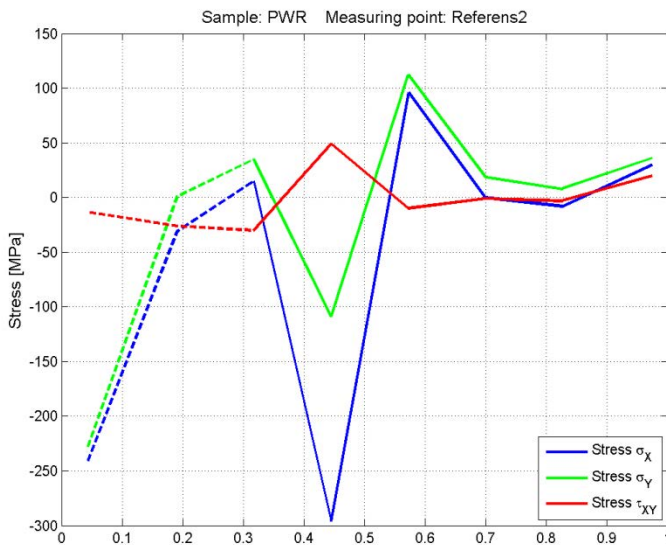
Figure A5: 29 Stresses calculated for Measuring point 63 on the BWR sample. For the shaded stresses the von Mises effective stress is larger than 70% of the yield stress and therefore they are not reliable



Hoop stress: σ_x				
Depth mm	σ_x MPa	σ_y MPa	τ_{xy} MPa	σ_e MPa
0.04	-174	-180	29	177
0.19	301	153	31	260
0.32	334	196	-65	290
0.45	313	140	72	271
0.57	-303	-210	10	268
0.70	-28	-10	47	27
0.83	2	-30	-1	31
0.97	-65	-67	5	66

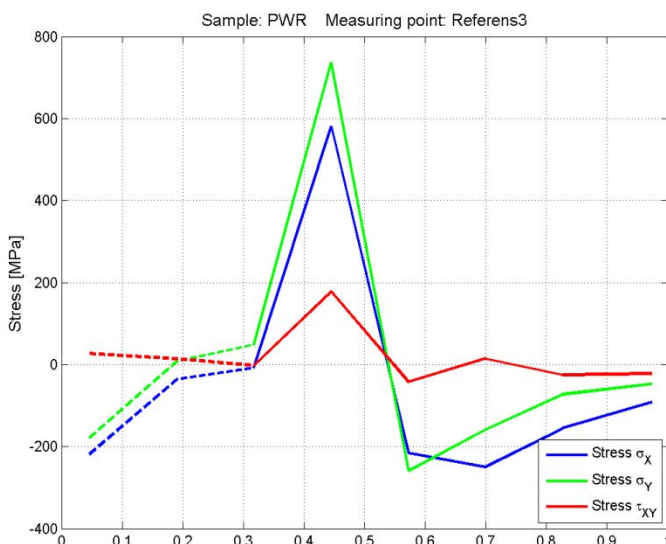
Figure A5: 30 Stresses calculated for Measuring point RI on the PWR sample. For the shaded stresses the von Mises effective stress is larger than 70% of the yield stress and therefore they are not reliable

Appendix 5



Hoop stress: σ_x				
Depth mm	σ_x MPa	σ_y MPa	τ_{xy} MPa	σ_e MPa
0.04	-243	-230	-13	236
0.19	-31	1	-26	30
0.32	15	35	-30	28
0.45	-296	-109	49	259
0.57	96	112	-10	104
0.70	0	19	-1	18
0.83	-8	8	-3	13
0.97	30	36	20	34

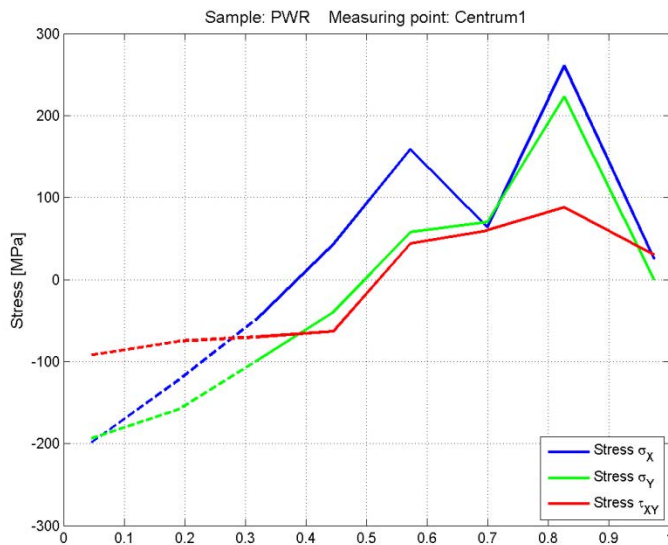
Figure A5: 31 Stresses calculated for Measuring point *R2* on the PWR sample. For the shaded stresses the von Mises effective stress is larger than 70% of the yield stress and therefore they are not reliable



Hoop stress: σ_x				
Depth mm	σ_x MPa	σ_y MPa	τ_{xy} MPa	σ_e MPa
0.04	-224	-184	27	207
0.19	-36	8	14	41
0.32	-7	48	-2	51
0.45	581	737	178	673
0.57	-215	-259	-42	239
0.70	-250	-159	14	219
0.83	-156	-73	-25	134
0.97	-92	-47	-22	79

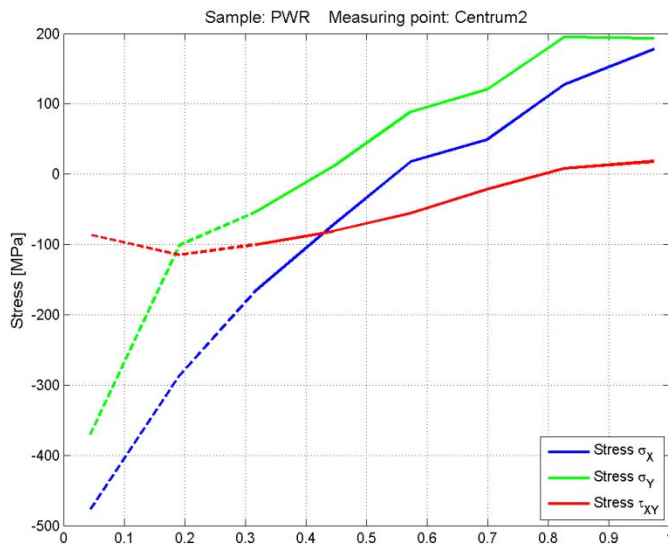
Figure A5: 32 Stresses calculated for Measuring point *R3* on the PWR sample. For the shaded stresses the von Mises effective stress is larger than 70% of the yield stress and therefore they are not reliable

Appendix 5



Depth mm	σ_x MPa	σ_y MPa	τ_{xy} MPa	σ_e MPa
0.04	-201	-195	-92	197
0.19	-122	-158	-75	142
0.32	-49	-100	-70	85
0.45	43	-40	-63	70
0.57	159	58	44	139
0.70	64	70	60	68
0.83	261	223	88	244
0.97	25	0	30	26

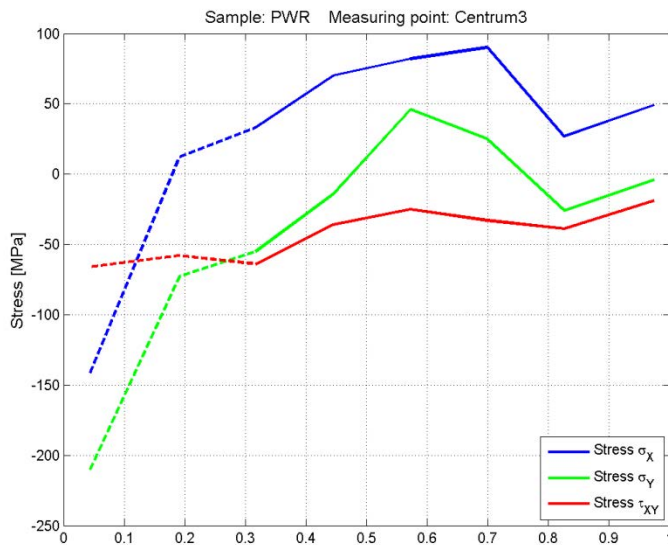
Figure A5: 33 Stresses calculated for Measuring point *C1* on the PWR sample. For the shaded stresses the von Mises effective stress is larger than 70% of the yield stress and therefore they are not reliable



Hoop stress: σ_y				
Depth mm	σ_x MPa	σ_y MPa	τ_{xy} MPa	σ_e MPa
0.04	-480	-374	-86	436
0.19	-287	-101	-115	251
0.32	-166	-54	-100	145
0.45	-72	11	-81	76
0.57	17	88	-56	79
0.70	49	120	-22	104
0.83	127	195	8	171
0.97	178	193	18	186

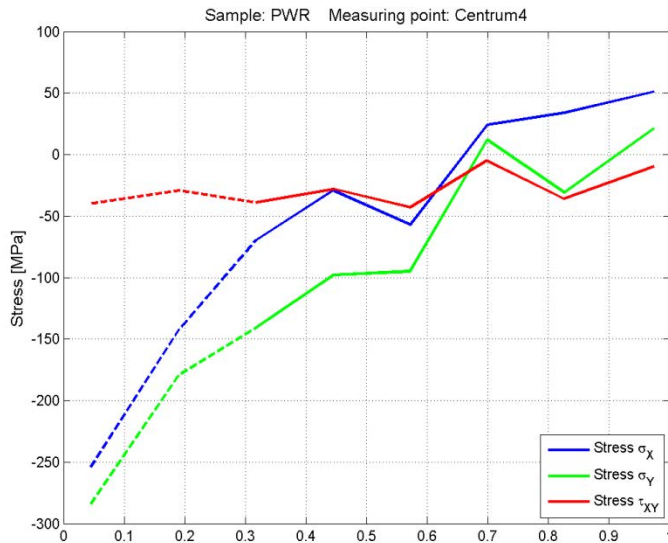
Figure A5: 34 Stresses calculated for Measuring point *C2* on the PWR sample. For the shaded stresses the von Mises effective stress is larger than 70% of the yield stress and therefore they are not reliable

Appendix 5



Hoop stress: σ_y				
Depth mm	σ_x MPa	σ_y MPa	τ_{xy} MPa	σ_e MPa
0.04	-143	-212	-66	186
0.19	12	-73	-58	78
0.32	33	-55	-64	75
0.45	70	-14	-36	77
0.57	82	46	-25	70
0.70	90	25	-33	79
0.83	27	-26	-39	44
0.97	49	-4	-19	50

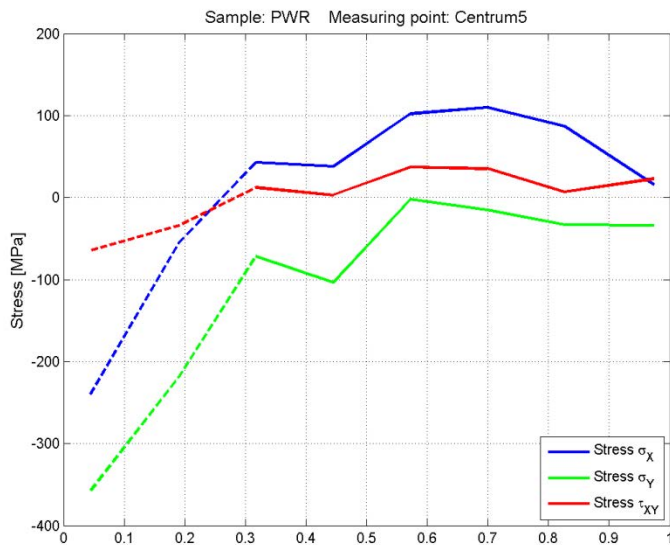
Figure A5: 35 Stresses calculated for Measuring point C3 on the PWR sample.



Hoop stress: σ_y				
Depth mm	σ_x MPa	σ_y MPa	τ_{xy} MPa	σ_e MPa
0.04	-256	-286	-40	272
0.19	-142	-179	-29	163
0.32	-70	-141	-39	121
0.45	-29	-98	-28	86
0.57	-57	-95	-43	82
0.70	24	12	-5	20
0.83	34	-31	-36	55
0.97	51	21	-10	44

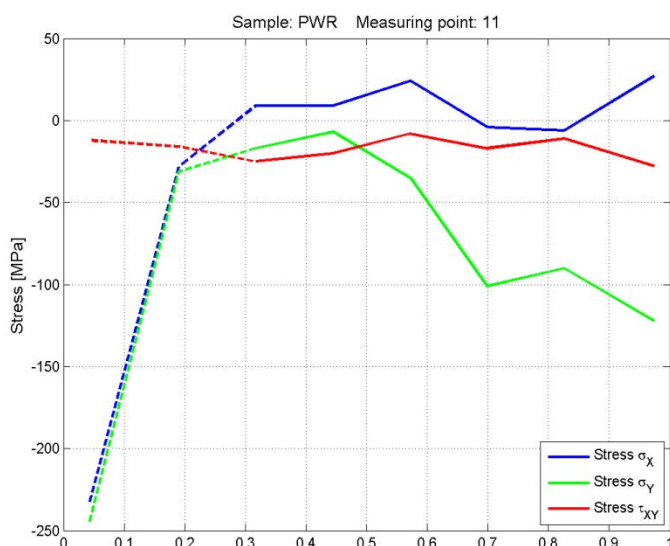
Figure A5: 36 Stresses calculated for Measuring point C4 on the PWR sample. For the shaded stresses the von Mises effective stress is larger than 70% of the yield stress and therefore they are not reliable

Appendix 5



Hoop stress: σ_y				
Depth mm	σ_x MPa	σ_y MPa	τ_{xy} MPa	σ_e MPa
0.04	-243	-360	-65	317
0.1	-55	-218	-34	196
0.32	43	-72	12	100
0.45	38	-104	3	127
0.57	102	-2	37	103
0.70	110	-15	35	118
0.83	87	-33	7	107
0.97	16	-34	23	45

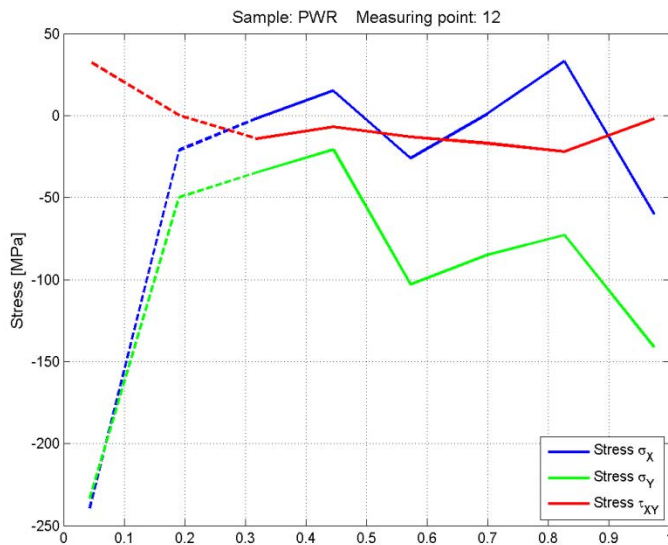
Figure A5: 37 Stresses calculated for Measuring point *C5* on the PWR sample. For the shaded stresses the von Mises effective stress is larger than 70% of the yield stress and therefore they are not reliable



Hoop stress: σ_y				
Depth mm	σ_x MPa	σ_y MPa	τ_{xy} MPa	σ_e MPa
0.04	-234	-246	-12	240
0.19	-28	-31	-16	28
0.32	9	-17	-25	21
0.45	9	-7	-20	11
0.57	24	-35	-8	51
0.70	-4	-101	-17	98
0.83	-6	-90	-11	86
0.97	27	-122	-28	137

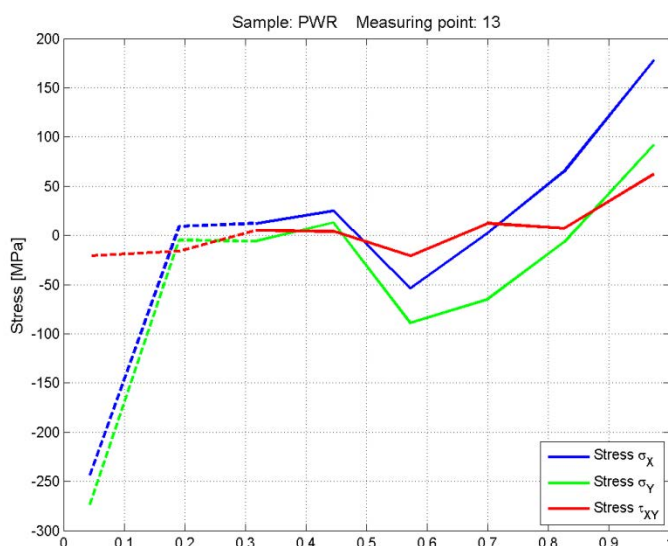
Figure A5: 38 Stresses calculated for Measuring point *11* on the PWR sample. For the shaded stresses the von Mises effective stress is larger than 70% of the yield stress and therefore they are not reliable

Appendix 5



Hoop stress: σ_y				
Depth	σ_x	σ_y	τ_{xy}	σ_e
mm	MPa	MPa	MPa	MPa
0.04	-241	-235	33	238
0.19	-21	-50	0	43
0.32	-2	-35	-14	33
0.45	15	-21	-7	30
0.57	-26	-103	-13	92
0.70	1	-85	-17	85
0.83	33	-73	-22	93
0.97	-60	-141	-2	122

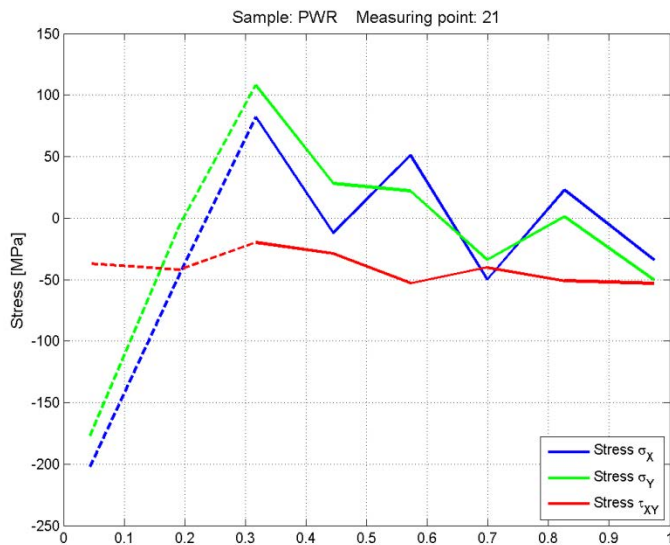
Figure A5: 39 Stresses calculated for Measuring point 12 on the PWR sample. For the shaded stresses the von Mises effective stress is larger than 70% of the yield stress and therefore they are not reliable



Hoop stress: σ_y				
Depth	σ_x	σ_y	τ_{xy}	σ_e
mm	MPa	MPa	MPa	MPa
0.04	-246	-276	-21	262
0.19	9	-5	-16	10
0.32	12	-6	5	16
0.45	25	13	4	21
0.57	-54	-89	-21	77
0.70	2	-65	12	66
0.83	65	-7	7	68
0.97	178	92	62	154

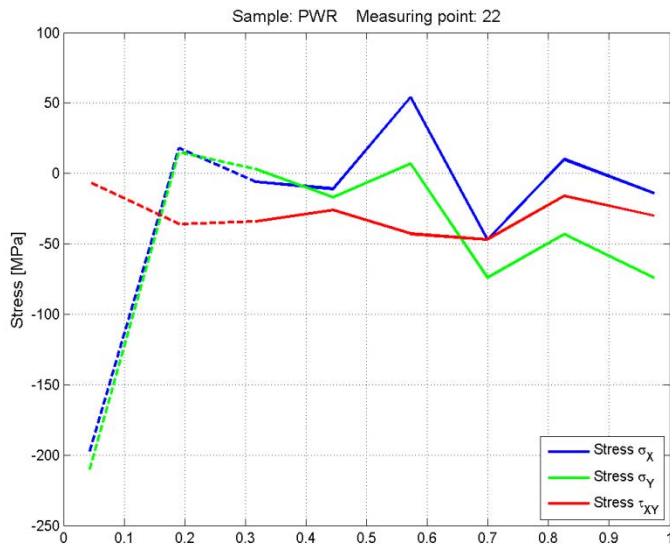
Figure A5: 40 Stresses calculated for Measuring point 13 on the PWR sample. For the shaded stresses the von Mises effective stress is larger than 70% of the yield stress and therefore they are not reliable

Appendix 5



Hoop stress: σ_y				
Depth mm	σ_x MPa	σ_y MPa	τ_{xy} MPa	σ_e MPa
0.04	-204	-179	-37	192
0.19	-46	-6	-42	41
0.32	82	108	-20	97
0.45	-12	28	-29	34
0.57	51	22	-53	42
0.70	-50	-34	-40	42
0.83	23	1	-51	18
0.97	-34	-50	-53	42

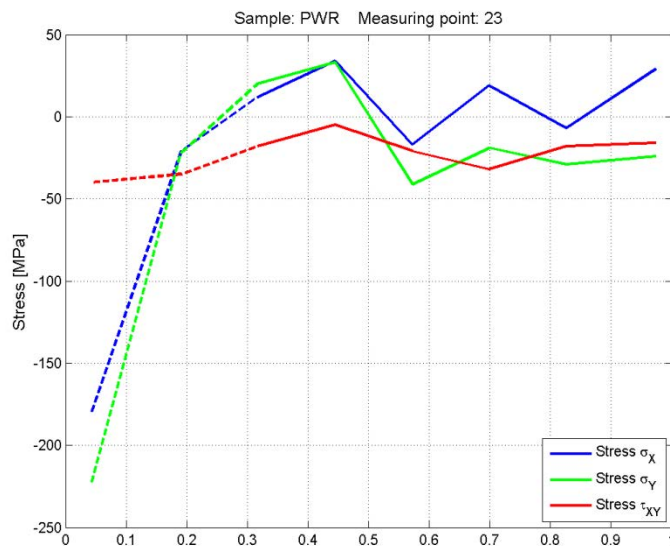
Figure A5: 41 Stresses calculated for Measuring point 21 on the PWR sample.



Hoop stress: σ_y				
Depth mm	σ_x MPa	σ_y MPa	τ_{xy} MPa	σ_e MPa
0.04	-199	-212	-6	205
0.19	18	15	-36	13
0.32	-6	3	-34	0
0.45	-11	-17	-26	12
0.57	54	7	-43	49
0.70	-47	-74	-47	63
0.83	10	-43	-16	48
0.97	-14	-74	-30	67

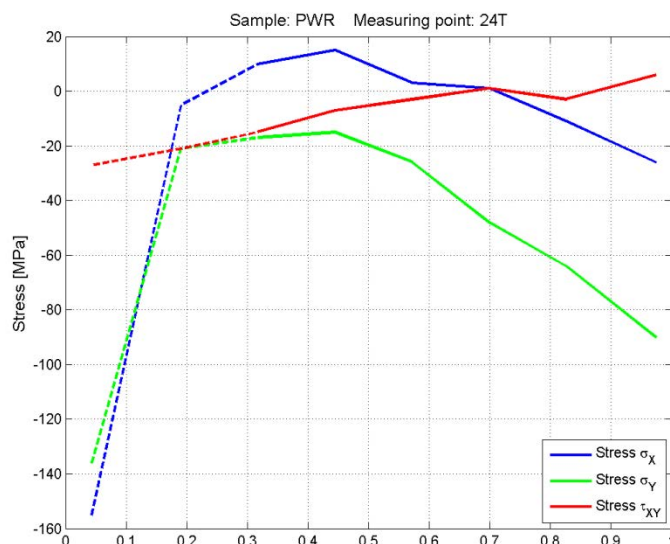
Figure A5: 42 Stresses calculated for Measuring point 22 on the PWR sample.

Appendix 5



Hoop stress: σ_y				
Depth mm	σ_x MPa	σ_y MPa	τ_{xy} MPa	σ_e MPa
0.04	-181	-224	-40	205
0.19	-21	-22	-35	18
0.32	12	20	-18	15
0.45	34	33	-5	33
0.57	-17	-41	-21	34
0.70	19	-19	-32	31
0.83	-7	-29	-18	25
0.97	29	-24	-16	45

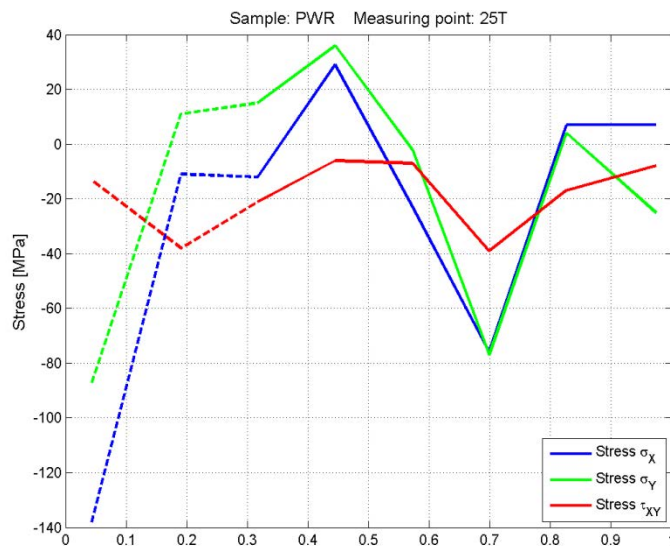
Figure A5: 43 Stresses calculated for Measuring point 23 on the PWR sample.



Hoop stress: σ_y				
Depth mm	σ_x MPa	σ_y MPa	τ_{xy} MPa	σ_e MPa
0.04	-156	-137	-27	147
0.19	-5	-21	-21	17
0.32	10	-17	-15	22
0.45	15	-15	-7	25
0.57	3	-26	-3	27
0.70	1	-48	1	48
0.83	-11	-64	-3	59
0.97	-26	-90	6	80

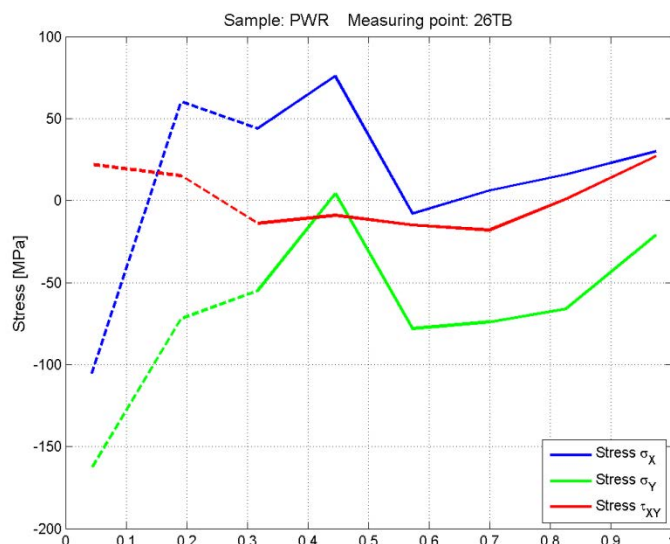
Figure A5: 44 Stresses calculated for Measuring point 24T on the PWR sample

Appendix 5



Hoop stress: σ_y				
Depth mm	σ_x MPa	σ_y MPa	τ_{xy} MPa	σ_e MPa
0.04	-139	-88	-13	121
0.19	-11	11	-38	15
0.32	-12	15	-21	22
0.45	29	36	-6	32
0.57	-23	-2	-7	21
0.70	-76	-77	-39	75
0.83	7	4	-17	0
0.97	7	-25	-8	28

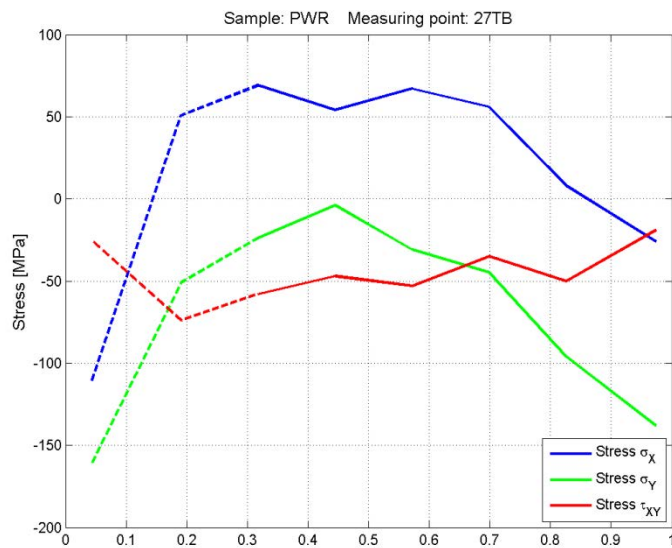
Figure A5: 45 Stresses calculated for Measuring point 25T on the PWR sample



Hoop stress: σ_y				
Depth mm	σ_x MPa	σ_y MPa	τ_{xy} MPa	σ_e MPa
0.04	-107	-164	22	144
0.19	60	-72	15	114
0.32	44	-55	-14	85
0.45	76	4	-9	73
0.57	-8	-78	-15	74
0.70	6	-74	-18	76
0.83	16	-66	1	75
0.97	30	-21	27	45

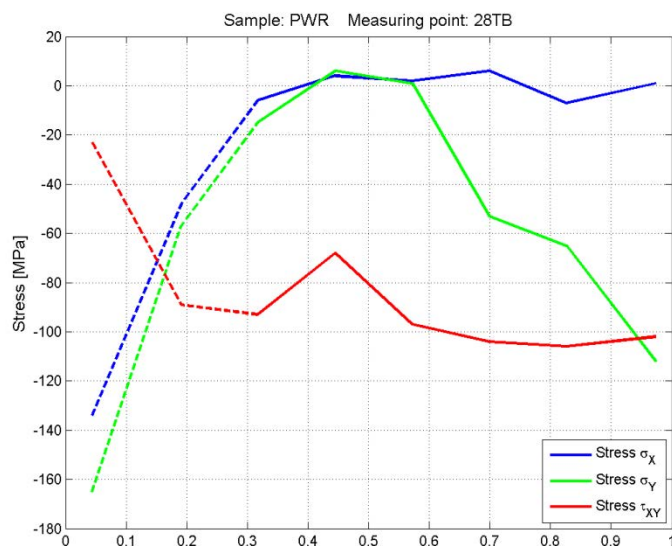
Figure A5: 46 Stresses calculated for Measuring point 26TB on the PWR sample

Appendix 5



Hoop stress: σ_y				
Depth [mm]	σ_x [MPa]	σ_y [MPa]	τ_{xy} [MPa]	σ_e [MPa]
0.04	-112	-162	-25	143
0.19	51	-51	-74	87
0.32	69	-24	-58	82
0.45	54	-4	-47	54
0.57	67	-31	-53	85
0.70	56	-45	-35	87
0.83	8	-96	-50	99
0.97	-26	-138	-19	126

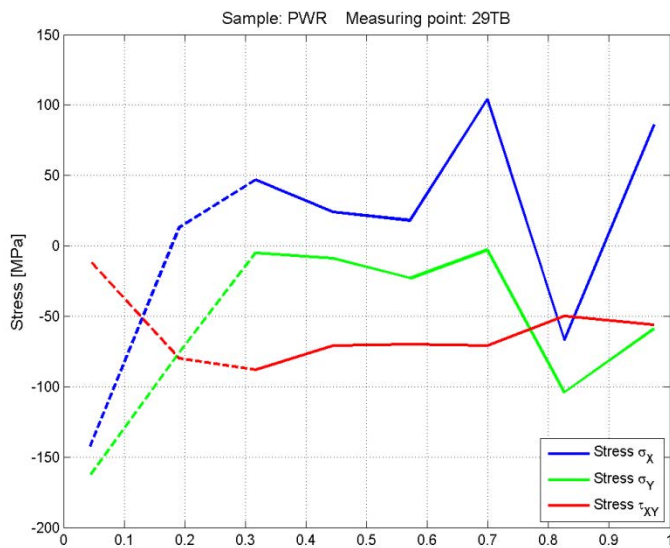
Figure A5: 47 Stresses calculated for Measuring point 27TB on the PWR sample



Hoop stress: σ_y				
Depth [mm]	σ_x [MPa]	σ_y [MPa]	τ_{xy} [MPa]	σ_e [MPa]
0.04	-135	-166	-22	152
0.19	-48	-57	-89	50
0.32	-6	-15	-93	0
0.45	4	6	-68	0
0.57	2	1	-97	0
0.70	6	-53	-104	53
0.83	-7	-65	-106	59
0.97	1	-112	-102	111

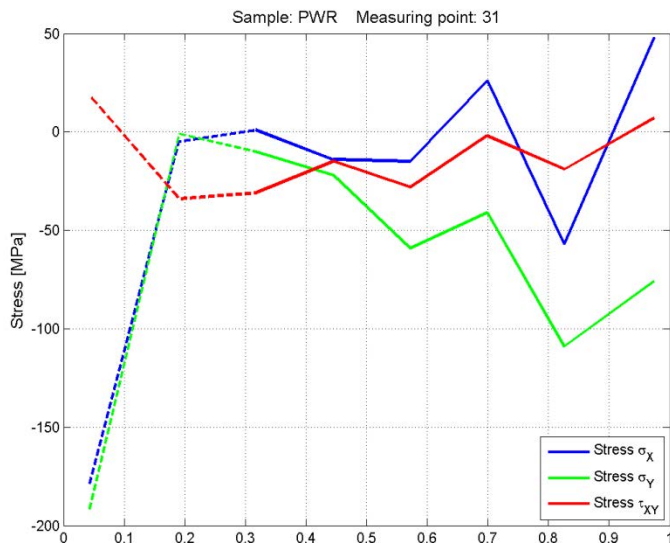
Figure A5: 48 Stresses calculated for Measuring point 28TB on the PWR sample

Appendix 5



Hoop stress: σ_y				
Depth [mm]	σ_x [MPa]	σ_y [MPa]	τ_{xy} [MPa]	σ_e [MPa]
0.04	-144	-164	-10	154
0.19	13	-76	-80	81
0.32	47	-5	-88	46
0.45	24	-9	-71	25
0.57	18	-23	-70	32
0.70	104	-3	-71	104
0.83	-67	-104	-50	90
0.97	86	-59	-56	125

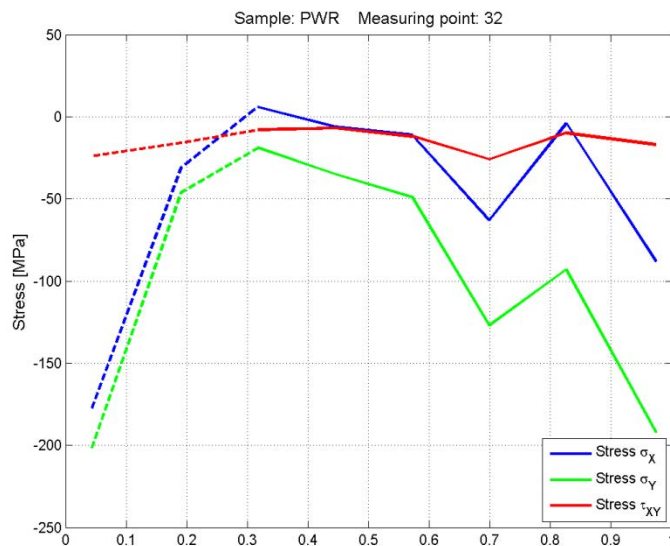
Figure A5: 49 Stresses calculated for Measuring point 29TB on the PWR sample



Hoop stress: σ_y				
Depth [mm]	σ_x [MPa]	σ_y [MPa]	τ_{xy} [MPa]	σ_e [MPa]
0.04	-180	-193	19	186
0.19	-5	-1	-34	0
0.32	1	-10	-31	4
0.45	-14	-22	-15	18
0.57	-15	-59	-28	52
0.70	26	-41	-2	58
0.83	-57	-109	-19	94
0.97	48	-76	7	108

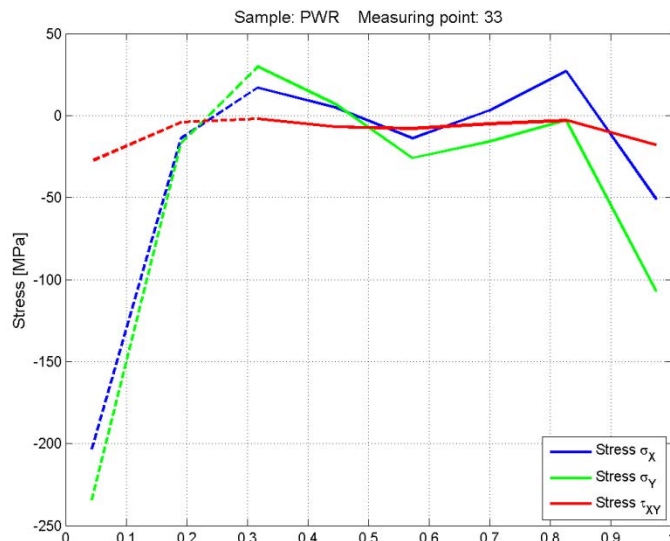
Figure A5: 50 Stresses calculated for Measuring point 31 on the PWR sample

Appendix 5



Hoop stress: σ_y				
Depth [mm]	σ_x [MPa]	σ_y [MPa]	τ_{xy} [MPa]	σ_e [MPa]
0.04	-179	-203	-24	191
0.19	-31	-46	-16	40
0.32	6	-19	-8	22
0.45	-6	-35	-7	32
0.57	-11	-49	-12	44
0.70	-63	-127	-26	109
0.83	-4	-93	-10	90
0.97	-88	-192	-17	166

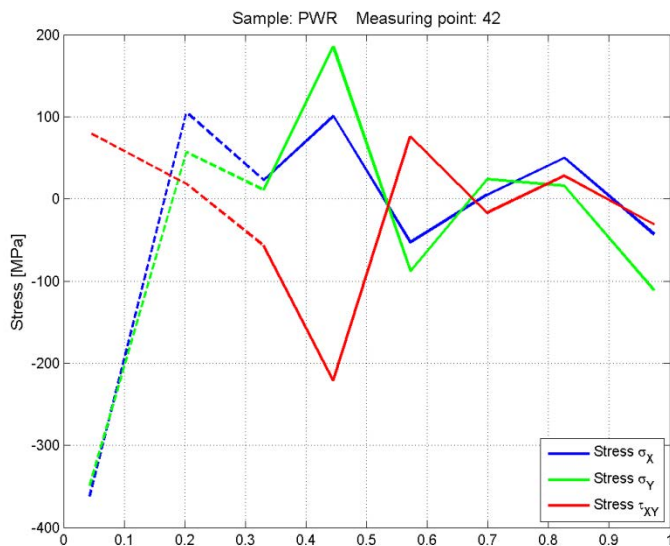
Figure A5: 51 Stresses calculated for Measuring point 32 on the PWR sample.



Hoop stress: σ_y				
Depth [mm]	σ_x [MPa]	σ_y [MPa]	τ_{xy} [MPa]	σ_e [MPa]
0.04	-205	-236	-28	221
0.19	-14	-17	-4	15
0.32	17	30	-2	25
0.45	5	7	-7	4
0.57	-14	-26	-8	22
0.70	3	-16	-5	17
0.83	27	-3	-3	28
0.97	-51	-107	-18	92

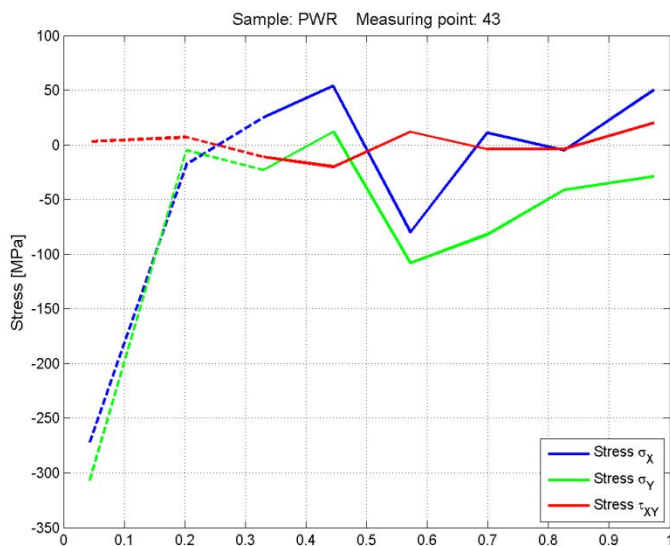
Figure A5: 52 Stresses calculated for Measuring point 33 on the PWR sample. For the shaded stresses the von Mises effective stress is larger than 70% of the yield stress and therefore they are not reliable

Appendix 5



Hoop stress: σ_y				
Depth [mm]	σ_x [MPa]	σ_y [MPa]	τ_{xy} [MPa]	σ_e [MPa]
0.04	-365	-352	81	359
0.19	105	57	18	91
0.32	23	11	-57	15
0.45	101	185	-221	158
0.57	-53	-88	76	78
0.70	5	24	-17	20
0.83	50	16	28	45
0.97	-43	-111	-31	96

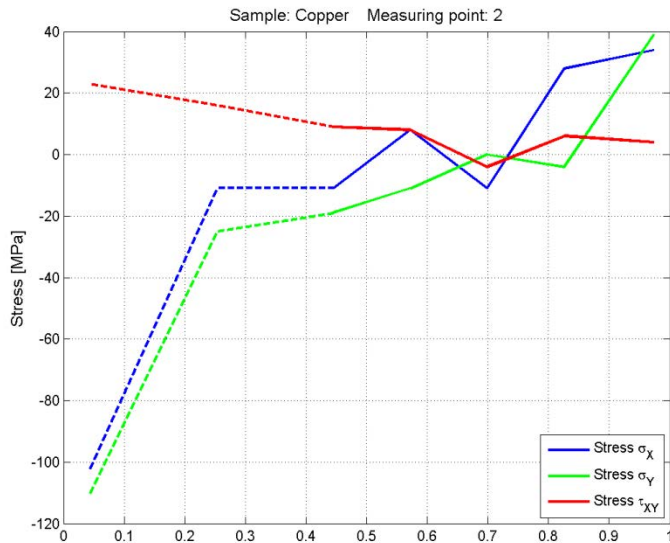
Figure A5: 53 Stresses calculated for Measuring point 42 on the PWR sample. For the shaded stresses the von Mises effective stress is larger than 70% of the yield stress and therefore they are not reliable



Hoop stress: σ_y				
Depth [mm]	σ_x [MPa]	σ_y [MPa]	τ_{xy} [MPa]	σ_e [MPa]
0.04	-274	-309	3	293
0.19	-18	-5	7	16
0.32	25	-23	-11	41
0.45	54	12	-20	48
0.57	-80	-108	12	97
0.70	11	-82	-4	87
0.83	-5	-41	-4	38
0.97	50	-29	20	69

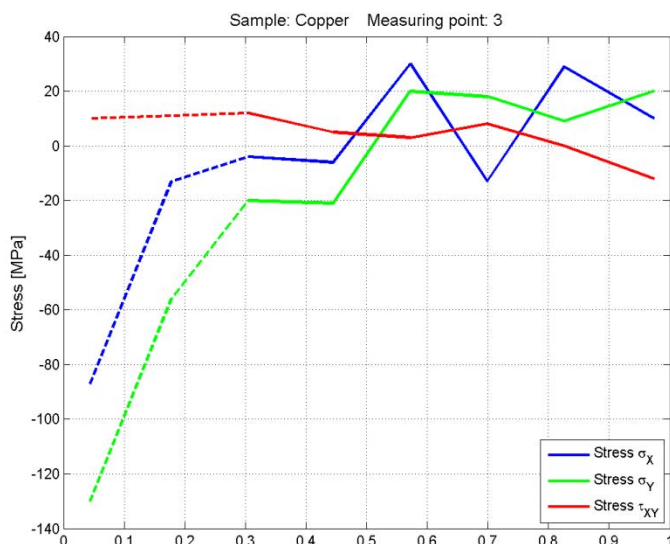
Figure A5: 54 Stresses calculated for Measuring point 43 on the PWR sample. For the shaded stresses the von Mises effective stress is larger than 70% of the yield stress and therefore they are not reliable.

Appendix 5



Depth mm	σ_x MPa	σ_y MPa	τ_{xy} MPa	σ_e MPa
0.04	-103	-111	23	108
0.19	-11	-25	16	23
0.32	-11	-19	9	17
0.45	8	-11	8	17
0.57	-11	0	-4	10
0.70	28	-4	6	30
0.83	34	39	4	37

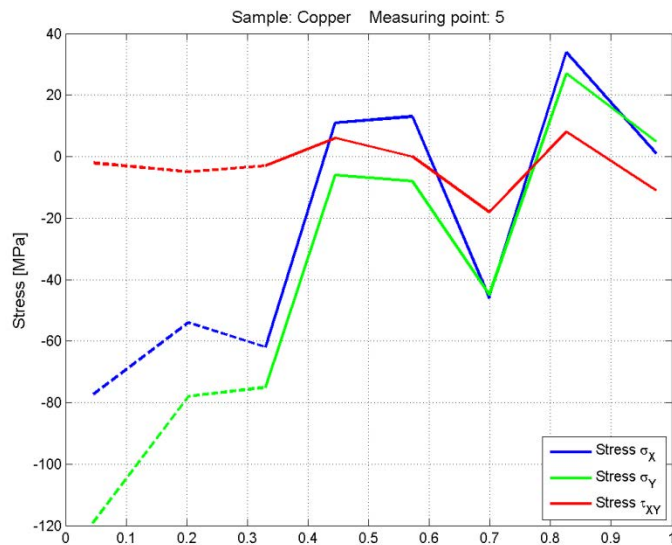
Figure A5: 55 Stresses calculated for Measuring point 2 on the Copper sample. For the shaded stresses the von Mises effective stress is larger than 70% of the yield stress and therefore they are not reliable



Depth mm	σ_x MPa	σ_y MPa	τ_{xy} MPa	σ_e MPa
0.04	-88	-131	10	116
0.19	-13	-56	11	51
0.32	-4	-20	12	19
0.45	-6	-21	5	19
0.57	30	20	3	27
0.70	-13	18	8	27
0.83	29	9	0	26
0.97	10	20	-12	16

Figure A5: 56 Stresses calculated for Measuring point 3 on the Copper sample. For the shaded stresses the von Mises effective stress is larger than 70% of the yield stress and therefore they are not reliable

Appendix 5



Depth mm	σ_x MPa	σ_y MPa	τ_{xy} MPa	σ_e MPa
0.04	-78	-120	-2	105
0.19	-54	-78	-5	69
0.32	-62	-75	-3	69
0.45	11	-6	6	16
0.57	13	-8	0	18
0.70	-46	-45	-18	45
0.83	34	27	8	31
0.97	1	5	-11	0

Figure A5: 57 Stresses calculated for Measuring point 5 on the Copper sample. For the shaded stresses the von Mises effective stress is larger than 70% of the yield stress and therefore they are not reliable

Appendix 5

Table A5: 6 The hoop stress at different depths at measuring points R1 and R2 in the BWR sample. For the shaded stress the von Mises effective stress is larger than 70% of the yield stress and therefore they are not reliable.

Depth mm	R1 MPa	R2 MPa
0.04	-187	-308
0.19	-5	-121
0.32	33	-18
0.45	31	7
0.57	16	-5
0.70	4	-19
0.83	36	-17
0.97	3	30

Table A5: 7 The hoop stress at different depths at measuring points 11, 12, 13, 21, 22 and 23 in the BWR sample. For the shaded stresses the von Mises effective stress is larger than 70% of the yield stress and therefore they are not reliable.

Depth mm	11 MPa	12 MPa	13 MPa	21 MPa	22 MPa	23 MPa
0.04	-256	-199	-273	-181	-227	-225
0.19	3	-32	-3	-11	-16	-32
0.32	31	34	31	20	15	8
0.45	21	33	26	28	19	33
0.57	-4	34	-4	1	37	-5
0.70	4	18	-26	-38	23	17
0.83	-40	-6	-14	-1	-21	-2
0.97	17	-43	-30	-19	54	-96

Table A5: 8 The hoop stress at different depths at measuring points 31, 32, 33, 34T and 35T in the BWR sample.

Depth mm	31 MPa	32 MPa	33 MPa	34T MPa	35T MPa
0.04	-164	-235	-202	-132	-129
0.19	61	34	9	3	14
0.32	89	102	26	30	11
0.45	58	42	31	-13	46
0.57	57	36	67	25	62
0.70	33	69	-40	9	31
0.83	62	79	41	9	39
0.97	26	-20	47	-35	-55

Appendix 5

Table A5: 9 The hoop stress at different depths at measuring points 36TB, 37TB, 38TB, 41, 42 and 43 in the BWR sample. For the shaded stresses the von Mises effective stress is larger than 70% of the yield stress and therefore they are not reliable.

Depth mm	36TB MPa	37TB MPa	38TB MPa	41 MPa	42 MPa	43 MPa
0.04	-129	-127	-150	-225	-218	-226
0.19	-17	-8	-3	17	50	-11
0.32	0	-7	11	127	95	66
0.45	0	14	0	80	76	51
0.57	-10	3	-3	109	93	55
0.70	-6	7	-24	139	55	59
0.83	30	-49	-22	138	34	51
0.97	-50	45	50	62	53	26

Table A5: 10 The hoop stress at different depths at measuring points 51, 52, 53, 61, 62 and 63 in the BWR sample. For the shaded stresses the von Mises effective stress is larger than 70% of the yield stress and therefore they are not reliable.

Depth mm	51 MPa	52 MPa	53 MPa	61 MPa	62 MPa	63 MPa
0.04	-317	-302	-172	-290	-279	-225
0.19	-104	-92	-78	-80	-58	-45
0.32	19	4	4	-15	-3	15
0.45	24	0	2	0	7	16
0.57	-19	9	-2	-53	13	4
0.70	-55	8	4	-77	-64	-34
0.83	11	-50	-47	-66	-18	-15
0.97	-7	-3	-5	-103	1	-3

Table A5: 11 The hoop stress at different depths at measuring points R1, R2 and R3 in the PWR sample. For the shaded stresses the von Mises effective stress is larger than 70% of the yield stress and therefore they are not reliable.

Depth mm	R1 MPa	R2 MPa	R3 MPa
0.04	-174	-243	-224
0.19	301	-31	-36
0.32	334	15	-7
0.45	313	-296	581
0.57	-303	96	-215
0.70	-28	0	-250
0.83	2	-8	-156
0.97	-65	30	-92

Appendix 5

Table A5: 12 The hoop stress at different depths at measuring points C2, C3, C4 and C5 in the PWR sample. For the shaded stresses the von Mises effective stress is larger than 70% of the yield stress and therefore they are not reliable.

Depth mm	C2 MPa	C3 MPa	C4 MPa	C5 MPa
0.04	-374	-212	-286	-360
0.19	-101	-73	-179	-218
0.32	-54	-55	-141	-72
0.45	11	-14	-98	-104
0.57	88	46	-95	-2
0.70	120	25	12	-15
0.83	195	-26	-31	-33
0.97	193	-4	21	-34

Table A5: 13 The hoop stress at different depths at measuring points 11, 12, 13, 21, 22 and 23 in the PWR sample. For the shaded stresses the von Mises effective stress is larger than 70% of the yield stress and therefore they are not reliable.

Depth mm	11 MPa	12 MPa	13 MPa	21 MPa	22 MPa	23 MPa
0.04	-246	-235	-276	-179	-212	-224
0.19	-31	-50	-5	-6	15	-22
0.32	-17	-35	-6	108	3	20
0.45	-7	-21	13	28	-17	33
0.57	-35	-103	-89	22	7	-41
0.70	-101	-85	-65	-34	-74	-19
0.83	-90	-73	-7	1	-43	-29
0.97	-122	-141	92	-50	-74	-24

Table A5: 14 The hoop stress at different depths at measuring points 24T, 25T, 26TB, 27TB, 28TB and 29TB in the PWR sample.

Depth mm	24T MPa	25T MPa	26TB MPa	27TB MPa	28TB MPa	29TB MPa
0.04	-137	-88	-164	-162	-166	-164
0.19	-21	11	-72	-51	-57	-76
0.32	-17	15	-55	-24	-15	-5
0.45	-15	36	4	-4	6	-9
0.57	-26	-2	-78	-31	1	-23
0.70	-48	-77	-74	-45	-53	-3
0.83	-64	4	-66	-96	-65	-104
0.97	-90	-25	-21	-138	-112	-59

Appendix 5

Table A5: 15 The hoop stress at different depths at measuring points 31, 32, 33, 42 and 43 in the PWR sample. For the shaded stresses the von Mises effective stress is larger than 70% of the yield stress and therefore they are not reliable.

Depth mm	31 MPa	32 MPa	33 MPa	42 MPa	43 MPa
0.04	-193	-203	-236	-352	-309
0.19	-1	-46	-17	57	-5
0.32	-10	-19	30	11	-23
0.45	-22	-35	7	185	12
0.57	-59	-49	-26	-88	-108
0.70	-41	-127	-16	24	-82
0.83	-109	-93	-3	16	-41
0.97	-76	-192	-107	-111	-29